Dissertation

submitted to the

Combined Faculty of Natural Sciences and Mathematics

of the Ruperto Carola University Heidelberg, Germany

for the degree of

Doctor of Natural Sciences

Presented by

Leonardo Traini, M.Sc.

born in: Loreto, Italy

Oral examination: 20th December, 2021

The role of tumor suppressor genes

PBRM1 and RPS6KA3 in primary liver cancer

Referees:

Prof. Dr. Ralf Bartenschlager

Prof. Dr. Darjus Felix Tschaharganeh

Summary

Primary liver cancer (PLC) is a major health concern, being the fifth most occurring cancer and the second most lethal worldwide. However, due to the lack of targetable mutations in patient tumors, treatment options are still limited. Therefore, identifying and characterizing new targetable mutations in PLC is of the utmost importance. In the present study, I interrogated publicly available human PLC sequencing data to detect and functionally characterize recurring genetic alterations, with the overall aim of identifying potential biomarkers exploitable by precision medicine.

PBRM1 is a component of the SWI/SNF epigenetic remodeling complexes and was found to be preferentially mutated in intrahepatic cholangiocarcinoma (iCCA) rather than hepatocellular carcinoma (HCC), thus suggesting a role as tumor initiator and/or cancer identity determinator. To gain further insight, I employed mouse models with liver-specific deletion or reversible downregulation of PBRM1 by CRISPR/Cas9 or RNA interference, respectively. In parallel, loss of PBRM1 was further investigated in these mouse models with NASH-inducing dietary models of HCC. Disrupting PBRM1 expression *in vivo* and *in vitro* showed no connection between PBRM1 expression status and its involvement in liver cancer initiation or liver cancer plasticity.

RPS6KA3 is a kinase protein that acts as an effector and negative feedback regulator of RAS/MAPK pathway. The results from this dissertation demonstrated that RPS6KA3 loss contributes to tumorigenicity *in vivo* and that the loss of RPS6KA3 leads to an upregulation of the MAPK pathway both *in vivo* and *in vitro* with murine and human HCC cell lines. Moreover, RPS6KA3-depleted murine xenograft tumors and orthotopically transplanted human HCC cells lines with low RPS6KA3 levels responded remarkably to trametinib, a FDA-approved MEK inhibitor. Thus, the results not only reveal RPS6KA3 as an important tumor suppressor in HCC but also implicate RPS6KA3 as a novel biomarker for MAPK pathway inhibitors in HCC patients.

Zusammenfassung

Primärer Leberkrebs (PLC) ist ein großes Gesundheitsproblem, da er weltweit die fünfthäufigste und zweittödlichste Krebserkrankung ist. Aufgrund des Fehlens von gezielt für Therapien verwendbare Mutationen in Patiententumoren, sind die Behandlungsmöglichkeiten jedoch immer noch begrenzt. Daher ist es von größter Bedeutung, neue gezielte Mutationen in PLC zu identifizieren und zu charakterisieren. In der vorliegenden Studie habe ich öffentlich verfügbare humane PLC-Sequenzierungsdaten abgefragt, um wiederkehrende genetische Veränderungen zu erkennen und funktionell zu charakterisieren, mit dem übergeordneten Ziel, potenzielle Biomarker zu identifizieren, die für die Präzisionsmedizin verwendbar sind.

PBRM1 ist eine Komponente der epigenetischen Remodellierungskomplexe von SWI/SNF und wurde vor allem im intrahepatischen Cholangiokarzinom (iCCA), und nicht im hepatozellulären Karzinom (HCC), mutiert festgestellt, was auf eine Rolle als Tumorinitiator und/oder Krebsidentitätsdeterminator hindeutet. Um weitere Erkenntnisse zu gewinnen, habe ich Mausmodelle mit leberspezifischer Deletion oder reversibler Herunterregulierung von PBRM1 durch CRISPR/Cas9 bzw. RNA-Interferenz verwendet. Parallel dazu wurde außerdem der Verlust von PBRM1 in diesen Mausmodellen mit NASH-induzierenden Ernährungsmodellen von HCC untersucht. Eine Beeinträchtigung der PBRM1-Expression *in vivo* und *in vitro* zeigte keinen Zusammenhang zwischen dem PBRM1-Expressionsstatus und seiner Beteiligung an der Entstehung von Leberkrebs oder der Plastizität von Leberkrebs.

RPS6KA3 ist ein Kinaseprotein, welches als Effektor und negativer Rückkopplungsregulator des RAS/MAPK-Signalwegs fungiert. Die Ergebnisse dieser Dissertation zeigten, dass der Verlust von RPS6KA3 *in vivo* zur Tumorigenität beiträgt und, dass der Verlust von RPS6KA3, sowohl *in vivo* als auch *in vitro* bei Maus- und Human-HCC-Zelllinien, zu einer Hochregulation des MAPK-Signalwegs führt. Darüber hinaus reagierten RPS6KA3-depletierte Maus-Xenotransplantat-Tumoren und orthotop transplantierte humane HCC-Zelllinien mit niedrigen RPS6KA3-Spiegeln bemerkenswert auf Trametinib, ein von der FDA zugelassener MEK-Inhibitor. Somit zeigen die Ergebnisse RPS6KA3 nicht nur als wichtigen

Tumorsuppressor bei HCC, sondern deuten auch auf RPS6KA3 als neuartigen Biomarker für MAPK-Signalweg-Inhibitoren bei HCC-Patienten hin.

Table of contents

List of Figures

List of Tables

List of Abbreviations

Abbreviation	Explanation
ACT	Adoptive cell therapy
AFP	Alpha fetoprotein
AJCC	American Joint Committee on Cancer
ALB	Albumin
ALT	Alanine aminotransferase
APOE	Apolipoprotein E
AST	Aspartate transaminase
BCLC	Barcelona Clinic Liver Cancer
BDL	Bile duct ligation
BRAF	B-Raf proto-oncogene
CNA	Copy number alterations
CCA	Cholangiocarcinoma
ccRCC	Clear cell renal cell carcinoma
CD-HFD	Choline-deficient high fat diet
CDKN2A	Cyclin dependent kinase inhibitor 2A
CRISPR	Clustered regularly interspaced short palindromic repeats
CTC	Blood-derived circulating tumor cells
ctDNA	Blood-derived cell-free tumor DNA
CTNNB1	Catenin beta 1
dCCA	Distal CCA
DNA	Deoxyribonucleic acid
Dox	Doxycycline
EGF	Epidermal growth factor
EGFR	Epidermal growth factor receptor
EPCAM	Epithelial cell adhesion molecule
FLC	Fibrolamellar HCC
GDP	Guanosine diphosphate
GFP	Green fluorescent protein
GTP	Guanosine triphosphate
HBV	Hepatitis B virus
HCC	Hepatocellular carcinoma
HCV	Hepatitis C virus
HER2	Erb-b2 receptor tyrosine kinase 2
HNF4A	Hepatocyte nuclear factor 4 alpha
HTVI	Hydrodynamic tail vein injection

iCCA	Intrahepatic CCA
IDH1	Isocitrate dehydrogenase (NADP(+)) 1
IHC	Immunohistochemistry
KRT19	Keratin 19
MAPK	Mitogen-activated protein kinase
MAX	MYC associated factor X
miRNA	Micro RNA
mRNA	Messenger RNA
MSKCC	Memorial Sloan Kettering Cancer Center
mTOR	Mechanistic target of rapamycin kinase
myr-AKT	Myristoylated AKT
NAFLD	Nonalcoholic fatty liver disease
NASH	Nonalcoholic steatohepatitis
NGS	Next generation sequencing
NICD	Notch intracellular domain
NK	Natural killer
NSCLC	Non-small cell lung cancer
ORF	Open reading frame
PBRM1	Polybromo 1
pCCA	Perihilar CCA
PCR	Polymerase chain reaction
PD-L1	Programmed cell death-ligand 1
p-ERK	Phosphorylated ERK
PI3K	Phosphatidylinositol 3-kinase
PKB	Protein kinase B
PLC	Primary liver cancer
RNA	Ribonucleic acid
RNAi	RNA interference
RPS6KA3	Ribosomal protein S6 kinase
RT-qPCR	Reverse transcriptase quantitative PCR
sgRNA	Single guide RNA
shRNA	Short hairpin RNA
SOX9	SRY-box transcription factor 9
SWI/SNF	Switch/sucrose non-fermenting
TAA	Thioacetamide
TCGA	The Cancer Genome Atlas
TCR	T-cell receptor
TERT	Telomerase reverse transcriptase

TIL	Tumor infiltrating lymphocytes
TP53	Tumor protein 53
TRP53	Transformation related protein 53
TSG	Tumor-suppressor genes
UICC	Union for International Cancer Control
VEGFA	Vascular endothelial growth factor A
WB	Western blot
WD	Western diet
WHO	World Health Organization
YAP1	Yes-associated protein 1

1 Introduction

1.1 The liver: structure and physiology

When observing the human body and the organs composing it, one cannot avoid to immediately notice the liver. This organ not only is one of the biggest (2% to 5% of the body weight can be attributed to it), but arguably is the organ with the most functions – more than 500. Moreover, the liver is famously one of the few organs with a unique ability for extreme regeneration, accompanied by its capacity for very precise mass regulation.[1]

1.1.1 Liver architecture

The liver's complex array of functions is orchestrated by an elegant, hierarchical structure (**Figure 1.1**).[1] In adults, the liver is structured into four lobes. Zooming in, liver lobes are composed by liver lobules, which can be roughly identified as hexagons with a central vein running through the middle and connected to portal triads at each vertex. The triad itself consists of a:

- Portal vein branch, carrying deoxygenated blood and digestion byproducts from the gut, and supplying around two thirds of the blood supply to the liver;
- Hepatic artery branch, carrying oxygenated blood, and accounting for around one third of the liver's blood supply;
- Bile ducts branch, lined by cholangiocytes and collecting bile from the hepatocytes.

Ultimately, the functional unit of the liver is represented by the hepatic lobule, spanning all the area between the portal triad and the central vein (**Figure 1.2**).[2] The unique dual nature of blood supply in the liver is observed in the lobule itself – oxygenated blood from the hepatic artery mixes with deoxygenated blood from the portal vein and finally drains in the central vein.[3] This, therefore, creates a strong gradient for oxygenated blood, nutrients, hormones, and other molecules, whose concentration decreases as blood flows towards the central vein. Eventually, in response to this gradient, both parenchymal and nonparenchymal cells in the

hepatic lobule cluster into different functional areas, in a process referred to as “liver zonation”.[4]

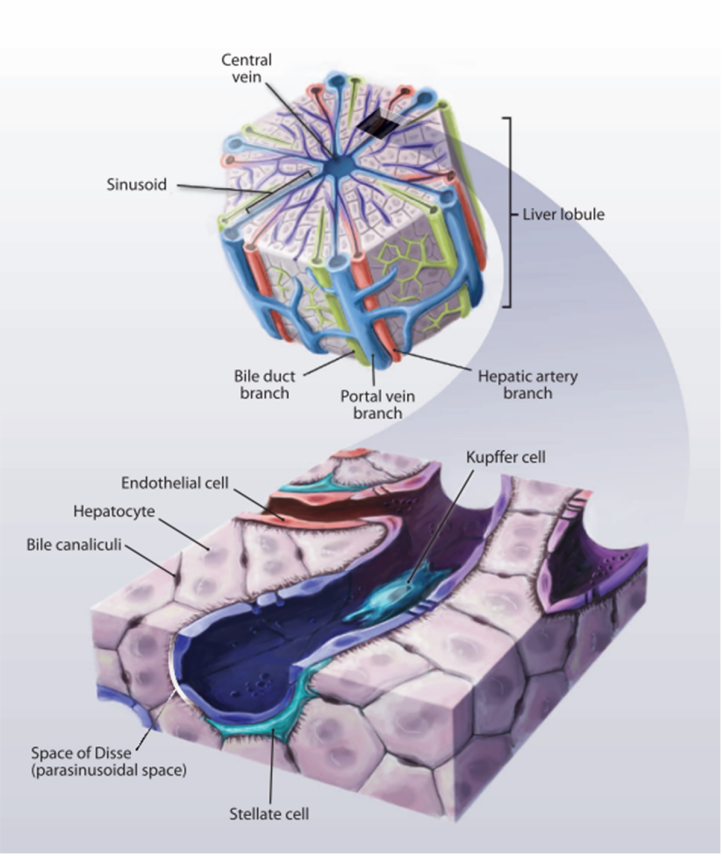

Figure 1.1 | The liver lobule. Shown in the picture is the liver lobule, the functional unit of the liver. Bhatia et al. (2014).[1]

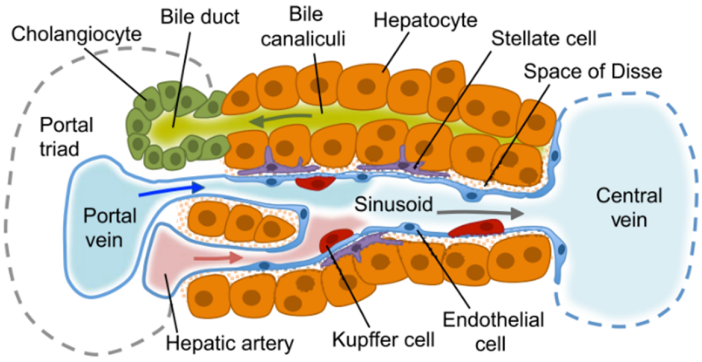

Figure 1.2 | The hepatic lobule: structure and cell types. Gordillo et al. (2015).[5]

1.1.2 Liver cell populations and their functions

When looking broadly at physiological functions of the liver, this organ plays pivotal roles in metabolism, digestion, detoxification, immune response and synthesis processes.[1,6] Such a multi-layered set of systemic functions is possible thank to an exquisite interplay among the heterogeneous population of cells inhabiting the liver.

In the parenchyma – the functional part of the organ, the liver is mostly composed of hepatocytes (~80% by mass) (**Figure 1.2**).[7] Hepatocytes are big (~20-30 μm) and cuboidal cells that are responsible for the majority of liver metabolic functions. Hepatocytic functions depend on the aforementioned liver zonation, which is regulated by a gradient of Wnt/β-catenin signaling. The pathway is more activated in the perivenous area and gradually decreases in strength as it approaches the periportal area. This gradient drives the downstream expression of different sets of genes along its axis and divides hepatocytes in three different subpopulations.[4,8] Hepatocytes in the outermost periportal area are subjected to the highest oxygen concentration and carry energy-demanding processes such as gluconeogenesis, β-oxidation, cholesterol biosynthesis, ureagenesis and protein secretion. In the middle zone, hepatocytes participate in iron homeostasis and modulation of insulin growth factors. Finally, less energy-demanding process are carried out in the perivenous area, where hepatocytes perform glycolysis, bile acid production and xenobiotic metabolism.[9]

When it comes to metabolism, the liver plays a critical role in detoxification of drugs and xenobiotics through the action of cytochrome P450 family of enzymes. Mainly, these enzymes' role is to convert drugs from an hydrophobic state into an hydrophilic one, which is more suitable for disposal through the bile or blood.[10] Metabolism in the liver is not exclusively limited to the removal of such substances, but is also linked with degradation and recycling of heme, through a multi-organ biotransformation process similar to the one employed with drugs. During this process, heme is converted into unconjugated bilirubin which, once bound to albumin, can be processed by the liver, leading to its excretion into the bile.[6] Lastly, the liver has a central role in biosynthesis and storage of glycogen,[11] triglycerides,[12] crucial components of the blood clotting cascade,[5] fat-soluble vitamins, and trace minerals, such as copper and iron.[13]

Hepatocytes synthesize and release bile into the bile canaliculi, whose bile flow is opposite to the blood flow. The bile is then drained into increasingly bigger ducts building the biliary tree to be stored in the gallbladder, and to ultimately be released into the duodenum, where it is important for digestion and absorption of lipids.[6] The biliary tree is lined by the second parenchymal cell of the liver – the cholangiocyte (also known as biliary epithelial cell).[5] When compared to hepatocytes, cholangiocytes are significantly smaller cells, normally classified as small (~9 μm) and large (~13 μm). While small cholangiocytes are poorly specialized, large cholangiocytes possess a major role in hepatocyte-derived bile maturation and biliary fluid secretion.[14,15]

Apart of these parenchymal cells, other cells are playing major supportive roles. One of these are Kupffer cells, the largest population of liver-specific macrophages, located in liver sinusoids, whose major function is endocytosis of pathogens present in the blood but also possess supporting roles in the maintenance of tissue homeostasis and bilirubin metabolism.[16] Another supportive cell type is the hepatic stellate cell, which constitutes the major type of mesenchymal cells in the liver. Hepatic stellate cells are located in the space of Disse, and when they are inactive, their main function is to store vitamin A. Upon liver damage, these cells deposit collagen in the liver tissue and play a central role in the development of hepatic fibrosis.[17,18]

The liver has also many important immunological properties. The majority of the liver blood supply is obtained from the gut through the portal vein, leading to the creation of a complex microenvironment in which parenchymal and immune cells are the first line of defense against pathogens and harmful substances. In a healthy liver, homeostasis is obtained by a fine-tuned cycle of phases of acute inflammation and resolution. In this physiological background, the liver-specific immune cells are able to distinguish between harmless dietary and microbial products while recognizing potential dangerous stimuli such as pathogens and tissue damage.[19]

1.2 Primary liver cancer

The liver is an extremely resilient organ and it acts as one of the first line of defense the body employs against the environment. Therefore, it is not surprising that this organ is subjected to continuous stress and damage, resulting in several types of pathologies. One of these, and the main subject of this thesis, is primary liver cancer (PLC). As of 2020, PLC ranks fifth in terms of incidence and third in terms of number of deaths worldwide when compared to other cancers types. Currently, liver cancer, with a 5-year survival rate of 18%, is one of the most lethal cancers globally, second only to pancreatic cancer.[20] Moreover, when compared to other cancer types, primary liver cancer is one of the few neoplastic diseases characterized by steady increase in incidence and mortality.[21] To put this into perspective, the World Health Organization (WHO) projected liver cancer to cause more than 1 million casualties in 2030 alone.[22]

Primary liver cancer is an umbrella term that comprises diverse cancers arising in the liver characterized by different histological and prognostic features. Among PLCs, the absolute most prevalent cancer type is hepatocellular carcinoma (HCC), accounting for around 80-90% of the total cases of primary liver cancers.[23] The second most common PLC, with 10-20% of total cases, is intrahepatic cholangiocarcinoma (iCCA), where the term ‘’intrahepatic” is commonly used to identify this neoplasm when it arises within the liver. This is of importance because cholangiocarcinomas (CCA) can arise anywhere in the biliary tree and, depending on the anatomical location, they can be categorized into intrahepatic CAA (iCCA, located in intrahepatic bile ducts), perihilar CCA (pCCA, arising outside the liver after the bile duct bifurcation) and distal CCA (dCCA, forming outside and the farthest from the liver) (**Figure 1.3**).[7]

The remaining PLC cases are other, rarer neoplasms, such as fibrolamellar HCC (FLC), mixed HCC-iCCA tumors and hepatoblastoma, the most common liver cancer among children.[24]

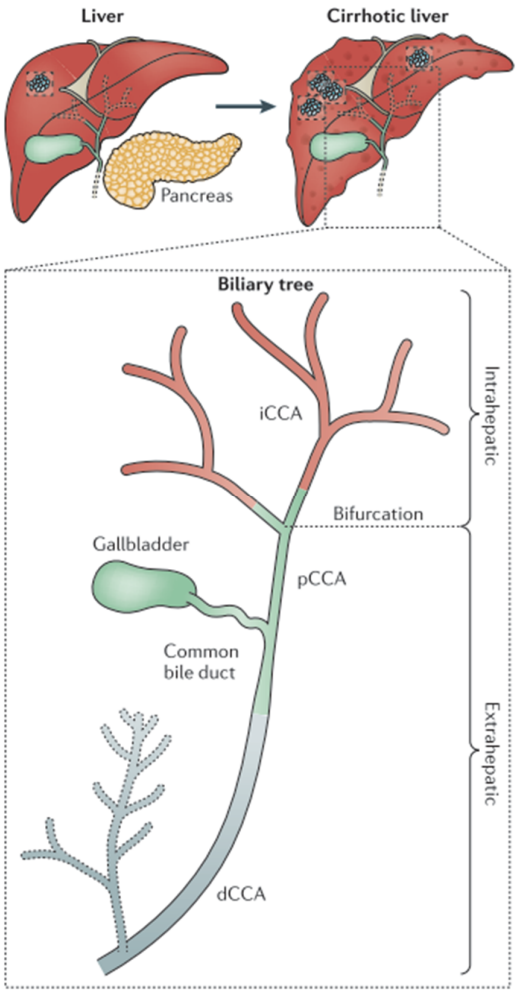

Figure 1.3 | The anatomy of the biliary tree. Depending on where CCA arises, it can be categorized as iCCA, pCCA or dCCA. Modified from Marquardt et al. (2015).[7]

1.2.1 A bird's-eye view on PLC: etiology, ethnicity and geography

When observing PLCs, specifically HCC and iCCA, their common feature is that their development takes decades. For both malignant neoplasms the initial stage is chronic liver damage, characterized by persistent inflammation and compensatory proliferation leading to accumulation of mutations. Over the years, this leads to a profound change in liver architecture, where a pro-oncogenic microenvironment is forming, usually accompanied by cirrhosis. The latter is an irreversible scarring of the liver, and, in 80 to 90% of diagnosed patients, the prerequisite for tumor initiation (**Figure 1.4**).[25,26]

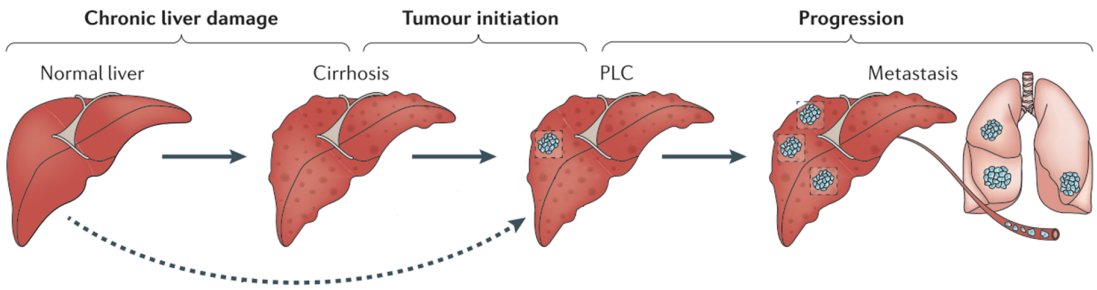

Figure 1.4 | Sequential progression of PLC. In the majority of cases, PLC progression requires cirrhosis to start. Sometimes, tumor initiation can also arise from a normal liver microenvironment. Modified from Marquardt et al. (2015).[7]

1.2.1.1 Virus- and parasite-induced carcinogenesis

Chronic liver damage can be induced by many different risk factors, among which we find predispositions caused by geographical location, ethnicity and gender. When focusing on HCC, hepatotropic viruses, such as hepatitis B virus (HBV) and hepatitis C virus (HCV), play a major role. 50% of worldwide cases of HCC are caused by HBV through its direct oncogenic effect. These cases cluster in areas, such as Asia and sub-Saharan Africa, where this virus is endemic, affecting mostly men with a 3-5 to 1 male to female ratio.[27,28] HCV infection, whose prevention is still hindered by the absence of a vaccine, acts by accelerating the onset of fibrosis and cirrhosis and is also strongly associated with HCC development.[29]

On the other hand, when it comes to iCCA, its gender-related incidence is lower, with a male to female ratio of 1.2-1.5 to 1,[7] with Hispanic ethnicities being the most affected, followed by Asian and Caucasian communities. Primary causes are sclerosing cholangitis, biliary tract inflammation and cysts, but also HBV and HCV infections. Moreover, some regions in Southeast Asia have the highest incidence of iCCA due to infection by hepatobiliary flukes *Opisthorchis viverrini* and *Clonorchis sinensis*, which are able to induce persistent inflammation in the liver and are recognized as *bona fide* carcinogens.[30]

1.2.1.2 NAFLD: an emerging cause of PLC

In the last two centuries, healthcare breakthroughs like vaccination have completely changed the way individuals can avoid contracting diseases. As much as vaccination against

human papillomavirus has been proven effective against the development of cervical cancer, HBV vaccination has been demonstrated to greatly help preventing the development of HCC, especially in the Western world.[31] Despite this, HCC cases in the Western world are still on the rise and recent studies have linked this phenomenon to obesity, metabolic syndrome, type 2 diabetes, sedentary lifestyles, and their resulting complications, such as nonalcoholic fatty liver disease (NAFLD), which is observed in around 24% of the general population.[32] As a matter of fact, a recent meta-analysis of nine studies has reported that in the Western population premorbid obesity is associated with doubling the risk of developing HCC-related mortality.[33]

NAFLD is an umbrella term that describes a spectrum of liver-associated diseases caused independently from alcohol consumption and characterized by an excessive storage of triglycerides in the cytoplasm of hepatocytes.[32] Initially, the liver presents with steatosis (fatty liver), which can progress gradually to extensive fat accumulation in combination with chronic inflammation and hepatocyte injury. This last stage is called nonalcoholic steatohepatitis (NASH) and can occur both in the presence or absence of fibrosis and cirrhosis.[34] Several risk factors, such as obesity, high-caloric intake, metabolic syndrome and age, can increase the risk of progressing through this gradient into more severe NAFLD and therefore also increasing the risk of developing HCC. Nonetheless, it is worth noting that disease progression is also, at least to a certain extent, dynamic and reversible (**Figure 1.5**).[32]

When it comes to mouse models of NAFLD, NASH, and resulting HCC, different diets have been developed to recapitulate the pathophysiology in a stepwise fashion. Of note, choline-deficient high-fat diet (CD-HFD) and western diet (WD, high-fat, high-cholesterol, high-fructose diet) have been reported to successfully model steatosis, fibrosis and obesity.[35,36] Moreover, CD-HFD has been shown to induce HCC development after 12 months with an incidence of 25% while WD has been shown to lead to HCC development after 8 to 13 months with an incidence of 89%.[35,36]

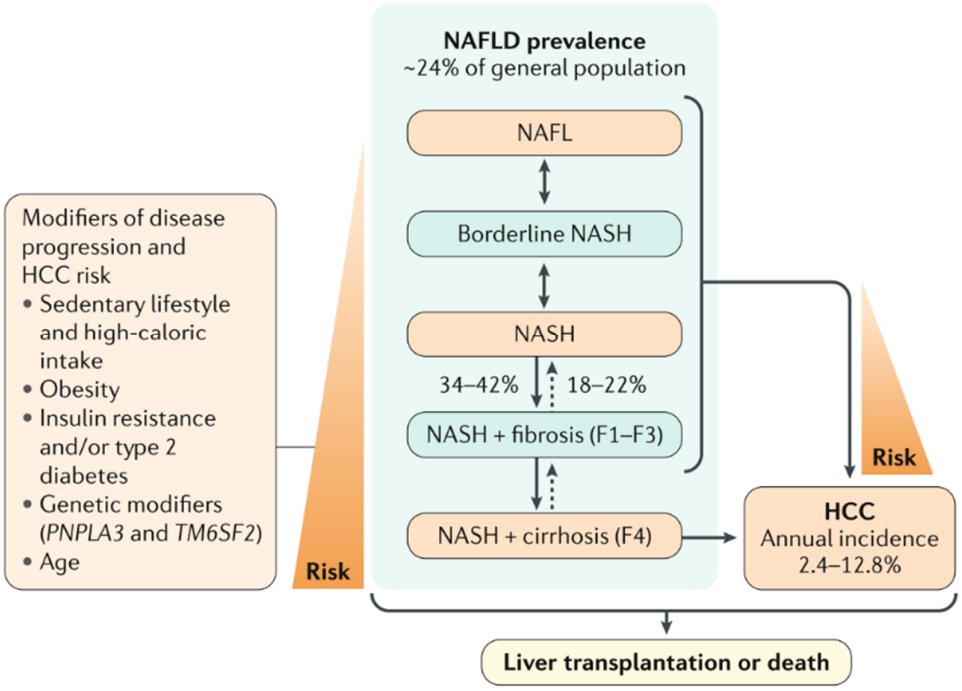

Figure 1.5 | NAFLD and HCC - Risk factors and progression. Unmodified from Anstee et al. (2019).[32]

1.2.2 Cellular reprogramming in liver tissue homeostasis and PLC

As already discussed in section 1.1, the liver is an extremely resilient organ, able to withstand extensive damage and to restore tissue homeostasis. Interestingly, when compared to other tissue types such as skin and blood, liver tissue regeneration was shown not to be driven by stem cell activation but rather by continuous replication of the parenchymal hepatocytic cells due to activation of Hippo/Yap and Wnt/β-Catenin pathways.[37–39] For mammals, proliferation of resident cells or differentiation from dedicated stem cells are among the most common ways of maintaining tissue homeostasis while in other animal kingdoms processes such as dedifferentiation and transdifferentiation are widely employed.[40] Surprisingly, cellular reprogramming and transdifferentiation is also observed in adult mammals in the liver, especially in the case of biliary-specific damage caused by, for example, bile duct ligation (BDL)[41] or toxin-mediated damage.[42] In these cases, hepatocytes transdifferentiate into cholangiocytes, e.g. due to activation of Notch signaling,

in a fashion similar to the one observed in liver development during embryogenesis, in which this pathway regulates differentiation of bipotential progenitor hepatoblasts into either hepatocytes or cholangiocytes.[43]

Given the high degree of cellular plasticity observed in liver development, it is not surprising that the same phenomenon is also observed in pathological settings. When focusing our attention on primary liver neoplasms and their cellular origin, the historical and common assumption is that HCC and iCCA derive from malignant transformation of resident hepatocytes and cholangiocytes,[44] respectively. However, recent genetic lineage tracing studies challenged this view. Guest and colleagues have shown that in the context of cholangiocyte-specific loss of transformation related protein 53 (*Trp53*) coupled with administration of a toxin called thioacetamide (TAA), cholangiocytes are the cell of origins of iCCA.[45] On the other hand, two other studies have demonstrated that hepatocytes can also give rise to iCCA. Sekiya and colleagues have shown this by firstly labeling hepatocytes and then by administrating TAA to the mice, while also showing Notch signaling involvement as pivotal in hepatocytic transdifferention.[46] Around the same time, Fan and colleagues have also confirmed the involvement of Notch signaling using a different model of hepatocytic lineage tracing (**Figure 1.6**).[47]

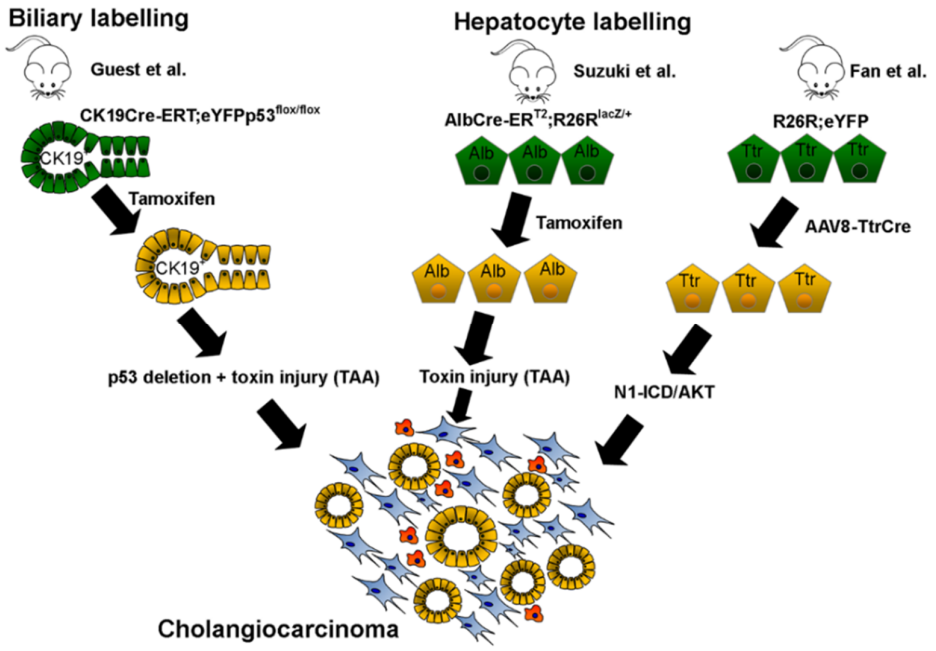

Figure 1.6 | iCCA can originate from both cholangiocyte and hepatocytes. Unmodified from Guest et al. (2017).[37]

The cellular plasticity characterizing the development of HCC and iCCA is not exclusively observed when only investigating the cell of origin of these malignancies, but also in the case of neoplastic tissues. A study from Tschaharganeh and colleagues employed a hydrodynamic tail vein injection (HTVI) mouse model to induce yes-associated protein 1 (*Yap1*) overexpression and *Trp53* loss, resulting in the formation of a progenitor undifferentiated liver tumor possessing the characteristics of neither HCC nor iCCA. Interestingly, the introduction of lineage-specific oncogenic signals in the genetic landscape of this progenitor tumor, such as knockdown of APC, which regulates Wnt signaling, and Notch intracellular domain (NICD) overexpression, which constitutively activates Notch pathway, leads to maturation of the tumor into HCC or iCCA, respectively[48].

Taken all together, these studies demonstrate that the cellular identity of adult liver cells is characterized by a high degree of plasticity and that HCC and iCCA can arise in a different fashion than commonly assumed.

1.2.3 Primary liver cancer treatment

When classifying HCC, the Barcelona Clinic Liver Cancer (BCLC) algorithm is the most widely used staging system which stratifies the disease into five stages by taking into account factors like liver function, performance status and tumor burden.[49] Depending on the stage of the disease, different therapeutic strategies are taken into consideration. Treatments for early stages, when liver function is still preserved and with the presence of fewer than three nodules (less than 3 cm in size), are either tumor resection, ablation, liver transplantation or trans-arterial chemoembolization.[50] More advanced stages, characterized by the presence of several nodules, impaired liver function, and metastasis are treated by systemic therapies, with the employment of first-line drugs like sorafenib, the first Food and Drug Administration (FDA)-approved drug for the treatment of HCC,[51] and second-line drugs like regorafenib, both multi-kinase inhibitors.[50] Systemic drug treatments are often the preferred course of action because diagnosis of HCC can be extremely difficult at early stages, as patients with small and resectable tumors are often asymptomatic and not diagnosed.[50,52] Despite the efforts in HCC treatment, the estimated survival time at later stages and after treatment with systemic therapies is still extremely low at around 1 year.[50] Moreover, several new drugs have failed to give positive results as first- and second-line therapeutic options after phase III clinical trials.[53] Thus, it will be important to identify new drug treatments for liver cancer.

On the other hand, iCCA is staged according to the American Joint Committee on Cancer/Union for International Cancer Control (AJCC/UICC) staging manual, which takes into account features such as vascular and periductal invasion, number of tumors and presence of metastasis.[54] Up to this day, treatment for iCCA is still limited to surgical resection, with recurrence rates up to 80%, and to palliative treatments.[55]

Often, drug treatments for cancer are combined with immunotherapy and cellular therapy, such as immune checkpoint blockade,[56] adoptive cell therapy (ACT) with tumor-infiltrating lymphocytes (TILs),[57] engineered T-cells (CAR T cells and T-cell receptor (TCR) engineered T-cells),[58,59] NK cells therapy[60] and personalized cancer vaccination.[61] In the case of PLC, the liver is a well-known immune tolerant organ, therefore immune checkpoint therapy is a complicated treatment option in this background.[62] As an example, anti-PD-1

therapy is an effective treatment for non-small cell lung cancer (NSCLC)[63] but, in the case of NASH-induced HCC, it was shown to reduce patient survival and stimulate HCC development.[64] Currently, for the treatment of HCC, many combinations of targeted therapies are being tested. Among these, different approaches include the adoption of adoptive cell therapy, CAR T cells and anti-CTLA-4 therapy.[62] More recently, the combination of atezolizumab and bevacizumab was used to treat unresectable HCC.[65] Atezolizumab acts as a programmed cell death-ligand 1 (PD-L1) inhibitor while bevacizumab inhibits vascular endothelial growth factor A (VEGFA). Their combination was shown to improve 12-month patient survival when compared to sorafenib treatment.[65] In conclusion, a promising solution in the future of PLC treatment lies in the identification and functional characterization of reliable biomarkers, whose specific vulnerabilities can ultimately be exploited by personalized medicine.

1.3 Cancer is a genetic disease

Cancer can be described from many different perspectives, but, ultimately, it can be defined as a genetic disease.[66] This perspective is of importance, because the genetic changes promoting neoplastic transformations can be exploited in the clinics for tailored treatments.[67] Such alterations can be either inherited or acquired over the course of lifetime through contact with carcinogenic substances (e.g. tobacco smoke or ultraviolet radiations) or simply by accumulation of unrepaired cell division errors.[66] Advances in sequencing technologies, especially the development of next-generation sequencing (NGS), have provided researchers with tools to better identify specific alterations occurring in cancer. Such genetic alterations can be categorized by the scale in which they affect DNA, from a single nucleotide substitution, to small deletions and insertions, copy number alterations (CNA) and finally to whole chromosomal rearrangements.[68,69]

Such features have been firstly and comprehensively summarized in 2000 by Hanahan and Weinberg and include sustained proliferative signaling, evasion of growth suppressors, invasion and metastasis, replicative immortality, induction of angiogenesis, and resistance to cell death.[70] This list was expanded in 2011 by the addition of hallmarks such as avoidance of immune destruction and deregulation of cellular energetics.[71] Moreover, in the same review

from 2011, the authors identified tumor-promoting inflammation and genome instability as crucial characteristics needed for the acquisition of the aforementioned cancer features.[71] Therefore, genes altered in cancer may be linked to the development of these hallmarks during cancer development and/or progression and, depending on their function, can be classified either as proto-oncogenes or as tumor suppressor genes (TSGs).[72]

1.3.1 Proto-oncogene activation

A proto-oncogene can be defined as a normal regulatory gene whose expression is involved in the regulation of cellular growth or proliferation. Gain-of-function mutations in these genes lead to activation (or conversion) of proto-oncogenes into oncogenes, whose expression leads to transformation of normal cells into tumoral cells by generally inducing aberrant cell proliferation and cellular division.[72]

From a molecular perspective, proto-oncogene activation can be induced in several ways. As an example, point mutations may lead to the translation of a constitutively active mutant of the original protein. One of the most notorious instances of this kind of mutation is observed in the Ras family of proteins, encoded by three genes in humans: *HRAS*, *KRAS,* and *NRAS*. Ras proteins are GTPases acting as molecular switches, whose intracellular signaling function is fulfilled by binding guanosine triphosphate (GTP) in the active state and hydrolyzing it into guanosine diphosphate (GDP), which results in the inactive state. Point mutations in the nucleotide binding domain lead to GDP uncoupling and preferential binding to GTP, inducing a constitutive activation of the Ras protein and therefore leading to an overactivation of the RAF/MEK/ERK kinase cascade and the phosphatidylinositol 3-kinase (PI3K)/protein kinase B (PKB)/AKT pathway, thereby increasing cell proliferation and cell survival.[73,74] In support of the oncogenic role of activating mutations in proto-oncogenes, *KRAS* mutations have been reported in several studies to occur in up to 10-16% of iCCAs.[75,76]

Another example of proto-oncogene activation is commonly observed in the case of c-MYC activation. When compared to Ras proteins mutation, c-MYC activation does not rely on activating mutations but rather on aberrant and deregulated overexpression of the normal protein due to gene amplification or increased messenger ribonucleic acid (mRNA) expression

caused by mutations of the internal ribosomal entry site.[77,78] c-MYC acts as a transcription factor of many genes and was even reported to regulate the expression of 15% of the human genome.[79] c-MYC binds to MYC associated factor X (MAX) to form a MYC-MAX heterodimer, which can then bind to open chromatin and regulate gene expression.[77] Physiologically, c-MYC is a key player involved in promoting cellular proliferation[80], inhibiting cellular differentiation[81] and apoptosis.[82] Neoplasms harboring c-MYC deregulation are associated with poorly differentiated and very aggressive phenotypes. c-MYC deregulation is widely considered to possess *bona fide* oncogenic potential and, in the case of PLC, its amplification is considered to be one of the most frequent gene alterations, observed in 18% of HCCs (TCGA, Firehose Legacy).

1.3.2 Tumor suppressor gene inactivation

On the other hand, when compared to proto-oncogenes, tumor suppressor genes have an opposite role. Their main function is to act as "gatekeepers" by preventing the development of cancer by properly regulating cell cycle, inhibiting proliferation, promoting apoptosis, and initiating DNA repair.[72,83] Moreover, in contrast to proto-oncogenes, TSGs oncogenic potential is caused by their homozygotic deletion, meaning that their mutations are of a recessive nature. Such a deletion can happen both at the genetic or epigenetic level, but also downstream of protein translation at the level of protein subcellular localization and proteosomal degradation.[84]

A textbook example of a TSG, which is often deleted in many different cancers, is tumor protein p53 (*TP53*). Its main function is to prevent tumor development through specific transcriptional activation after being activated by oncogenic stimuli such as oncogene expression, DNA damage, and metabolic dysfunction.[85,86]

1.3.3 Identification of genetic alterations in HCC and iCCA

Given the current advances in sequencing technologies, genetic profiling of PLCs is an essential and powerful tool with a pivotal role in the identification of potential driver genes, pathways and therapeutic targets in order to better characterize and treat liver cancer.[53] The cBioPortal for Cancer Genomics[87] software allows for such analyses by acting as a database

collecting publicly-available human cancer sequencing data. Such datasets include the ones belonging to Memorial Sloan Kettering Cancer Center (MSK), and The Cancer Genome Atlas (TCGA) program.[88]

These tools are able to provide a snapshot of the genetic alterations present in PLCs. More specifically, in the case of iCCA, a cohort comprised of 412 samples was recently added to the cBioPortal database, and identified mutations in *TP53*, *KRAS*, isocitrate dehydrogenase (NADP(+)) 1 (*IDH1*) and cyclin dependent kinase inhibitor 2A (*CDKN2A*) as the most prevalent in this subtype of PLC.[75] On the other hand, when looking at HCC, recent studies have included their own genomic characterization by whole-exome and oncovirome sequencing, ultimately defining the landscape of the most mutated genes – *TP53*, catenin beta 1 (*CTNNB1*) and in the promoter of telomerase reverse transcriptase (*TERT*).[89,90] The TCGA research network also performed genomic characterization of HCC on their own cohort of 363 patient samples not only by the analysis of DNA copy number alterations and somatic mutations but also by integrating the evaluation of DNA methylation and the expression of mRNA, microRNA (miRNA) and protein in the tissue samples. Ultimately, this study proposed an integrated molecular landscape of the genetic alterations in HCC and their interaction through signaling pathways (**Figure 1.7**).[90]

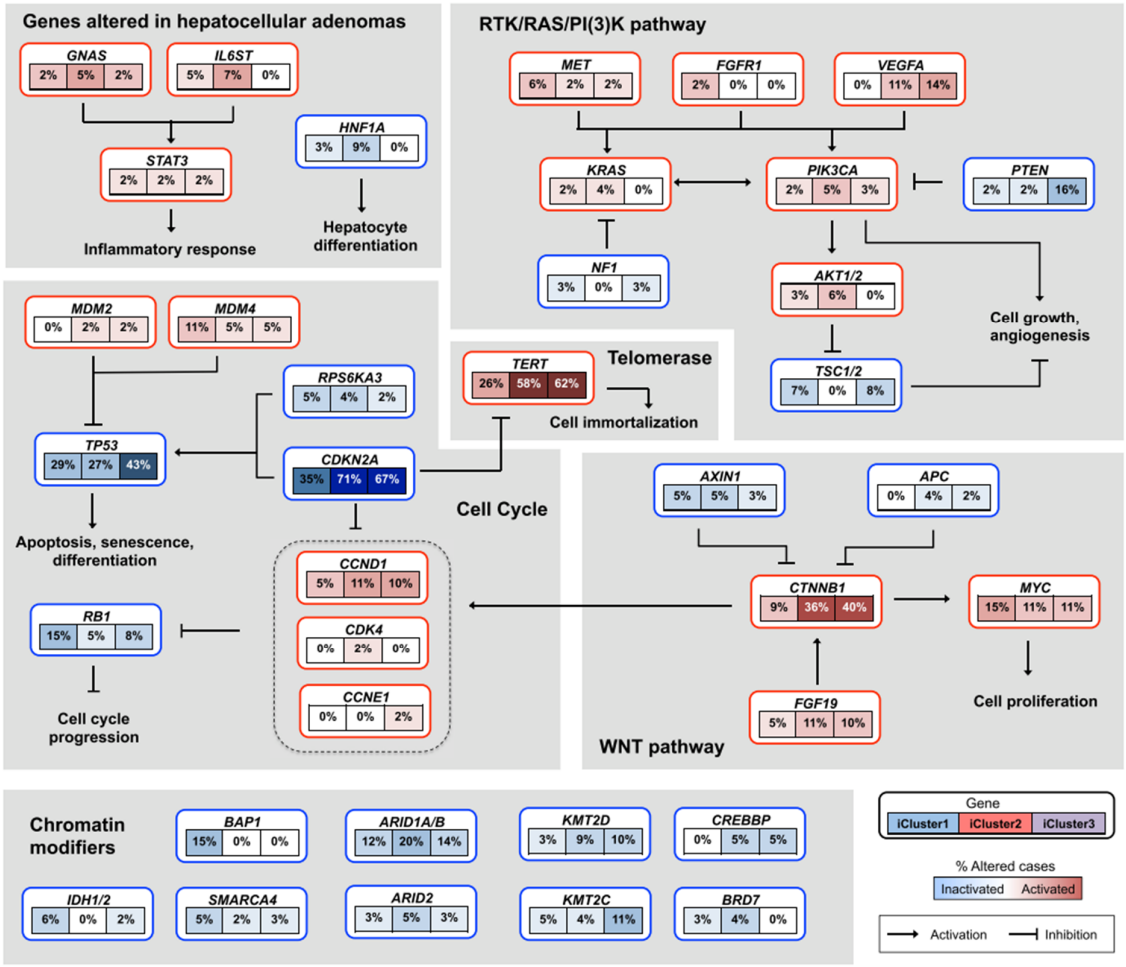

Figure 1.7 | Integrated molecular comparisons of the genetic alterations in HCC and their interaction through signaling pathways. Data was obtained from five different platforms (DNA copy number, DNA methylation, mRNA expression, miRNA expression and protein expression) and was integrated into three clusters corresponding to the three boxes below each gene name and associated with demographic, pathologic and molecular features of the cohort patients. Unmodified from The Cancer Genome Atlas Research Network (2017).[90]

1.3.3.1 Towards precision medicine in cancer

Historically, phase II and III clinical trials have always been drug-centered, revolving around the use of cytotoxic drugs (e.g. sorafenib and regorafenib) to indiscriminately treat neoplastic features shared among many patients.[91] In the last years, the *status quo* of clinical trials has increasingly shifted from drug-centered to patient-centered studies in the pursuit of precision medicine, whose major aim is to provide individualized therapy to cater for specific patient's needs based on the analysis of their biomarkers.[92,93] Such biomarkers are

currently identified mainly by the employment of genomics,[94] often integrated with transcriptomics[95] and proteomics,[96] but also by the analysis of blood-derived cell-free tumor DNA (ctDNA)[97] and blood-derived circulating tumor cells (CTCs).[98]

In the context of precision medicine, a biomarker can be defined as a drug-actionable driver mutation, which is able to initiate and progress tumorigenicity.[99] As an example, BRAF activating mutations are considered driver mutations in melanoma. These mutations are detected in ~50% of melanoma cases and lead to an upregulation of the mitogen-activated protein kinase (MAPK) pathway, leading to aberrant cellular proliferation. Patients with this genetic background are treated with and respond to B-Raf proto-oncogene (BRAF) inhibitor (vemurafenib) treatment.[100] Similarly, other examples include targeting of erb-b2 receptor tyrosine kinase 2 (HER2)-positive metastatic breast cancer with trastuzumab, epidermal growth factor receptor (EGFR)-driven NSCLC with gefitinib or mechanistic target of rapamycin kinase (mTOR) inhibition with temsirolimus in renal cell carcinoma.[101] Oftentimes, tumors initially relapse after an initial response to targeted therapy and a combinatorial approach is required for treatment. For instance, a recent study demonstrated that treating advanced HCC with lenvatinib leads to drug resistance through upregulation of EGFR. Meaningful treatment response was then obtained by combining lenvatinib treatment with gefitinib, a EGFR inhibitor.[102]

Precision medicine is an exponentially growing field, allowing for patient-centered tailoring of drug regimens to target specific driver mutations. In this context, identification and functional characterization of novel drug-actionable genetic drivers is pivotal in the development of targeted cancer therapy.

1.3.3.2 The epigenetic modifier Polybromo 1

Interesting genes often mutated in cancers are the ones encoding for epigenetic modifiers, which are a class of proteins involved in epigenetics, which can be defined as the study of how gene activity can be regulated without direct changes in the DNA sequence.[103,104] These modifiers play an important role in gene expression and the determination of cellular identity through the activation of several epigenetic processes.[105]

When examining proteins involved in nucleosome positioning in PLC, an interesting epigenetic modifier to be taken into consideration is Polybromo 1 (PBRM1), a widely recognized cancer driver mutated in 41% of clear cell renal cell carcinomas (ccRCC).[106] Interestingly, when surveying whole-genome sequencing data of PLC, *PBRM1* is shown to be preferentially mutated in iCCA when compared to HCC (**Figure 1.8**). Moreover, its mutations in iCCA are also reported in literature[107–109] and were even described to be occurring in up to 23.1% of the iCCA[110].

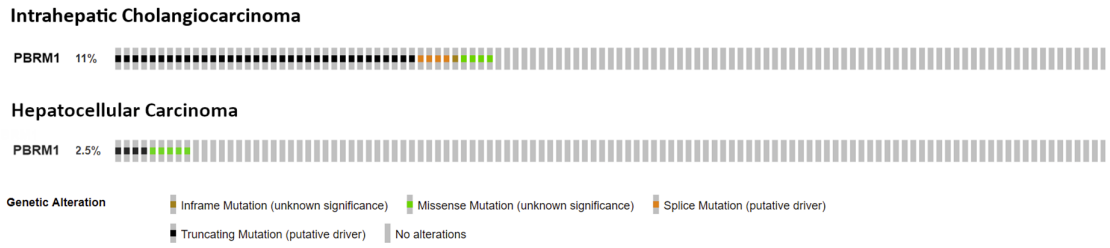

Figure 1.8 | PBRM1 mutations in PLC. Top row shows PBRM1 mutation frequencies in iCCA and bottom row show mutation frequencies in HCC, as obtained from cBioPortal.

PBRM1 belongs to the family of switch/sucrose non-fermenting (SWI/SNF) chromatin remodeling complexes, so-called for being firstly identified in *Saccharomyces cerevisiae*.[111] These complexes are already well-known in cancer research as many of their subunits are often mutated in many neoplasms and are widely considered to be TSGs.[111,112] In mammals, proteins belonging to the SWI/SNF remodelers have central roles in specifying cellular identity and maintaining stem cell pluripotency through a highly orchestrated control of gene expression.[111] More specifically, these complexes have been demonstrated to regulate lineage expression and to have a role in development.[113,114] Moreover, they regulate key target pathways, such as cell cycle progression[115] or context-dependent regulation of MYC activation.[116,117] Furthermore, they are involved in cellular migration and, therefore, in cancer they have been found to be also implicated in metastasis.[118]

SWI/SNF complexes aggregate in massive multi-subunit complexes (~1.14 MDa) and are categorized into BAF and PBAF, with PBRM1 being present exclusively in the latter (**Figure 1.9A**).[119] The function of genes encoding for the SWI/SNF is to interact with nucleosomes, which forces them to slide on or detach from the double-stranded DNA. This mechanism leads to the generation of new sites that can be accessible to gene expression activators or repressors (**Figure 1.9B**).[111] PBRM1 itself is a key element in the PBAF complex because it possesses seven tandem bromodomains that are responsible for interpreting the histone acetylation code.[120]

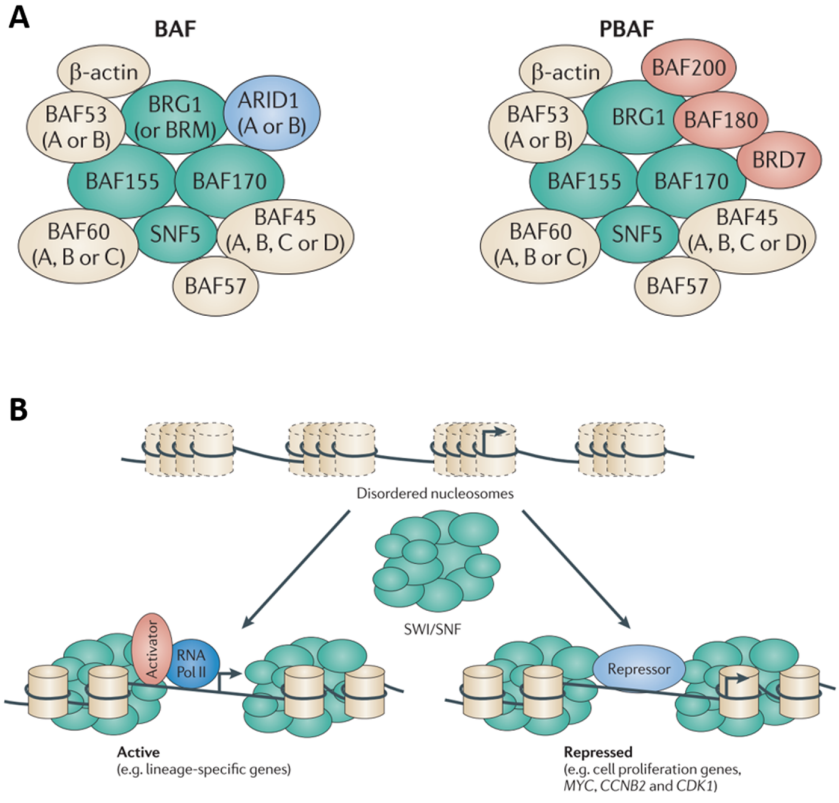

Figure 1.9 | SWI/SNF complexes and their mechanism of action. (A) BAF and PBAF complexes in mammals. PBRM1 (also called BAF180 as in this figure) belongs exclusively in the PBAF complex. **(B)** SWI/SNF complexes function is to interact with nucleosome and slide or eject them from DNA, thus activating or repressing gene expression through the exposure or hindering of genetic material. Modified from Wilson and Roberts (2011).[111]

1.3.3.3 Ribosomal protein S6 kinase A3 is a regulator of the MAPK pathway

Genetic alterations in cancer are potential therapeutic targets and could be exploited by drugs that are already approved by the FDA. As an example, around 50% of melanomas possess activating mutations in *BRAF*. A selective inhibitor called vemurafenib is already used in the clinics to treat patients with this mutation in metastatic melanomas with an initial tumor regression in 81% of them.[121] *BRAF* mutations in melanoma lead to aberrantly high levels of activation of the MAPK pathway. This phenomenon is observed in many cancers and caused by mutations in proteins involved in the regulation of the pathways itself, such as *NRAS* mutations in melanoma and *KRAS* mutations in colorectal adenocarcinoma. Interestingly, in the case of HCC, these mutations appear repeatedly, with low frequency and their functional relevance in the regulation of the RAS/MAPK in this neoplasm is still not well understood. Among these potential targets, ribosomal protein S6 kinase A3 (*RPS6KA3*) is one of the most promising, being mutated in around 4% of HCCs (**Figure 1.10A**).

RPS6KA3 is a kinase protein and an effector of the MAPK pathway, acting downstream of ERK and therefore modulating cellular processes such as cell cycle progression, protein synthesis and cell survival.[74] Interestingly, RPS6KA3 not only acts as a downstream effector of the MAPK pathway, but also as a negative feedback regulator of the pathway itself by phosphorylation and inhibition of SOS.[122] Therefore, inactivating mutations in this gene could relieve the negative feedback regulation and lead to an overactivation of the RAS/MAPK pathway, thus contributing to a subsequent neoplastic transformation (**Figure 1.10B**).

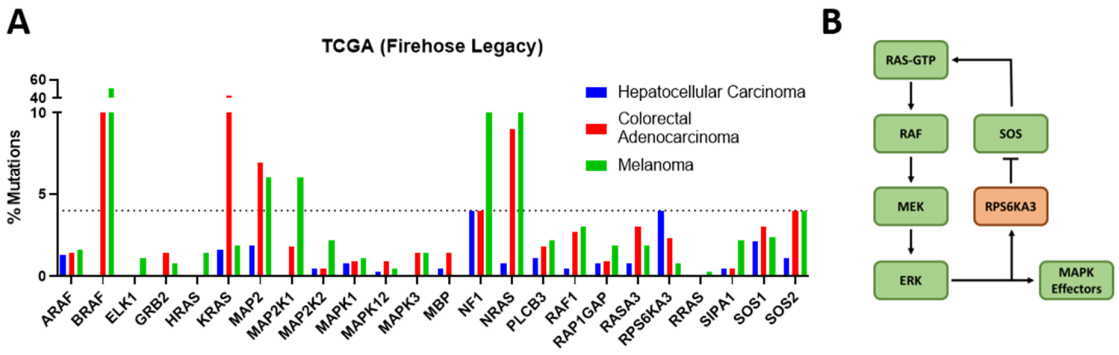

Figure 1.10 | MAPK-associated gene mutations and RPS6KA3 function. (A) The x-axis shows the names of MAPK-associated genes and the y-axis the frequency of their mutations in hepatocellular carcinoma, colorectal adenocarcinoma and melanoma. **(B)** RPS6KA3 acts as an effector of the MAPK pathway and as a negative feedback regulator of the pathway itself via phosphorylation and inhibition of SOS. Data obtained from cBioPortal.[87]

2 Aim of the thesis

The aim of the thesis was to interrogate the heterogenic mutational landscape of PLC for functional characterization of so far unexplored recurring genetic mutations, in both iCCA and HCC.

First, I was investigating the role of PBRM1 in PLC. PBRM1 is preferentially mutated in iCCA and therefore, the aim of the first part of the PhD project was to systematically dissect its role in liver cancer development and cellular plasticity. The molecular function of PBRM1 was probed *in vivo* and *in vitro* in the context of different oncogenic stimuli by HTVI and in NASH background with the use of CD-HFD and WD dietary models. Parallel experiments were also performed *in vitro* with the employment and genetic engineering of human HCC and iCCA cell lines.

The second aim of the project was to clarify the role of loss-of-function mutations in RPS6KA3. Mutations in this protein are exclusively found in HCC and it plays a role as a negative feedback regulator in the RAS/MAPK pathway, therefore could potentially link a genetic alteration to therapeutic intervention. The tumorigenic potential of RPS6KA3 loss in HCC was studied *in vivo* by coupling the protein loss with known oncogenic stimuli. Human and mouse HCC cell lines were engineered to knock-out or overexpress RPS6KA3 in order to investigate its functional role by *in vitro* assays. Human HCC cell lines, as well as their isogenic versions, were employed to generate xenograft tumors and orthotopic transplantations in immunodeficient mice. These models were also used to probe the response to drug treatments.

3 Materials and Methods

3.1 Materials

3.1.1 Chemicals, reagents and mediums

All chemicals were purchased from AppliChem, Carl Roth, Merck Millipore, SERVA and Sigma-Aldrich. Chemicals for bacteria medium preparation (Bacto Tryptone, Bacto Yeast Extract, Bacto Agar, NaCl) was ordered from BD Biosciences. All restriction enzymes used for cloning were purchased from New England Biosciences.

Table 3.1 | Chemicals, reagents and mediums

Name	Catalog No.	Manufacturer
10 mM dNTPs	R0191	Thermo Scientific
10X Cell Lysis Solution	9803S	Cell Signaling Technology
2-Mercaptoethanol	M3148	Thermo Fisher Scientific
Blasticidin S HCl	A1113903	Thermo Fisher Scientific
Bradford reagent	5000006	Bio-Rad
BSA (Protein quantification)	B9000S	New England Biolabs
CellTiter Blue	G8081	Promega
Clarity Western ECL Substrate	170-5060	Bio-Rad Laboratories
Collagenase D	11088866001	Sigma-Aldrich
Dispase II	4942078001	Sigma-Aldrich
DMEM	D6429	Sigma-Aldrich
Doxycycline hyclate	J60579-22	Alfa Aesar
Ethidium bromide	E/P800/03	Thermo Fisher Scientific
FBS	10270-106	Gibco
Herculase II Fusion DNA Polymerase	600677	Agilent Technologies
Hoechst 33342	62249	Thermo Fisher Scientific
Isoflurane	TU 061220	Zoetis
Murine EGF	315-09	PeproTech
NEB Stable Competent E. Coli	C3040	New England Biolabs
NEBuffer 2	B7002	New England Biolabs
NEBuilder HiFi DNA Assembly Master Mix	E2621	New England Biolabs
Page Ruler protein ladder	26616	Thermo Fisher Scientific
PBS	D8537	Sigma-Aldrich
Penicillin-Streptomycin	P0781	Sigma-Aldrich

Pimasertib	S1475	Selleck Chemicals
Polybrene	107689	Sigma-Aldrich
Polyethylenimine (PEI)	23966-1	Polysciences Europe GmbH
Power SYBR Green PCR Master Mix	4367659	Thermo Fisher Scientific
Protease Inhibitor Cocktail	11836170001	Sigma-Aldrich
Proteinase K	3115852001	Sigma-Aldrich
PureCol	5005	CellSystems
Puromycin	BP2956-100	Thermo Fisher Scientific
Q5 DNA Polymerase	M0593L	New England Biolabs
Ravoxertinib	S7554	Selleck Chemicals
Ready Mix Red Taq PCR Reaction Mix	R2523	Sigma-Aldrich
REDTaq ReadyMix PCR Reaction Mix	2648-20RXNR	Sigma-Aldrich
Regorafenib	S1178	Selleck Chemicals
rSAP	M0371L	New England Biolabs
Sorafenib	S7397	Selleck Chemicals
T4 DNA Lligase Buffer	B0202S	New England Biolabs
T4 ligase	M0202M	New England Biolabs
T4 Polynucleotide Kinase (PNK)	M0201	New England Biolabs
T7 Endonuclease I	M0302L	New England Biolabs
Trametinib	S2673	Selleck Chemicals
Trypsin-EDTA Solution	T4049	Sigma-Aldrich
Ulixertinib	S7854	Selleck Chemicals

3.1.2 Consumables

Microcentrifuge tubes, Falcon tubes, serological pipettes, and cell culture plastic ware were purchased from Sarstedt and Eppendorf. Other consumables were obtained from:

Table 3.2 | Consumables

Item	Catalog No.	Manufacturer
BeadBlaster 24	55D1032-15	Biozym
GOT/AST-PIII	9903140	Fujifilm
GPT/ALT-PIII	9903150	Fujifilm
TBIL-PIII	9903240	Fujifilm
Tissue-Tek OCT	4583	Sakura
Virus filters (w/0.45 µm)	514-0063	VWR International

3.1.3 Buffers and solutions composition

Unless specified, all buffers were prepared in water:

Table 3.3 | Buffers and solutions composition

Buffer	Composition
10X MGB (10 mL)	6.7 mL 1 M Tris (pH 8.8) 830 µL 2 M $(NH_4)_2SO_4$ 650 µL 1 M $MgCl_2$
10X SDS-PAGE Running buffer (2 L)	60.6 g 0.25 M Trizma base 288.5 g 1.92 M Glycine 20 g 1% SDS
10X SDS-PAGE Transblot buffer (2 L)	60.8 g 0.25 M Trizma base 288.26 g 1.92 M Glycine
50X Phosphatase Inhibitor	5 mM Sodium fluoride 1 mM Sodium orthovanadate 1 mM Sodium pyrophosphate 1 mM Beta-glycerophosphate
Antigen retrieval buffer pH 6.0 (1 L)	22.94 g tri-sodium citrate 5 mL Tween 20
Crystal violet staining solution (1 L)	0.5g Crystal Violet 27 mL 37% Formaldehyde 100 mL 10X PBS 10 mL Methanol
Genotyping lysis solution (10 mL)	1 mL 10X MGB 500 µL 10% Triton X 100 µL β-Mercaptoethanol 200 µL Proteinase K (20 mg/mL)
Lysis buffer (protein extraction)	10% 10X lysis buffer 10% 10X protease inhibitors 2% 50X phosphatase inhibitors

3.1.4 Antibodies

Table 3.4 | Antibodies

Name	Catalog No.	Manufacturer	Dilution/application
Actin-HRP	A3854	Sigma-Aldrich	1:20000 (WB)
Alexa Fluor 488-DAC	AB2340375	Jackson ImmunoResearch Laboratories	1:250 (IF)
Alexa Fluor 568-DAG	A11058	Invitrogen	1:250 (IF)
Alexa Fluor 594-DAR	A21207	Invitrogen	2 drops/mL (IF)
GFP	ab13970	Abcam	1:500 (IF)
GFP (D5.1)	2956	Cell Signaling Technology	1:1000 (WB)
HNF4a (C-19)	sc-6556	Santa Cruz	1:50 (IF)
KRT19	ab52625	Abcam	1:100 (IF)
PBRM1	A301-591A	Bethyl Laboratories	1:1000 (WB)
p-ERK	4370S	Cell Signaling Technology	1:2000 (WB)
RPS6KA3	5528S	Cell Signaling Technology	1:1000 (WB)
tot-ERK	9102S	Cell Signaling Technology	1:1000 (WB)
Vinculin	V9131-.2ML	Sigma-Aldrich	1:5000 (WB)

3.1.5 Mouse lines

Every mouse strain was housed and controlled daily in the DKFZ animal facilities.

Table 3.5 | Mouse lines

Name	Abbreviation	Origin
B6-Tg(Alb-cre)21Mgn Gt(ROSA)26Sortm1(CAG-rtTA3)Slowe Col1a1tm1(TRE-Pbrm1.622-shRNA)Dkfz	shPbrm1.1	In-house breeding
B6-Tg(Alb-cre)21Mgn Gt(ROSA)26Sortm1(CAG-rtTA3)Slowe Col1a1tm1(TRE-Pbrm1.2875-shRNA)Dkfz	shPbrm1.2	In-house breeding
B6-Tg(Alb-cre)21Mgn Gt(ROSA)26Sortm1(CAG-rtTA3)Slowe Col1atm1(TRE-Renilla.713-shRNA)Dkfz	shRen	In-house breeding
C57BL/6N	C57BL/6N	Janvier
NOD.Cg-Prkdc^{scid} Il2rg^{tm1Wjl}/SzJ (NSG)	NSG	DKFZ animal husbandry

3.1.6 Mouse diets

Table 3.6 | Mouse diets

Name	Specifications	Catalog No.	Manufacturer
CD-HFD	Rodent diet with 45 kcal% fat without added choline	D05010402	Research Diets
Doxycycline	6.25% Doxycycline hyclate	TD.08541	Envigo
WD	Rodent diet with 40 kcal% fat (mostly non trans-fat primex), 20 kcal% fructose and 2% cholesterol	D16022301	Research Diets

3.1.7 Equipment

Table 3.7 | Equipment

Equipment	Type	Manufacturer
Cell culture hood	HERAsafe	Heraus
Centrifuge	Fresco 17	Thermo Scientific
Centrifuge	Megafuge 16R	Thermo Scientific
Dissectoscope	MZ10 F	Leica
Electrophoresis power supply	EV202	Consort
Flow Cytometer	11HT	Guava
Gel and WB developer	FluorChem M	ProteinSimple
Heat block	Dri-Block DB100/4	Techne
Homogenizer	Precellys 24	Bertin Instruments
Light microscope / camera	BX51 / XC30	Olympus
Microplate reader	FLUOstar Omega	BMG LABTECH
Pipette set	Discovery Comfort	HTL Lab Solutions
RT-qPCR system	QuantStudio 3	Thermo Scientific
Scanner	Perfection V370 Photo	Epson
Sonicator	Transsonic T460/H	Elma
Spectrophotometer	NanoDrop ND-100	Thermo Scientific
Thermal cycler	Arktik	Thermo Scientifc
Widefield microscope	Cell Observer	Zeiss

3.1.8 Kits

Table 3.8 | Kits

Name	Catalog No.	Manufacturer
Herculase II Fusion Polymerase Kit	600675	Agilent
Puregene Core Kit A	158445	Qiagen
QIAGEN Plasmid *Plus* Midi Kit	12945	Qiagen
QIAprep Spin Miniprep Kit	27106	Qiagen
QIAquick Gel Extraction Kit	28706X4	Qiagen
QIAQuick PCR Purification Kit	28106	Qiagen
RNeasy Mini Kit	74106	Qiagen
TaqMan Reverse Transcription	N8080234	Applied Biosystems

3.1.9 Plasmids

Table 3.9 | Plasmids

Name	Description	Origin
CMV-SB13	Sleeping beauty transposase expression vector	AG Tschaharganeh, DKFZ, Heidelberg
lentiCRISPR v2	Lentiviral backbone expressing SpCas9 and sgRNA under U6 promoter	Addgene, 52961
MLPe (pMSCV-LTR-miR-E-PGK-Puro-IRES-GFP)	Retroviral vector for shRNA expression	AG Tschaharganeh, DKFZ, Heidelberg
pLenti6.2/V5-DEST	Lentiviral expression vector under CMV promoter	Thermo Fisher, V36820
pLenti6.2/V5-DEST-PBMR1	Lentiviral PBRM1 expression vector under CMV promoter	AG Tschaharganeh, DKFZ, Heidelberg
pLKO.U6-EFs-GFP-P2A-Blasticifin	Lentiviral backbone expressing SpCas9 and sgRNA under U6 promoter	AG Tschaharganeh, DKFZ, Heidelberg
pMD.2G	VSV-G envelope expressing plasmid	Addgene, 12259
pMSCV-puro-mycRSK2wt	Retroviral vector for RPS6KA3 expression	Addgene, 15827
psPAX2	Viral packaging plasmid	Addgene, 12260
pT3-EF1a-HRASG13V	Transposon-based $HRAS^{G13V}$ expression plasmid	AG Tschaharganeh, DKFZ, Heidelberg
pT3-EF1a-KRASG12D	Transposon-based $KRAS^{G12D}$ expression plasmid	AG Tschaharganeh, DKFZ, Heidelberg

pT3-EF1a-MYC	Transposon-based c-MYC expression plasmid	AG Tschaharganeh, DKFZ, Heidelberg
pT3-EF1a-myrAKT	Transposon-based myr-AKT expression plasmid	AG Tschaharganeh, DKFZ, Heidelberg
pT3-EF1a-YAPS127A	Transposon-based YAP^{S127A} expression plasmid	AG Tschaharganeh, DKFZ, Heidelberg
pX330-U6-Chimeric_BB-CBh-hSpCas9	SpCas9 and chimeric guide RNA expression plasmid	Addgene, 42230

3.1.10 Oligonucleotides

All nucleotides were ordered from Sigma-Aldrich.

3.1.10.1 RT-qPCR primers

Table 3.10 | RT-qPCR primers

Name	Sequence (5' – 3')
Afp for (human)	AGGGTGTTTAGAAAACCAGCTACC
Afp rev (human)	TGCAGCAGTCTGAATGTCCG
Alb for (human)	ATGCCCCGGAACTCCTTTTC
Alb rev (human)	CGAAGTTCATCGAGCTTTGGC
Apoe for (human)	CAGCGGAGGTGAAGGACG
Apoe rev (human)	GTGATTGGCCAGTCTGGAGG
Epcam for (human)	GAGATGGGTGAGATGCATAGGG
Epcam rev (human)	AAGATGTCTTCGTCCCACGC
Gapdh for (mouse)	TGTCCGTCGTGGATCTGAC
Gapdh rev (mouse)	CCTGCTTCACCACCTTCTTG
Krt19 for (human)	ACAGCCACTACTACACGACC
Krt19 rev (human)	GTTCCGTCTCAAACTTGGTTCG
Pbrm1 for (mouse)	CTCGTGTGGGCAGAATTGAG
Pbrm1 rev (mouse)	GACAGCACTGCACATTTCCC
RPL41 for (human)	AAACCTCTGCGCCATGAGAG
RPL41 rev (human)	AGCGTCTGGCATTCCATGTT
Sox9 for (human)	CTCTGGAGACTTCTGAACGAGAG
Sox9 rev (human)	GTTCTTCACCGACTTCCTCCG

3.1.10.2 PCR primers

Table 3.11 | PCR primers

Name	Sequence (5’ – 3’)
Col1a1.1	TTCAGACAGTGACTCTTCTGC
Col1a1.2	AATCATCCCAGGTGCACAGCATTGCGG
Col1a1.3	CTTTGAGGGCTCATGAACCTCCCAGG
Cre for	TGCCACGACCAAGTGACAGC
Cre rev	CCAGGTTACGGATATAGTTCATG
mirE-EcoRI rev	TTAGATGAATTCTAGCCCCTTGAAGTCCGAGGCAGTAGGCA
mirE-XhoI for	TACAATACTCGAGAAGGTATATTGCTGTTGACAGTGAGCG
Rosa26.1	AAAGTCGCTCTGAGTTGTTAT
Rosa26.2	GCGAAGAGTTTGTCCTCAACC
Rosa26.3	CCTCCAATTTTACACCTGTTC
sgPbrm1.1 for	AAAGCTGCTTGTAAACTCTGGG
sgPbrm1.1 rev	ATCACATGAAACTGGAGTGTGG
sgPbrm1.2 for	TCCTCTCCACAGGAAAAAGAAG
sgPbrm1.2 rev	GGTGTGAGGAAGCTTGAGAAAT
sgPbrm1.3 for	TACAGGCCTCTCAGGCTTACAT
sgPbrm1.3 rev	CTGAGCCATCTTTCTAGCACCT
sgPbrm1.4 for	TGCATGTCTGAAATTTGTTGTG
sgPbrm1.4 rev	TGGCTGAGACAGGAAAAAGAAT

3.1.10.3 sgRNAs

Table 3.12 | sgRNAs

Name	Sequence (5’ – 3’)
sgGFP	GGGCGAGGAGCTGTTCACCG
sgPbrm1 (human)	GTTGTGGTATAGCTGAGTGC
sgPbrm1.1 (mouse)	GATCAAGGCACACTGGCTGA
sgPbrm1.2 (mouse)	GGTGTCTTCATCAAATCCCA
sgPbrm1.3 (mouse)	GTATGTCTATGTTGAACCTG
sgPbrm1.4 (mouse)	GCAACTGGGCCCTGCAAAGG
sgPten (mouse)	GTTTGTGGTCTGCCAGCTAA
sgRps6ka3.1 (human)	GGCTGATGTGCATTAGCACT
sgRps6ka3.2 (human)	GTCACACATCATGTAAAGGA
sgTrp53 (mouse)	GACCCTGTCACCGAGACCCC

3.1.10.4 Short Hairpin RNA (shRNA)

All the shRNAs in the PhD project were designed with splashRNA internet resource.

Table 3.13 | Short hairpin RNAs (shRNAs)

Name	Sequence (5' – 3')
shPbrm1.1917 (mouse)	TGCTGTTGACAGTGAGCGCGCGAATGAAAATTTTATTCAATAGTGAAGCCAC AGATGTATTGAATAAAATTTTCATTCGCTTGCCTACTGCCTCGGA
shPbrm1.2509 (mouse)	TGCTGTTGACAGTGAGCGACAAGACATAGATTCTATGGTATAGTGAAGCCAC AGATGTATACCATAGAATCTATGTCTTGGTGCCTACTGCCTCGGA
shPbrm1.2575 (mouse)	TGCTGTTGACAGTGAGCGCCCAGAGTCTTTGATCTACAAATAGTGAAGCCAC AGATGTATTTGTAGATCAAAGACTCTGGTTGCCTACTGCCTCGGA
shPbrm1.2875 (mouse)	TGCTGTTGACAGTGAGCGCCAGGAGCATATGTTTGAAGTATAGTGAAGCCAC AGATGTATACTTCAAACATATGCTCCTGATGCCTACTGCCTCGGA
shPbrm1.622 (mouse)	TGCTGTTGACAGTGAGCGCGAGTATGATGATGTTAATCTATAGTGAAGCCAC AGATGTATAGATTAACATCATCATACTCTTGCCTACTGCCTCGGA
shPbrm1.781 (mouse)	TGCTGTTGACAGTGAGCGCGACGATGAAGATGATGACGAATAGTGAAGCCA CAGATGTATTCGTCATCATCTTCATCGTCTTGCCTACTGCCTCGGA
shPbrm1.961 (mouse)	TGCTGTTGACAGTGAGCGCCCAGACTATTATGCAATAATTTAGTGAAGCCACA GATGTAAATTATTGCATAATAGTCTGGATGCCTACTGCCTCGGA
shRen	TGCTGTTGACAGTGAGCGCAGGAATTATAATGCTTATCTATAGTGAAGCCACA GATGTATAGATAAGCATTATAATTCCTATGCCTACTGCCTCGGA
shRps6ka3.1 (mouse)	TGCTGTTGACAGTGAGCGCTGCCGTGAAGATTATTGATAATAGTGAAGCCAC AGATGTATTATCAATAATCTTCACGGCAATGCCTACTGCCTCGGA
shRps6ka3.2 (mouse)	TGCTGTTGACAGTGAGCGCGCCGTGAAGATTATTGATAAATAGTGAAGCCAC AGATGTATTTATCAATAATCTTCACGGCATGCCTACTGCCTCGGA

3.1.11 Internet resources

Table 3.14 | Internet resources

Resource	Website
CHOPCHOP	http://chopchop.cbu.uib.no/
HUGO Gene Nomenclature database	https://www.genenames.org/
Mouse Nomenclature database	http://www.informatics.jax.org/mgihome/nomen/
NEBioCalculator	https://nebiocalculator.neb.com/#!/ligation
PubMed	https://pubmed.ncbi.nlm.nih.gov/
splashRNA	http://splashrna.mskcc.org/

3.1.12 Software

Table 3.15 | Software

Software	Company/Source
Dissectoscope software	Leica Application Suite
Excel 2016	Microsoft
Gimp	Gimp Development Team
Inkscape	Inkscape Project
Microscope software	Olympus cellSens Entry
Mendeley Desktop	Elsevier
PowerPoint 2016	Microsoft
Prism 8	GraphPad
SnapGene	GSL Biotech LLC
Word 2016	Microsoft

3.2 Methods

3.2.1 Animal experiments

All animal experiments were approved by the regional board Karlsruhe, Germany.

3.2.1.1 Hydrodynamic tail-vein injection

For HTVI, 8 weeks old female C57BL/6N mice were injected with 2 mL (corresponding to 10% of body weight) of sterile 0.9% NaCl solution containing the plasmids of interest were injected into the tail vein within 5 to 7 seconds. Depending on the vector used, this technique allowed for liver-specific gene knockouts and/or overexpression by *in vivo* transfection of hepatocytes. The quantities of each plasmid injected for each mouse were as follow: 20 µg for pX330-based plasmid for gene knockout and 10 µg for pT3-EF1a-based plasmids for transposon-mediated gene overexpression. CMV-SB was also injected to allow genomic integration of the transposon and was added in the injection cocktail as 1/5 of the total amount of pT3-EF1a plasmids injected. All injections in the mice were performed by Lena Wendler, Kai Volz and Darjus Tschaharganeh.

3.2.1.2 Subcutaneous cell injection and xenograft measurement

Mice were anesthetized with isoflurane with the following settings for the isoflurane flow: druckluft 1-1.5 bar, flowmeter 2-2.5 L/min, isoflurane vaporizer 3-3.5 vol%, scavenger 45-50. 5 x 10^6 human cells diluted in 100 µL were injected in both flanks. Measurements were performed with a caliper and tumor volume was measured with the following formula: tumor volume = (length x width^2)/2.

3.2.2 Genotyping

1 µL of each sample was used for PCR and 24 µL of master mix was added. The master mix was composed of 12.5 µL RedTaq, 1µL of each primer and water until 24 µL. The samples were then amplified by PCR with the following program: denaturation at 95°C for 5 minutes, 35amplification cycles of 95°C for 30 seconds, 58°C for 30 seconds, 72°C for 1 minute and finally 72°C for 3 minutes. The samples were then directly loaded in 1% agarose gel containing ethidium bromide diluted at 1:20000.

3.2.3 Cell Culture

All cells were cultures at 37°C in 5% CO_2. Cells were cultured in Dulbecco's Modified Eagle Medium (DMEM) supplemented with 10% fetal bovine serum (FBS) and 1% penicillin and streptomycin (DMEM+/+). Mouse cell lines were cultured on collagen-coated plates (PureCol, 0.05 mg/mL). Primary cell cultures were passaged until other contaminating cell types were absent.

3.2.3.1 Primary cell line derivation

Liver tumors were resected with sterile instruments. 10 mg of tissue was mechanically disrupted with a scalpel and incubated in 1-2 mL of 4 mg/mL collagenase IV and dispase medium (dissolved w/v in serum-free DMEM). Cells were then centrifuged at 1500 rpm for 5 minutes, followed by supernatant replacement with fresh DMEM+/+. Once established, the primary cell lines were tested for mycoplasma contamination.

3.2.3.2 Virus production

For lentivirus production, HEK293T cells were plated one day before transfection in 10 cm plates. On day 1, the following transfection mix was prepared: 1 mL DMEM, 8 µg psPAX2, 2.5 µg pMD.2G, 10 µg of vector and 60 µL of polyethylenimine (PEI, 1 µg/µL). The mixture was firstly vortexed for 5 seconds and incubated for 30 minutes at room temperature and then it was added in a dropwise fashion on top of 80%-90% confluent HEK293T cells. 24 hours post-transfections the medium was replaced and 48 hours after transfection viral supernatant was harvested and filtered through 0.45 µm cellulose acetate membrane filters. For retrovirus production HEK293T-gp cells were employed. The same protocol as of lentiviral production was followed, with the exception of the transfection mix: 1 mL DMEM, 2.5 µg pMD.2G, 20 µg of vector and 60 µL of polyethylenimine (PEI, 1 µg/µL).

3.2.3.3 Transduction

The day before transduction, the target cells were plated in 6-well plates with a concentration of 1 x 10^5 cells/well. The next day, the cells were transduced with viral supernatants in the presence of polybrene (4 µg/mL). 2 days after transduction cells were selected with puromycin (2 µg/mL) or blasticidin (10 µg/mL), dependent on the plasmid.

3.2.3.4 Proliferation assay

For proliferation assay, mouse cell lines (7500 cells/well) and human cell lines (30000 cells/well) were seeded in triplicates in 12-well plates. Cells were split before confluency and their concentration was measured with the Guava flow cytometer. The step was repeated until the end of the assay.

3.2.3.5 Cell titer blue assay

Mouse cell lines (500-1000 cells/well) were seeded in sextuplicates in 96-well plates. Measurements were performed by the addition of cell titer blue (20 µL of CTB in 100 µL of DMEM), incubation of the plate at 37°C for 3 hours and measurement of fluorescence with the Omega plate reader (excitation: 560 nm, emission: 590 nm).

3.2.3.6 Colony formation assay

Depending on the growth speed of each cell lines, different cell concentrations were seeded. Mouse cell lines (50-200 cells/well) and human cell lines (750 – 3000 cells/well) were seeded in 12-well plates and let grow up to 10-14 days. Staining was performed by adding 0.5 mL of crystal violet solution to each well and incubating for 30 minutes on an orbital shaker. After removing and washing the plates with water, the plates were scanned at 1200 dpi. Quantification of the assays was performed with the freely available ImageJ plugin "ColonyArea".[123]

3.2.3.7 Preparation of cell lines for subcutaneous injection in NSG mice

For subcutaneous injection of cells in NSG mice, cells were cultured in T175 flasks. Cells were trypsinized, resuspended and counted. The required number of cells was collected, centrifuged at 1000 rpm for 5 minutes. Supernatant was discarded, the pellet was washed with PBS and then centrifuged at 1000 rpm for 5 minutes. Washing steps were repeated three times. Finally, the pellet was diluted in PBS for cell injection in a concentration of 5 x 10^6 cells per 100 µL.

3.2.4 Sample preparation

3.2.4.1 Mouse samples

Mice were sacrificed by cervical dislocation. Immediately after termination, tissue samples were snap-frozen in dry ice for subsequent protein, mRNA and gDNA extraction. The remaining tissue was prepared for IHC. Part of it was embedded and frozen into OCT while the remaining was placed in 4% paraformaldehyde for 3 days at 4°C before being embedded in formalin.

3.2.4.2 Cell samples

Cells were immediately processed to extract protein, mRNA or gDNA. In some cases, cells were harvested and frozen for storage at -20°C in the lysis buffer required for the specific macromolecule extraction (see 383.2.4.3, 3.2.4.5 and 3.2.4.6).

3.2.4.3 Protein extraction

3.2.4.3.1 Initial lysis for cells

Cells were placed on ice and washed with cold PBS. Lysis buffer was added to the plates (100 µL/well in 6-well plates and 500 µL/well in 10 cm dishes). Cells were then scraped and placed in 1.5 mL tubes.

3.2.4.3.2 Initial lysis for tissues

Tissue samples were placed into dry ice and fragments of approximately 3 – 8 mm^3 were snapped with the help of a disposable scalpel. The tissue was homogenized in BeadBlaster tubes. The lysate was then moved to a 1.5 mL tube.

3.2.4.3.3 Common protocol for cells and tissues

After lysate collection, the samples were sonicated 30 seconds, vortexed and placed in ice for 1 minute and then sonicated again for 30 seconds. The tubes were then centrifuged at 13300 rpm for 10 minutes at 4°C. The supernatant was finally transferred in a new 1.5 mL tube.

3.2.4.4 Protein quantification

Proteins were quantified by Bradford Protein Assay. The dye reagent was prepared by diluting 1 part of Bradford reagent concentrate with 4 parts water. For each protein measurement, BSA standards were prepared with the following concentrations: 0, 5, 10, 15, 20 and 25 µg/µL. For each sample to measured, 1 µL of protein was added to 1 mL of diluted Bradford reagent, which was then vortexed and incubated for 10 minutes at room temperature. 150 µL of each standard and sample were then dispensed in triplicates in a 96-well plate and their absorbance was measured at 595 nm with the Omega spectrophotometer. Microsoft Excel was used to generate the standard curve and to extrapolate the samples' protein concentration.

3.2.4.5 mRNA extraction

All mRNA extractions were performed by using the RNeasy Mini Kit (Qiagen).

3.2.4.6 gDNA extraction

All gDNA extractions were performed by using the Puregene Core Kit A (Qiagen).

3.2.4.7 gDNA extraction for genotyping

Tails and ear punches were collected and shipped by the DKFZ animal facility. 200 µL of genotyping lysis solution were added for each sample, which was then incubated overnight at 55°C. Samples were then boiled at 95°C for 15 minutes and centrifuged at 13000 rpm for 5 minutes.

3.2.4.8 Plasmid extraction

All plasmid extractions were performed by following manufacturer specifications from the following kits: QIAprep Spin Miniprep Kit and QIAGEN Plasmid *Plus* Midi Kit (Qiagen).

3.2.5 Western blotting

The samples for Western blotting were prepared as follow: 30 µg of protein (when possible), 4µL of loading buffer and water until 20 µL. The sample were then boiled at 95°C for 5 minutes and loaded into the acrylamide gel. Samples were ran at 100 V until they transitioned from the stacking gel into the running gel and then were ran at 130 V until the front ran out. Transblotting was carried on at 120 V for 1 hour and 30 minutes. Membrane saturation was performed in 5% milk in TBS-T for 1 hour at room temperature. All antibodies were diluted in 5% milk in TBS-T (**Table 3.4**). Diluted primary antibodies were incubated on the membrane at 4°C O/N. Afterwards the blots were washed with TBS-T for 3x 5 minutes. Diluted HRP-conjugated secondary antibodies were incubated on the membrane for 1 hour at room temperature. Next, the blots were washed with TBS-T for 3x 5 minutes. Signal detection was performed after incubating the membranes with ECL solution.

3.2.6 Quantitative reverse transcription PCR (RT-qPCR)

Total RNA was extracted by using the RNeasy Mini Kit (Qiagen) and was then converted in cDNA with TaqMan Reverse Transcription kit with the following program: 25°C for 10 minutes, 37°C for 30 minutes, 95°C for 5 minutes. Next, the DNA was diluted 1:20. 1 µL of diluted cDNA, SYBR Green Master Mix and respective primers (**Table 3.10**). Each RT-qPCR reaction was performed in triplicate by using the QuantStudio 3 system (Thermo Fisher). The expression of the genes taken under examination was normalized to housekeeper gene expression *RPL41* for human samples and *Gapdh* for mouse samples. The ΔCt method was used to calculate the fold change in transcript expression.

3.2.7 Immunofluorescence

On day one, the slides were deparaffinized in xylol for 3x 5 minutes, rehydrated in 96% EtOH for 2x 5 minutes, 70% EtOH 1x 5 minutes and deionized in water for 5 minutes. The slides were then dipped into antigen retrieval buffer and incubated for 8 minutes in the pressure cooker to facilitate antigen retrieval. The slides were then cooled in running water, dried and the tissue area was marked with a hydrophobic pen. The slides were then blocked with 5% BSA in PBS + 0.05% Triton X for 1 hour at room temperature. After discarding the blocking solution, primary antibody was diluted in 5% BSA and added to the slides for incubation at 4°C O/N. On day two the slides were washed with PBS for 3x 5 minutes before adding the secondary antibody diluted in 5% BSA. The incubation lasted 1 hour at room temperature and was carried on in a dark chamber. The slides were then washed with PBS for 3x 5 minutes and incubated with Hoechst solution (Hoechst dye 1:1000 in PBS) for 1 minute at room temperature in the dark. Afterwards slides were embedded in mounting medium and left drying overnight.

3.2.8 Tissue stainings and immunohistochemistry

All H&E stainings and some IHC stainings were performed by the CMCP & wissensch.-histologisches Labor in the Pathology Institute, Heidelberg. All the immunological IHC stainings related to the CD-HFD transgenic mouse model were performed by the histological laboratory of Prof Dr Mathias Heikenwälder (AG Heikenwälder, DKFZ, Heidelberg). Remaining

IHC stainings were also performed by Kai Volz and Luise Butthof (AG Tschaharganeh, DKFZ, Heidelberg).

3.2.9 Cloning

3.2.9.1 sgRNA

For sgRNA cloning, vectors pX330 (pX330-U6-Chimeric_BB-CBh-hSpCas9), lentiCRISPR v2 and pLKO (pLKO.U6-EFs-GFP-P2A-Blasticifin) were used as backbones, respectively for gene knockout in HTVI and *in vitro* experiments. pX330 was digested with BbsI at 37°C while lentiCRISPR v2 was digested with BsmBI at 55°C. Both vectors were incubated for 4-6 hours. 1 µL of rSAP was then added to the digestion mix for 45 minutes at 37°C to dephosphorylate the DNA ends. Afterwards, PCR purification was performed (see 3.2.9.3).

In parallel, the top and bottom sgRNAs were annealed in the following mixture: 0.5 µL PNK, 1 µL T4 ligase buffer, 1µL 10 µM top sgRNA, 1µL 10 µM bottom sgRNA, 6.5 µL water. The oligos were annealed with the following program: 37°C for 30 minutes, 95°C for 5 minutes, -2°C/sec until 85°C, -0.1°C/sec until 25°C, 4°C forever. The annealed product was then diluted 1:250 and used for ligation with the digested vectors (see 3.2.9.4).

3.2.9.2 shRNA

Short hairpin RNAs were designed as 97-mer oligos in the splash RNA website. The oligos were then diluted to a final concentration of 0.05 ng/µL and PCR-amplified in the following mix: 35.75 µL nuclease-free water, 10 µL 5X Her II Pol Buffer, 1.25 µL dNTPs (10 µM), 1.25 µL mirE-XhoI primer, 1.25 µL mire-EcoRI primer, 0.5 µL Herculase II polymerase, 1 µL 97-mer (0.05 ng/µL). PCR program: 95°C for 2 minutes,30 cycles of 95°C for 20 seconds, 54°C for 20 seconds, 72°C for 30 seconds and finally 72°C for 3 minutes. PCR product and vector (pMSCV-LTR-miR-E-PGK-Puro-IRES-GFP) were then digested with EcoRI-HF and XhoI and then ligated.

3.2.9.3 PCR purification

Buffer PB was added five times the amount of the PCR sample volume. The solution was transferred to a QIAquick spin column and centrifuged 1 minute at 13300 rpm. The column was washed with 750 µL of buffer PE and centrifuged 1 minute at 13300 rpm. After discarding the flowthrough, the same centrifugation step was repeated. 30 µL of pre-warmed buffer EB (60°C) were added to the spin column and let incubate for 10 minutes. The column was finally placed in a 1.5 mL tube and centrifuged for 1 minute at 13300 rom to collect the eluate.

3.2.9.4 Ligation

Ligations were performed in the following mix: 0.5 µL T4 ligase, 1 µL 10X T4 ligase buffer, 50 ng digested vector, 1µL of 1:250 diluted annealing product and water until 10 µL. The mix was then incubated for 1 hour at room temperature. 2 µL of the ligated mix was then used for bacterial transformation.

3.2.9.5 Gibson assembly

Overexpression vector pLenti6.2/V5-DEST-Pbrm1 was cloned by Gibson assembly. Briefly, the pLenti6.2/V5-DEST vector was linearized by digestion with BamHI. In parallel, *PBRM1* ORF was designed with 20 bp overlapping overhangs and ordered as dsDNA (gBlock, Integrated DNA Technologies). The fragments were then assembled with Gibson Assembly Master Mix (NEB #E2611) for 1 hour at 50°C. Vector and fragments amounts were determined by using NEBioCalculator.

3.2.9.6 Bacterial transformation

Stable bacteria (C3040, NEB) were generated in-house. For the amount of plasmid product used for transformation, refer to the dedicated section. 25 µL of stable bacteria were mixed with the plasmid and incubated for 10 minutes on ice. Bacteria were then heat-shocked for 45 seconds at 42°C. Samples were then incubated on ice for 3 minutes. Bacteria were then plated on ampicillin-containing agar plates and incubated O/N at 32°C to allow colony formation.

3.2.9.7 Gel extraction

During cloning, specific DNA fragments were extracted from agarose gels in order to be used for downstream cloning. Such extractions were performed by following the specifications on the QIAquick Gel Extraction kit.

3.2.9.8 Sequencing

All sequencing was carried on by Microsynth Seqlab GmbH.

3.2.10 T7 endonuclease assay

3T3 Hras cells transfected with the guide of interested and were harvested at day 3 post-transfection. gDNA was extracted using the Qiagen Puregene Core Kit A. Before starting the assay, primers specific to the guide of interest were designed and tested, so that the alignment temperature would result in a ~350 bp product with a single specific band. The primers used can be found in **Table 3.11**. The bands were amplified in the following reaction mix: 10 µL 5X Q5 Buffer, 2.5 µL 10 µM forward primer, 2.5 µL 10 µM reverse primer, 1 µL 10 mM dNTPs, 0.5 µL Q5 Hot Start DNA Polymerase, 400 ng gDNA and nuclease-free water until 50 µL. The PCR program was as follows: 98°C for 30 seconds, 35 cycles of 98°C for 10 seconds, established annealing temperature for 10 seconds, 72°C for 20 seconds and finally 72°C for 2 minutes. Part of the amplicon was ran on agarose gel to check for specific amplification while the remaining was PCR purified (3.2.9.3). Reannealing mix was prepared with 200 ng of DNA, 2 µL of 10X NEB2 buffer in a total reaction volume of 19 µL. PCR products were then denatured and reannealed to form heteroduplexes with the following program: 95°C for 5 minutes, -2°C/sec until 85°C, -0.1°C/sec until 25°C, 4°C forever. 1 µL of T7 endonuclease 1 was then added to the 10 µL annealing reaction mix and incubated at 37°C for 35 minutes. The final mix was then loaded on an agarose gel to check for the editing.

3.2.11 Statistical analysis

The statistical analysis was performed with GraphPad Prism 8. The type of statistical analysis employed is specified in the figure caption. Significance levels are depicted as *: $p < 0.05$, ** : $p < 0.01$, *** : $p < 0.001$, **** : $p < 0.0001$, n.s.: not significant.

4 Results

4.1 Investigating the role of PBRM1 in liver cancer initiation and cellular plasticity

4.1.1 Generation and validation of transgenic mice harboring doxycycline-responsive expression of shPbrm1

In order to study the function of Pbrm1 in the liver I employed a state-of-the-art transgenic mouse model by crossing Alb-Cre mice with CAGs-LSL-rtTA3 x TGM shPbrm1 mice.[124] This transgenic mouse strain allows liver-specific and doxycycline-dependent short hairpin (shRNA) expression, and thus is ideally suited to study Pbrm1 *in vivo* in a reversible manner. A schematic overview of the transgenes is summarized in **Figure 4.1A**. Briefly, tissue specificity is conferred by inserting CRE recombinase downstream of the albumin (*Alb*) promoter, therefore restricting expression of this protein to liver cells. CRE recognizes the LoxP sites in the *Rosa26* locus and excises the stop codon placed in between the Caggs-promoter and the reverse tetracyclin-transactivator 3 (rtTA3), thereby allowing for expression of rtTA3 along with the red fluorescent reporter mKate2 (**Figure 4.1A**). Administration of doxycycline (Dox), a tetracycline analog, in the diet of the mice leads to rtTA3 binding and activation of the TRE promoter, homed downstream of the *Col1a1* locus, which drives the expression of a shRNA targeting *Pbrm1,* which is fused with GFP (**Figure 4.1B**). As the system is based on RNA interference (RNAi), withdrawal of Dox from the diet shuts down the shRNA expression and permits endogenous re-expression of the target protein.

To check whether the transgene system was exclusively targeted in liver tissue, mice were administered Dox chow for two weeks and liver, kidneys, heart, lungs, guts and stomach were collected. Dissectoscope pictures were taken to check for mKate2 and green fluorescent protein (GFP) expression. As expected, the reporter expression was solely observed in the liver, whereas the other organs did not show any fluorescence signal (**Supplementary Figure 1**).

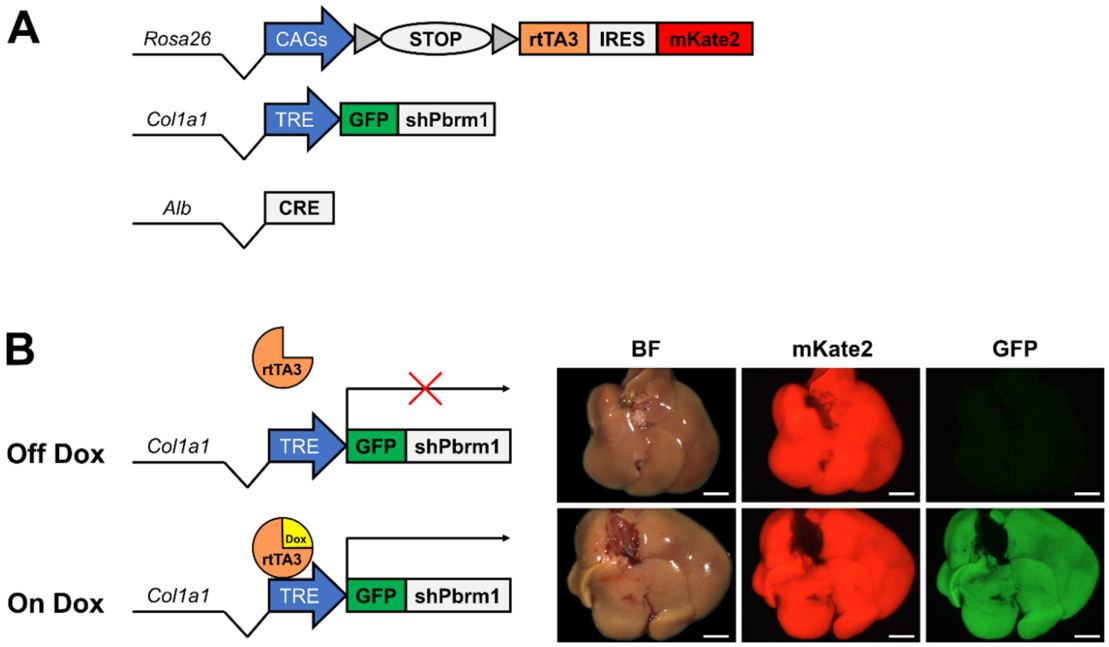

Figure 4.1 | The Alb-Cre x CAGs-LSL-rtTA3 x TGM shPbrm1 strains. (A) Schematic representation of the transgenes present in the strain. **(B)** On the left, the RNAi mechanism of action. On the right, the double fluorescent report system. mKate2 is always expressed in the liver tissue while GFP signal is observed as a reporter only when the short-hairpin is expressed after Dox administration. Scale bar = 5 mm.

4.1.1.1 *In vitro* and *in vivo* validation of shPbrm1-induced knockdown

In order to model PBRM1 loss in this transgenic mouse model, shRNAs were designed, cloned into retroviral expression vectors and tested for their knockdown ability in NIH/3T3 cells under single copy integration conditions (MOI < 0.3). Western blot (WB) analysis four days after Puromycin selection showed strong protein suppression with tested shPbrm1 constructs. When compared to the control shRNA (shRen) targeting *Renilla luciferase*, a gene not present in the mammalian genome, PBRM1 levels were reduced by 92% and up to 100% (**Figure 4.2A**). shPbrm1.622 (shPbrm1.1) and shPbrm1.2875 (shPbrm1.2) were then chosen to generate the two independent transgenic mouse strains. shRNAs were cloned in respective targeting vectors and the targeting vectors in combination with a plasmid encoding FLPe recombinase were then electroporated into murine ES cells containing the *Col1a1* homing cassette and CAGs-LoxP-STOP-LoxP-rtTA3-IRES-mKate2 downstream of the *Rosa26* locus.[124] After successful integration, ES clones were used for blastocyst injection and the resulting chimeric mice were then crossed with Alb-Cre mice to obtain the transgenic mouse strain

outlined in **Figure 4.1A**. A control strain (shRen) was also generated with the same approach, by inserting the non-targeting shRNA (shRen) downstream of the *Col1a1* locus.

In order to validate PBRM1 knockdown *in vivo*, mice from each experimental strain were either kept on normal diet or fed with Dox diet for two weeks. Mice were sacrificed and mRNA as well as proteins were extracted from whole liver lysates. Reverse transcriptase quantitative polymerase chain reaction (RT-qPCR) clearly showed a downregulation in *Pbrm1* mRNA levels in both mouse strains after administration of Dox diet, especially for shPbrm1.1 (**Figure 4.2B**). Accordingly, WB analysis showed PBRM1 protein downregulation for shPbrm1.1 in on Dox conditions as well as expression of GFP, which is coupled to the shRNA expression. However, I could not observe a decrease of PBRM1 protein expression after administration of Dox diet in shPbrm1.2 despite the expression of GFP as a reporter (**Figure 4.2C**). Furthermore, PBRM1 knockdown was validated by immunohistochemistry (IHC), where PBRM1, being normally localized in the nucleus, was downregulated and could not be detected in on Dox shPbrm1.1 mice (**Figure 4.2D**).

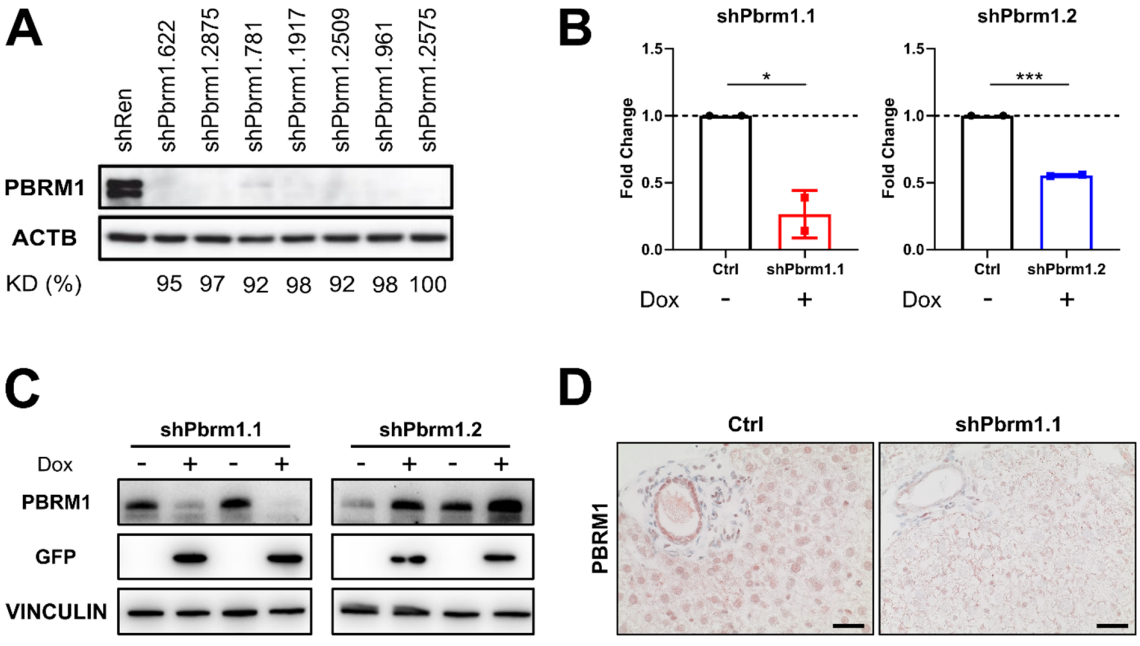

Figure 4.2 | *In vitro* and *in vivo* validation of shPbrm1-induced knockdown. (A) Western blot from NIH/3T3 cell lysates. shRen = non-targeting control. KD = knockdown. Experiment performed by Darjus Tschaharganeh **(B)** RT-qPCR of *Pbrm1* from liver lysates. Student's t-test, N = 2. **(C)** Western blot of liver lysates protein. **(D)** Representative IHC from ShPbrm1.1. Scale bar = 20 µm.

4.1.1.2 shPbrm1 is expressed in both hepatocytes and cholangiocytes

Albumin is a well-known protein largely expressed in liver tissue. Since CRE expression – and the subsequent expression of shRNAs – is dependent on the activity of the *Albumin* promoter, I investigated in which liver cell types the LSL cassette recombined and where the shRNA was expressed in the transgenic mouse model.

For this purpose, both shPbrm1.1 and shPbrm1.2 transgenic mice received Dox diet for two weeks in order to activate shPbrm1 and GFP expression. To evaluate shPbrm1 expression in liver parenchymal cells, I performed double-immunofluorescence staining for cell specific markers (hepatocyte nuclear factor 4 alpha [HNF4A] for hepatocytes and keratin 19 [KRT19] for cholangiocytes) in combination with staining for GFP expression. Analyses of the immunofluorescent signal revealed that GFP, and therefore shPbrm1, was expressed in both hepatocytes and cholangiocytes (**Figure 4.3**). Surprisingly, when assessing the shPbrm1.2 GFP staining, I noticed a mosaic pattern in its expression, with less than 50% of the tissue expressing the reporter. This may in part explain the failed knockdown of PBRM1 protein levels under Dox conditions previously observed in whole liver lysates (**Figure 4.2C**, shPbrm1.2). Considering this phenotype, shPbrm1.2 mice were not employed for further experiments.

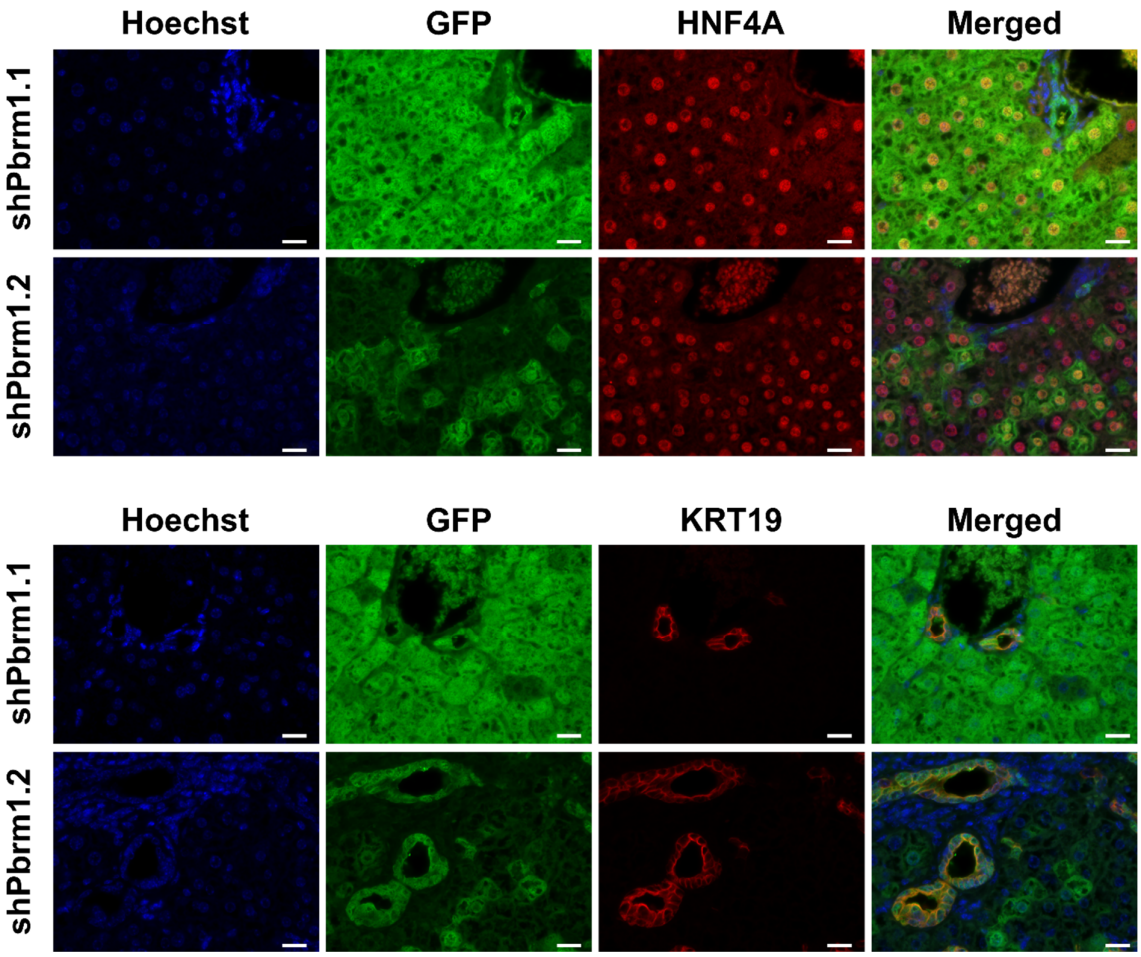

Figure 4.3 | shPbrm1 is expressed in both hepatocytes and cholangiocytes. Top: Double-immunofluorescence showing co-localization of GFP and HNF4A expression in hepatocytes. Bottom: Double-immunofluorescence showing co-localization of GFP and KRT19 expression in cholangiocytes. Scale bar = 20 µm.

4.1.2 PBRM1 loss is not involved in liver cancer plasticity

Overexpression of myristoylated AKT (myr-AKT), a constitutive active form of AKT, was shown to induce HCC formation in mouse liver after 28 weeks.[125] In other reports, it was demonstrated that combining myr-AKT overexpression with *Notch2*[47] or *Yap* overexpression[126] led to the formation of iCCA, meaning that NOTCH and YAP could dictate the phenotypical switch between the two PLCs. Given the high prevalence of PBRM1 mutations in intrahepatic cholangiocarcinomas, I hypothesized that PBRM1 loss could play an analogous role when coupled with myr-AKT overexpression. In order to investigate the role of PBRM1 in this process shPbrm1.1 and shRen mice were injected with a plasmid enabling

sleeping beauty-mediated myr-AKT overexpression (pT3-EF1a-myrAKT) by HTVI and the cohorts were then split into two groups, with one receiving normal diet and the other receiving Dox chow to allow shRNA expression. Of note, HTVI allows only for transfection of hepatocytes and not cholangiocytes *in vivo*. Following HTVI, survival of the cohorts was investigated for up to 12 months. After sacrifice, histological analysis of the liver tissue revealed no tumor development (**Figure 4.4A**).

To further characterize the role of PBRM1 in liver cancer cell plasticity, I investigated PBRM1 loss in an additional transdifferentiation setting. Previous reports showed that HTVI-induced overexpression of YAP coupled with loss of Trp53 in the livers of FVBN mice led to the formation of progenitor tumors within six weeks after the injection.[48] Moreover, adding transposon-mediated expression of NICD in this background switched the phenotype to iCCA.[48] I hypothesized that PBRM1 loss could act as a phenotypical switch as described for NICD overexpression. Thus, shPbrm1.1 mice underwent HTVI with a saline solution cocktail containing plasmids allowing for transposon-mediated YAP overexpression (pT3-EF1a-YAP) and plasmids enabling clustered regularly interspaced short palindromic repeats (CRISPR)/Cas9-mediated *Trp53* knockout (pX330-sgTrp53). Then, the cohort was again split in two, with one group receiving normal chow and the other receiving Dox food and thus knocking down PBRM1. The same experimental setting was performed with shRen mice. After HTVI, I palpated mice weekly to assess tumor formation. After 28 weeks, tumors appeared in all shPbrm1.1 mice on Dox in which PBRM1 was knocked down, but not in shPbrm1.1 mice off Dox and not in shRen mice on and off Dox (**Figure 4.4B**). The liver nodules, being obtained in the on Dox cohort, expressed both reporters mKate2 and GFP. Moreover, histological evaluation of the tumors identified them as HCC, therefore not supporting the original hypothesis of PBRM1 as a molecular switch in cellular differentiation. Additionally, I tried to recapitulate the phenotype by HTVI in wild-type C57BL/6N mice. The same plasmids permitting YAP overexpression and *Trp53* knockout were employed while *Pbrm1* knockout was induced by using pX330-sgPbrm1 plasmids. Mice were palpated weekly and sacrificed at week 28 post-HTVI. Surprisingly, histological analysis of the Yap;sgTrp53;sgPbrm1 cohort showed no tumor formation (**Figure 4.4C**). Together, these data show that PBRM1 does not

affect liver cancer plasticity, but rather its loss collaborates with YAP overexpression and Trp53 loss to give rise to HCC.

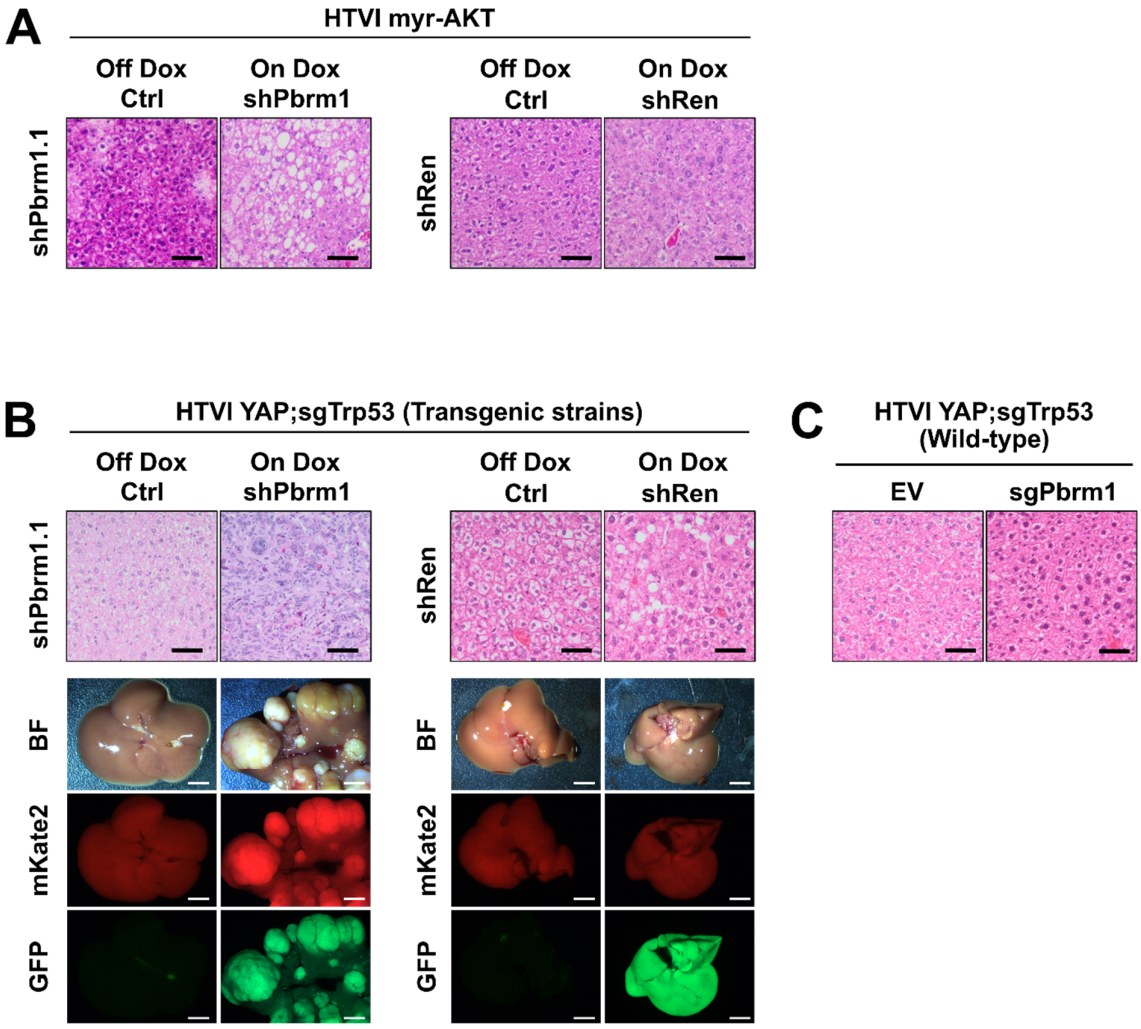

Figure 4.4 | Investigating the role of PBRM1 loss in liver cancer plasticity. (A) Representative H&E staining of the cytoarchitecture in the livers of myr-AKT HTVI in shPbrm1.1 and shRen mice. Scale bar = 100 µm. N = 5. **(B)** Top: representative H&E staining showing the cytoarchitecture of HTVI livers of shPbrm1.1 and shRen mice upon YAP overexpression and TRP53 loss. Scale bar = 100 µm. Bottom: corresponding representative dissectoscope pictures. Scale bar = 5 mm. N = 5. **(C)** Representative H&E staining showing the cytoarchitecture of HTVI livers of wild-type C57BL/6N mice upon YAP overexpression, TRP53 loss and PBRM1 loss. Scale bar = 100 µm. N = 5.

4.1.3 PBRM1 loss does not collaborate with known HCC and iCCA genetic alterations to initiate liver cancer

To further interrogate the function of PBRM1 in liver cancer initiation, CRISPR/Cas9 technology was employed to disrupt endogenous expression of *Pbrm1*. I designed four single guide RNAs (sgRNAs) targeting *Pbrm1* and cloned them in an expression vector (pX330). This vector enables simultaneous expression of the sgRNA and Cas9 nuclease, therefore allowing Cas9-mediated gene editing. The vectors were successively transfected into the murine fibroblast cell line 3T3. Three days after transfection, gDNA was extracted and the *Pbrm1* loci containing the expected mutations were PCR-amplified. To assess the presence of the mutations, the amplicons were digested with T7 endonuclease I, which is able to recognize and digest mismatched DNA, such as the one expected to arise after Cas9-mediated gene editing. T7 endonuclease I-mediated digests obtained from the transfected cells demonstrated that all the four pX330-sgPbrm1 plasmids were able to generate mutations in the *Pbrm1* locus (**Figure 4.5A**).

Guide sgPbrm1.4 (henceforth called sgPbrm1) was finally chosen to abolish endogenous *Pbrm1* expression for *in vivo* HTVI experiments. I investigated the potential outcomes of the association of PBRM1 loss with other oncogenic alterations commonly observed in HCC and iCCA and their combined potential to generate primary liver cancer. I modeled gene loss by employing pX330 plasmids enabling for CRISPR/Cas9-mediated gene knockout, whereas gene overexpression was mediated by the sleeping beauty transposon plasmids containing the gene of interest downstream of the EF1a promoter. The plasmid cocktail solutions were then hydrodynamically tail-vein injected in wild-type C57BL/6N mice, leading to selective *in vivo* transfection of hepatocytes. Plasmids allowing for *Pbrm1* knockout (pX330-sgPbrm1) were coupled with plasmids enabling for either *Pten* knockout (pX330-sgPten), *Myc* overexpression (pT3-EF1a-MYC), *Trp53* knockout (pX330-sgTrp53) or $Kras^{G12D}$ overexpression (pT3-EF1a-KRASG12D). As a control, the same combinations were injected with a pX330 plasmid expressing a non-targeting guide against *GFP* instead of *Pbrm1*. Unfortunately, 12 months after the injection, all the combinations in which PBRM1 was knocked out failed to trigger tumor formation (**Figure 4.5B**). Of note, the cohort in which PTEN was knocked out (with or

without PBRM1 loss) developed hepatocytic steatosis, recapitulating a phenotype previously described.[127] Surprisingly, the Myc;sgGfp cohort was the only one developing liver tumors with full penetrance within 9 to 11 weeks. I attributed this tumorigenic potential to sgGFP off-target effects and pX330 empty vector was successively employed as a control vector for all the following *in vivo* and *in vitro* experiments. Together, these experiments showed that PBRM1 loss does not contribute to initiate liver cancer in cooperation with well-known HCC and iCCA drivers.

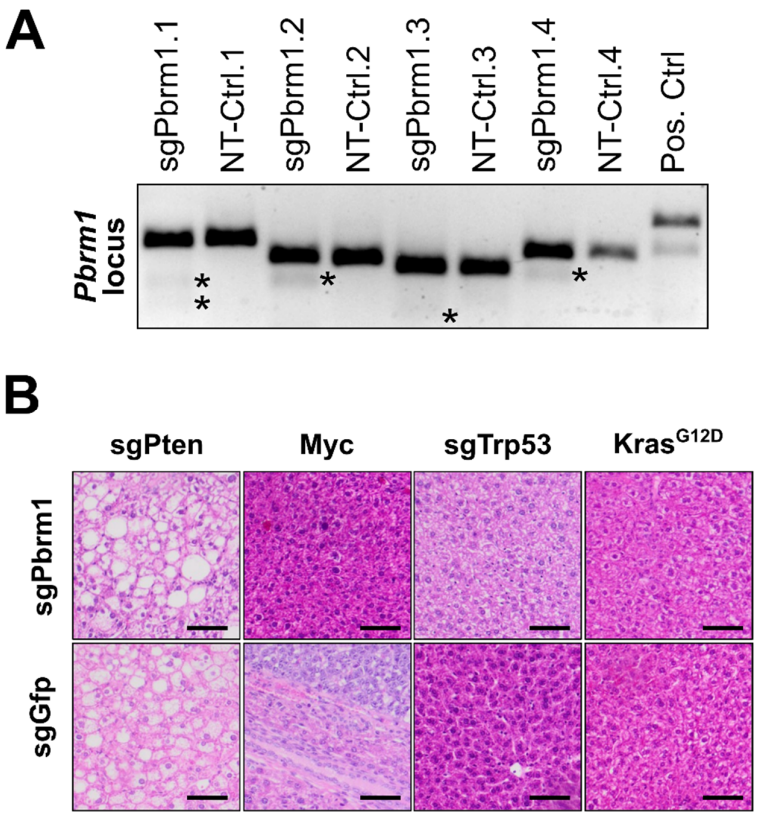

Figure 4.5 | PBRM1 loss does not collaborate with known HCC and iCCA genetic alterations to initiate liver cancer. (A) Agarose gel showing the results of the T7 endonuclease I assay. Asterisks = edited bands. NT = non-transfected, non-edited, negative control. Pos. Ctrl = positive control. **(B)** Representative H&E staining, showing the cytoarchitecture of livers upon HTVI in wild-type mice. Scale bar = 100 µm. N = 5.

4.1.4 Exploring the interplay between PBRM1 loss and CD-HFD-induced NASH

Given that in the western world, NASH is considered to be one of the leading causes involved in the development of HCC, I investigated whether PBRM1 loss in NASH background could be linked to an increased tumorigenicity or to a phenotypical switch in determining the development of a specific type of PLC. To do so, I employed the transgenic mouse strains and coupled them with CD-HFD administration as a dietary model inducing NASH and HCC after 12 months.

4.1.4.1 PBRM1 loss in not involved in tumor initiation and cellular plasticity in CD-HFD-fed mice

Both shPbrm1.1 and shRen mice were administered CD-HFD. For each strain, half of the cohort received a supplement of Dox water in order to activate the expression of their respective shRNAs while the other half was kept exclusively on CD-HFD as a control. Six mice per cohort were sacrificed after 6 months since the beginning of the treatment, while the remaining were sacrificed after 12 months. As shown in **Figure 4.6A**, tumor incidence in both strains after 12 months (5.3% to 15.8%) was lower than the previously reported of 25%.[35] Histological evaluation of the tumors categorized them as HCC and no significant difference in tumor incidence between on Dox and off Dox conditions, both with shPbrm1.1 and shRen mice. Together, these data indicate that PBRM1 loss in CD-HFD-induced NASH background is not implicated in increased tumorigenicity and liver cancer plasticity.

The long-term effects of CD-HFD in shPbrm1.1 and shRen strains were also studied by assessing body weight over time. This parameter was measured monthly from week 8 after the start of the diet. For both strains, mice who did not receive Dox in their chow gained significantly more weight when compared to mice expressing the shRNA, therefore such an increase can be attributed to Dox-dependent effects (**Figure 4.6B**). I next investigated liver damage and impaired liver function, expecting that the loss of PBRM1 would affect these parameters. Therefore, I measured the serum levels of surrogate liver impairment biomarkers such as liver transaminases alanine aminotransferase (ALT) and aspartate transaminase (AST), as well as of bilirubin. Serum was collected from the mice every two months. When looking

at ALT and AST levels, liver damage increased over the course of the 12 months for all the conditions under examination. Surprisingly, when looking at ALT levels in shPbrm1.1 mice, PBRM1 knockdown at month 6 significantly reduces the transaminase levels when compared to the control, implying that the PBRM1 could confer a protective effect against liver damage during NASH development. Conversely, the opposite was observed after 2 months of diet when analyzing AST levels, suggesting that PBRM1 might play context-dependent roles during different time-points of NASH development (**Figure 4.6C**).

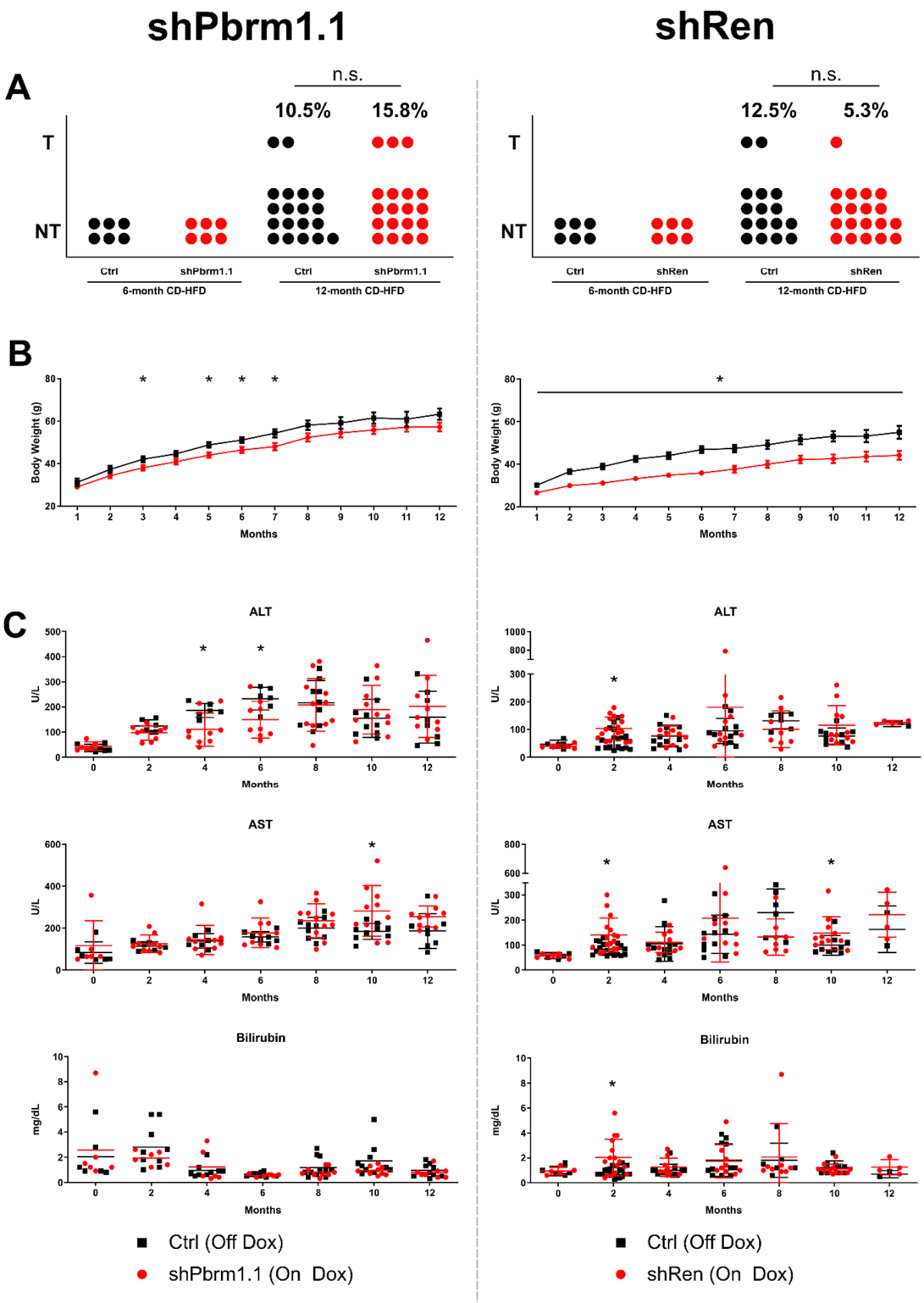

Figure 4.6 | Tumorigenicity and liver damage in CD-HFD-fed mice. Left column shows data related to ShPbrm1.1 while right column shows data related to Strain Ctrl. **(A)** Tumor incidence after 6 and 12 months since the start of CD-HFD administration. Each symbol represents a single mouse. Chi-squared test. **(B)** Body weight. Bars = SEM. Student's t-test. **(C)** ALT, AST and bilirubin serum levels. Bars = SD. Student's t-test.

4.1.4.2 Loss of PBRM1 is not involved in reshaping the microenvironment in CD-HFD-fed mice

In the case of CD-HFD, the interplay between hepatocytes and immune cells, more specifically $CD8^+$ and natural killer T (NKT) cells, is crucial in the transition of NASH into HCC.[35] In order to determine whether PBRM1 loss has an impact on the immunological landscape, liver sections of the CD-HFD cohort from both shPbrm1.1 and shRen strains were stained with several markers of immune cells. The markers investigated were B220 for B cells, CD3 for all T cells, CD4 for T helper cells, monocytes, macrophages and dendritic cells, MHCII for antigen-presenting cells, F4/80 for Kupffer cells and NKp46 for NK cells. After histological quantification in liver parenchyma, $B220^+$ cell infiltration appeared to be significantly higher after 12 months of CD-HFD when PBRM1 was knocked down (**Figure 4.7A**). The quantification of other immunological marker stainings showed no statistically significant change in the amount of immune cell infiltrates (data not shown). Overall, PBRM1 loss did not have a significant role in reshaping the immune microenvironment in the parenchyma of livers after 6 and 12 months of CD-HFD. Other than looking at immune cells, the samples were also stained for cleaved Caspase-3, Ki67 and by Sirius Red staining to investigate changes in apoptosis, hepatocytic proliferation and fibrosis, respectively. Also in this case, no significant changes were detected except for an increased intrinsic apoptosis with PBRM1 knockdown after 6 months of CD-HFD (**Figure 4.7B**). Together, the data showed that PBRM1 loss in CD-HFD-induced HCC model does not have a significant role in reshaping the microenvironment from the point of view of immunological infiltrate, apoptosis, hepatocytic proliferation and fibrosis.

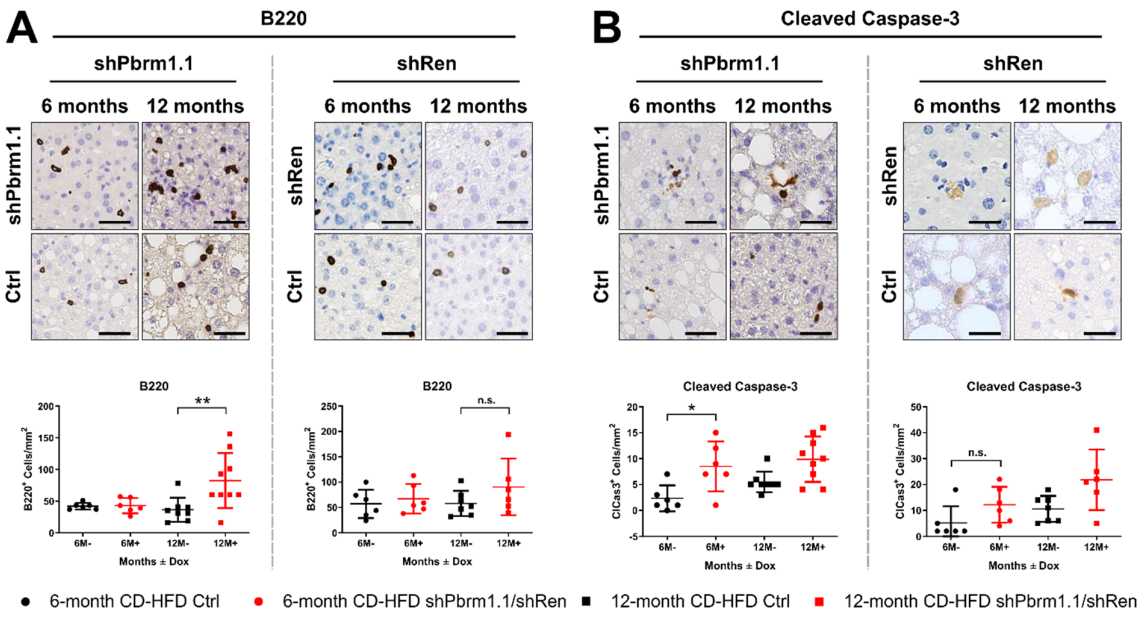

Figure 4.7 | Histological characterization of CD-HFD-fed mice. Pictures show immunological stainings after 6 and 12 months of CD-HFD administration in shPbrm1.1 and shRen mice **(A)** Representative IHC and quantification of B220⁺ cells. **(B)** Representative IHC and quantification of cleaved Caspase-3⁺ cells. Bars = SD. Ordinary one-way ANOVA (multiple comparisons). N ≥ 6.

4.1.4.3 *In vitro* assays of primary cell lines derived by CD-HFD-fed mice show no functional differences upon PBRM1 loss

I next characterized the tumors obtained from the CD-HFD-fed shPbrm1 strain cohort on Dox. As stated previously, the tumors were classified as HCCs after histological evaluation of H&E stainings. In support of this, the tumors stained positively for HNF4A, a marker for hepatocytic lineage, and negatively for KRT19, a marker for cholangiocytic differentiation (**Figure 4.8A**). Conversely, when staining for GFP, I unexpectedly observed that the reporter was mosaically expressed in the parenchyma and was completely absent within all of the tumors. Since GFP expression is coupled with shPbrm1 expression, this meant that over time transgene expression was silenced *in vivo* (**Figure 4.8A-B**). To better characterize this phenotype, I established two different primary cell lines (#1 and #2) from two tumors obtained from shPbrm1.1 mice after 12 months of CD-HFD coupled with Dox water (**Figure 4.8A**, cell lines #1 and #2). Both primary cell lines were established in Dox medium and, interestingly, when analyzing them by flow cytometry, at least 90% of the cell population expressed GFP. This meant that the gene silencing observed in the tumors *in vivo* was

reversed when transferring the cells *in vitro* (**Figure 4.8C**). I attributed this phenomenon to a decreased bioavailability of Dox *in vivo* due to a disrupted cytoarchitecture in NASH tissues. To check whether the transgene system was still functional in the established primary cell lines, both were cultured for nine days in Dox medium to keep PBRM1 knocked down and in normal medium to allow for shPbrm1 silencing and re-expression of PBRM1. In both cell lines, removing Dox from the medium allowed for PBRM1 re-expression and GFP disappearance, meaning that the transgene system was indeed still functional, at least *in vitro* (**Figure 4.8D**). These cell lines were then used in cell culture assays to probe for functional effects of PBRM1 expression on cell proliferation. Proliferation assay was employed to analyze long-term (40 days) proliferative potential. Cell titer blue assay was used as a parallel assay to assess a shorter term proliferation potential (13 days). Both of them showed that re-expressing PBRM1 did not affect cellular proliferation (**Figure 4.8E-F**). To exclude silencing of the transgene system as a bias in the assays, the percentage of GFP^+ cells was also measured by flow cytometry over time, showing that the transgene system was still functional up to 40 days (**Figure 4.8E**).

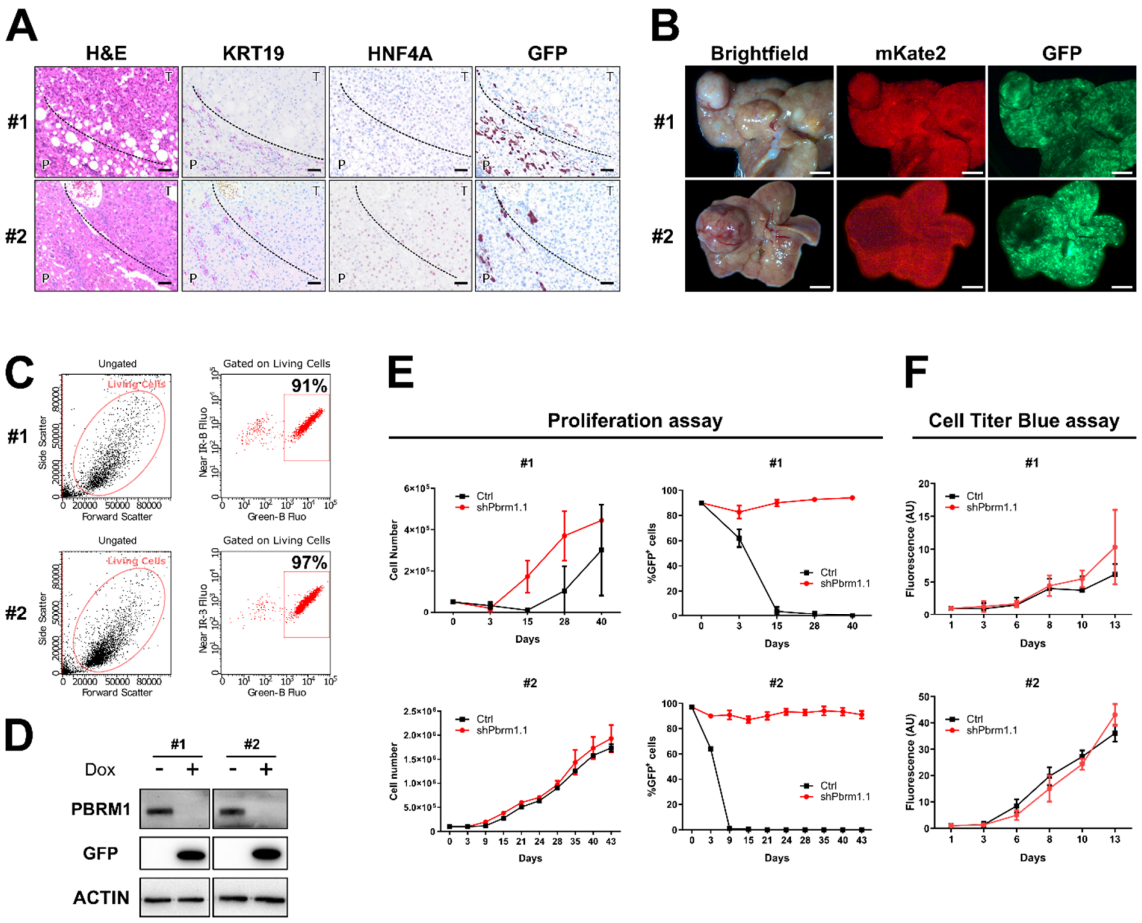

Figure 4.8 | *In vitro* functional assays of primary cell lines derived by CD-HFD-fed mice. (A) H&E and IHC stainings obtained from two livers in the CD-HFD shPbrm1.1 on Dox cohort. Dashed lines delineate the separation between liver parenchyma (P) and primary liver tumor (T). Scale bar = 100 µm **(B)** Dissectoscope pictures depicting two livers from shPbrm1.1 12-month CD-HFD On Dox cohort. Scale bar = 5 mm. **(C)** Flow cytometry analysis of primary cell lines obtained from tumor #1 and #2. **(D)** Western blot showing PBRM1 re-expression after withdrawing Dox from cell culture medium. **(E)** Proliferation assay. Percentage of GFP^+ cells over time is shown on the right. **(F)** Cell Titer Blue assay. Bars = SD. N = 1.

4.1.4.4 Sequencing of drug-targetable genomic alterations identify potential targets collaborating with PBRM1 loss in CD-HFD-induced tumor initiation

In order to investigate the mutational landscape of CD-HFD-induced HCC samples and identify potential partners collaborating with PBRM1 loss to drive tumor initiation, genomic DNA was extracted from two control (off Dox) tumors and three shPbrm1.1 (on Dox) tumors along with gDNA from the previously established cell lines. The gDNA was then sequenced with MSK-IMPACT, an oncopanel intended to identify the presence of drug-targetable

mutations. An activating mutation in HRAS (*Hras*^{G13V}) was observed in a tumor (#2) and primary cell line (#1) with PBRM1 knockdown but not in control samples with normal PBRM1 expression, leading to the hypothesis that HRAS^{G13V} could be a potential candidate co-operating with PBRM1 loss leading to tumor initiation (**Figure 4.9A**). To test this hypothesis, HTVI experiments were performed by injecting plasmids allowing for PBRM1 knockout (pX330-sgPbrm1) and transposon-mediated mutated HRAS^{G13V} overexpression (pT3-EF1a-HRASG13V). Following HTVI, mice were palpated daily and finally, once the cohort was sacrificed after 28 weeks, no tumor was observed (**Figure 4.9B**). Together, these data demonstrated that NASH-induced damage gives rise to a highly mutationally heterogeneous background. Unfortunately, modeling one of these mutations by HTVI in wild-type mice did not recapitulate tumor initiation as observed in CF-HFD-fed mice.

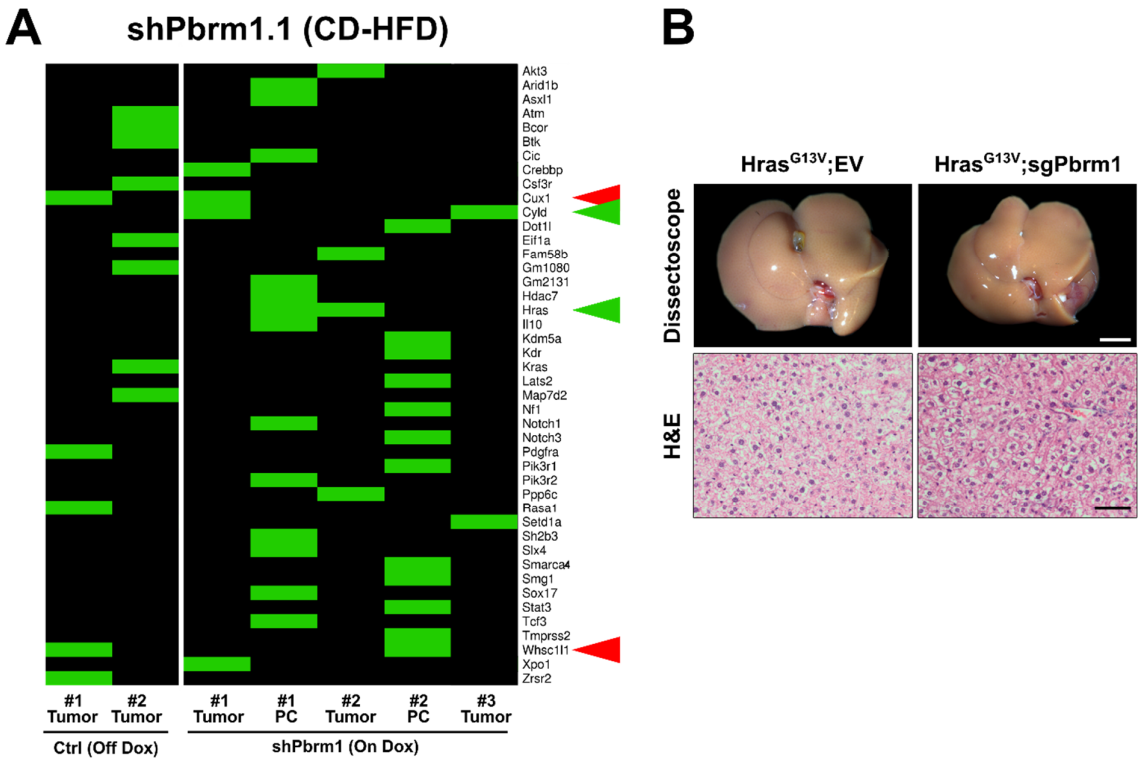

Figure 4.9 | Overview of genomic alterations in CD-HFD-derived HCCs. (A) Heatmap showing mutational hits obtained from the MSK-IMPACT oncopanel. Red arrows indicate reoccurring mutations in both Ctrl and shPbrm1 samples. Green arrows indicate reoccurring mutations exclusively in shPbrm1 samples. PC = Primary cell lines. Equal number = primary cells from respective tumor. **(B)** Dissectoscope and H&E staining pictures from the Hras^{G13V};sgPbrm1 HTVI experiments. Scale bar (white) = 5 mm. Scale bar (black) = 100 µm.

4.1.5 Exploring tumorigenicity and liver damage in WD-induced NASH coupled with PBRM1 loss

In parallel to CD-HFD, western diet (WD) was also used as an additional model of NASH-induced HCC. Previous reports demonstrated that administering WD to DIAMOND mice led to NASH and HCC development with 89% incidence within 8-13 months.[36] Analogous to CD-HFD, I investigated whether loss of PBRM1 in this background could lead to a shift in tumorigenicity or a lineage differentiation from HCC into iCCA. To this end, both shPbrm1.1 and shRen mice were administered WD. For each strain, half of the cohort received a supplement of Dox water in order to activate the expression of their respective shRNAs while the other half was kept exclusively on WD as a control. Mice were terminated after 12 months. As shown in **Figure 4.10A**, tumor incidence in both strains after 12 months (0% to 15.8%) was lower than the previously reported of 89%, probably due to inter-strain differences. Histological evaluation of the tumors also categorized them as HCC and showed no significant difference in tumor incidence between on Dox and off Dox conditions, for both shPbrm1.1 and shRen mice. Together, these data indicate that PBRM1 loss in combination with WD-induced NASH is not implicated in increasing tumorigenicity and liver cancer plasticity. Also in this cohort, the long-term effects of WD in shPbrm1.1 and shRen strains were studied by assaying body weight over time. This parameter was measured monthly from week 4 after the start of the diet. Also with WD and for both strains, mice who did not receive Dox in their chow gained significantly more weight when compared to mice expressing the shRNA, therefore such an increase can be attributed to Dox-dependent effects (**Figure 4.10B**). I then measured the serum levels of ALT and AST, as well as of bilirubin. Serum was collected from the mice every two months. When looking at ALT and AST levels, liver damage increased over the course of the 12 months for all the conditions under examination. Interestingly, also in the case of WD, when looking at ALT and AST levels in shPbrm1.1 mice, PBRM1 knockdown at month 4 significantly reduces the transaminases levels when compared to the off Dox control, implying that PBRM1 could confer a protective effect against liver damage during NASH development (**Figure 4.10C**). Also in this experimental setting, the results showed that in the background of WD-induced NASH, PBRM1 loss failed to increase tumor initiation or act as molecular switch in liver cancer differentiation.

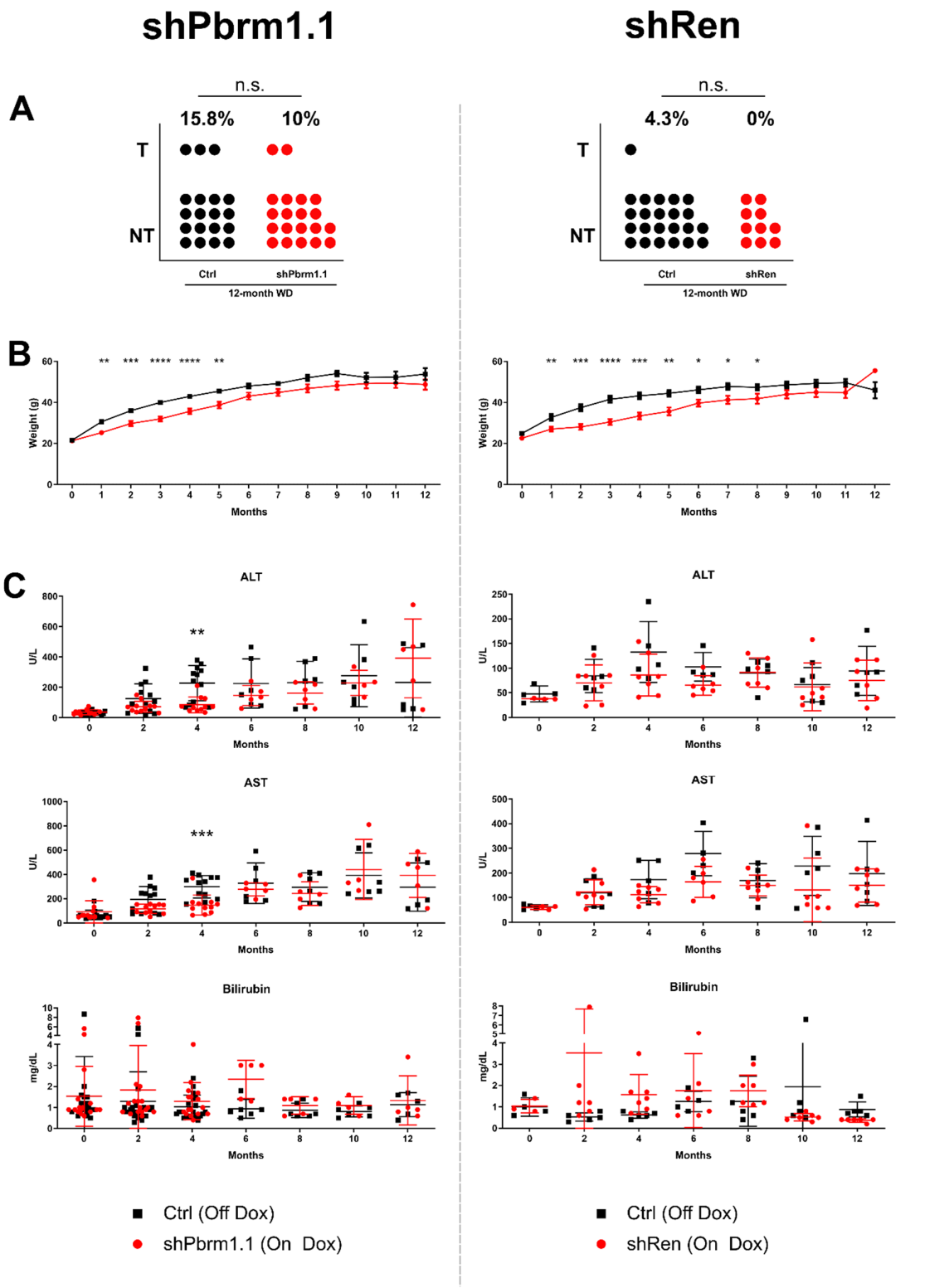

Figure 4.10 | Tumorigenicity and liver damage in WD-fed mice. Left column shows data related to ShPbrm1.1 while right column shows data related to Strain Ctrl. **(A)** Tumor incidence after 12 months since the beginning of WD administration. Each circle represents a single mouse. Chi-squared test. **(B)** Body weight. Bars = SEM. Student's t-test. **(C)** ALT, AST and bilirubin serum levels. Bars = SD. Student's t-test.

4.1.6 PBRM1 expression does not have functional implications in human isogenic cell lines

Additionally to the murine experiments, I investigated the functional role of PBRM1 *in vitro* in human HCC and iCCA cell lines. The aim of these experiments was to observe whether the manipulation of PBRM1 expression in human cell lines would lead to a change in phenotype, both from the perspective of cellular proliferation and cellular identity. First, I stratified a panel of human HCC and iCCA cell lines by PBRM1 expression (**Figure 4.11A**). I selected SNU-182 and HepG2 as HCC cell lines, which strongly express PBRM1 in order to knock it out and HuH-28 as iCCA cell line in which PBRM1 is not expressed in order to overexpress it. This choice was in line with the project's original hypothesis, stemmed from the observation that PBRM1 is normally present in HCC but not in iCCA. A sgRNA against human *Pbrm1* was designed with CHOPCHOP, cloned into a lentiviral vector (lentiCRISPR v2) and transduced into SNU-182 and HepG2 cells to knockout *Pbrm1*. PBRM1 overexpression was obtained by cloning human *PBRM1* open reading frame (ORF) into a lentiviral overexpression vector (pLenti6.2/V5-DEST) and then by transducing it into HuH-28 cells. After antibiotic selection, successful knockout and overexpression was tested via western blot analysis in the resulting isogenic cell lines (**Figure 4.11B**).

The isogenic cell lines were then used for proliferation assays. PBRM1 knockout in SNU-182 cells significantly slowed down cell proliferation while HepG2 and HuH-28 cells showed no difference in proliferation upon manipulation of PBRM1 expression (**Figure 4.11C**). Cellular growth was also investigated in parallel by colony formation assay. SNU-182 proliferation showed the same pattern as in the proliferation assay, while HepG2 growth was higher when PBRM1 was knocked out (**Figure 4.11D**). Finally, a panel of cellular differentiation markers was selected for mRNA quantification on the transcriptional level in the isogenic cell lines. Hepatocytic markers albumin (*ALB*) and apolipoprotein E (*APOE*), cholangiocytic markers keratin 19 (*KRT19*) and epithelial cell adhesion molecule *(EPCAM*), and progenitor markers alpha fetoprotein (*AFP*) and SRY-box transcription factor 9 (*SOX9*) were quantified by RT-qPCR. Since PBRM1 is an epigenetic modifier, changes in gene expression are not expected to occur immediately, therefore, the readout employed was the fold change relative to the

control cell line at day 0, week 1, week 2 and week 3 after viral transduction and cell selection. I hypothesized that PBRM1 knockout in HCC cell lines would lower the expression of hepatocytic markers and increase the expression of cholangiocytic markers. On the other hand, I expected that overexpression of PBRM1 in the iCCA cell line would obtain the opposite phenotype. In the case of SNU-182, *ALB* levels decreased while *EPCAM* levels increased. For HepG2, *KRT19* levels increased at week 2 but then dropped dramatically at week 3. More interestingly, HepG2 is generally considered to possess a "progenitor" phenotype and for this cell line progenitor markers *AFP* and *SOX9* gradually decreased over time, possibly meaning a loss of an undifferentiated state. Finally, in the case of HuH-28 no major changes were observed (**Figure 4.11E**). Together, the data collected from these initial *in vitro* experiments with the human isogenic cell lines did not lead to conclusive results, and, despite significant differences observed in proliferation and colony forming assays, the biological relevance of such differences seemed elusive.

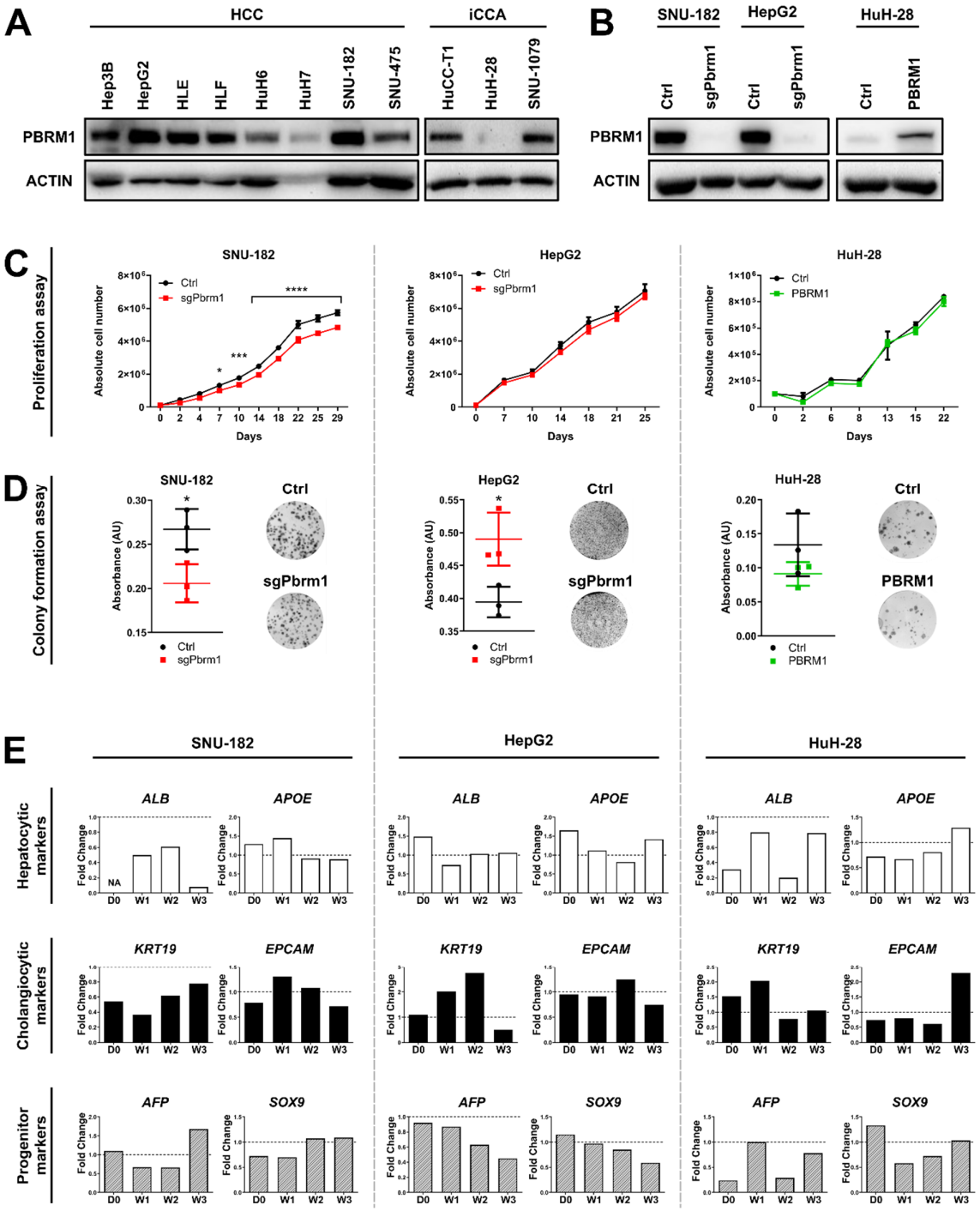

Figure 4.11 | PBRM1 expression does not have functional implications in isogenic human cell lines. (A) PBRM1 expression in a panel of HCC and iCCA cell lines. **(B)** Generation of isogenic cell lines by PBRM1 knockout and overexpression. **(C)** Proliferation assays of isogenic cell lines. Bars = SD. N = 1. **(D)** Colony formation assay of isogenic cell lines. Bars = SD. N = 1. **(E)** RT-qPCR data showing the fold change in gene expression after PBRM1 knockout or overexpression. In white, hepatocytic markers, in black, cholangiocytic markers, in grey, progenitor markers. D0 = Day 0, W1 = week 1, W2 = week 2, W3 = week 3 (after transduction). N = 1. NA = not available.

4.2 RPS6KA3 is a potent tumor suppressor and potential predictive biomarker in liver cancer

4.2.1 RPS6KA3 is the most frequently mutated gene in the RAS/MAPK pathway in HCC

As previously introduced, RSP6KA3 is a very promising candidate to be studied in HCC as, when compared to other RAS/MAPK players, it is often mutated. RPS6KA3 not only acts as an effector of the RAS/MAPK pathway, but was also shown to act as a negative feedback regulator by phosphorylation and inhibition of SOS. In order to test RPS6KA3 modulation of RAS/MAPK in HCC, a set of human HCC tissue microarrays was firstly stained for RPS6KA3 to stratify for high- and low-RPS6KA3-expressing tumors. Next, the microarrays were also stained for phosphorylated ERK (p-ERK) levels, a surrogate marker of RAS/MAPK pathway activation. p-ERK staining quantification showed that low RPS6KA3 expression is significantly associated with high p-ERK levels while the opposite was observed for low RPS6KA3 expression, meaning that RPS6KA3 expression status modulates RAS/MAPK activation in human HCC (**Figure 4.12A**).

In order to study the same effect in a murine setting, an effort was made in looking for partners that, when mutated alongside RPS6KA3, could lead to tumor initiation. The HTVI mouse model was employed to answer this question by injecting two different plasmids allowing for CRISPR/Cas9-mediated *Rps6ka3* knockout (pX330-sgRps6ka3.1 and pX330-sgRps6ka3.2) coupled with a transposon-based plasmid allowing for MYC overexpression (pT3-EF1a-MYC). From this cohort, one mouse receiving sgRps6ka3.2 developed a tumor 50 days after the injection (**Figure 4.12B**). Also in this case, RAS/MAPK pathway modulation was assessed by staining for RPS6KA3 and p-ERK, alongside a Myc;sgTrp53 tumor as a control. Also in this experimental setting, the absence of RPS6KA3 was correlated to high p-ERK expression (**Figure 4.12C**). Together, these results indicate that RPS6KA3 acts as a negative feedback regulator of the RAS/MAPK pathway in human and murine HCC tumors.

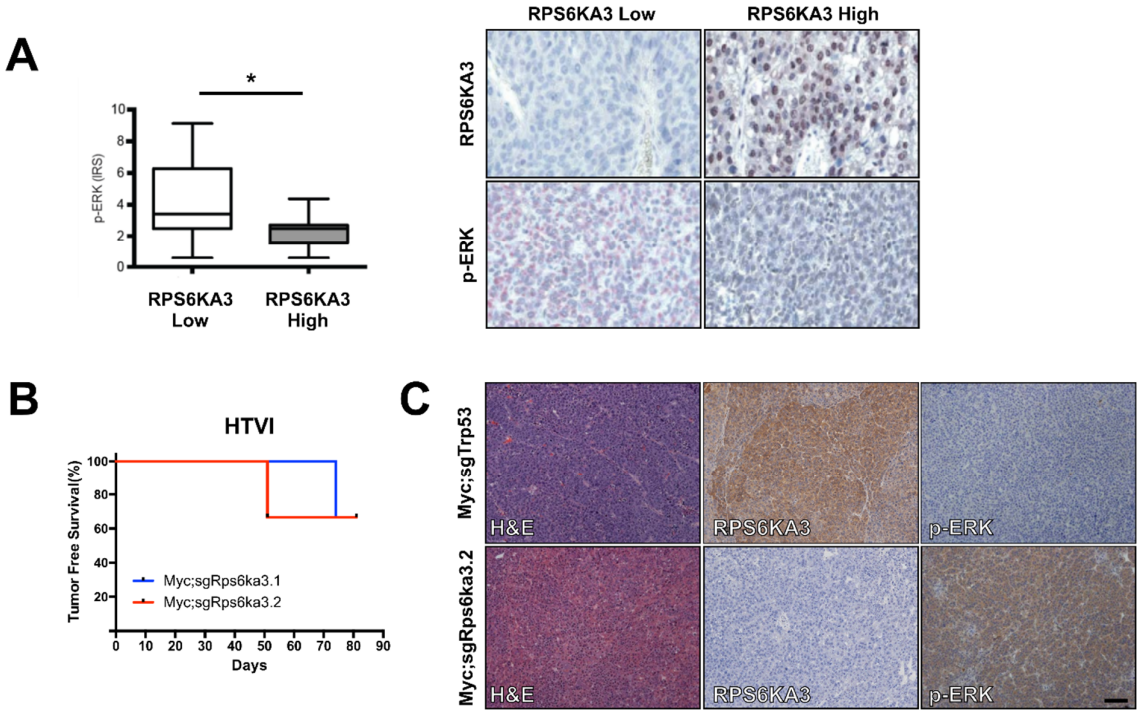

Figure 4.12 | RPS6KA3 expression levels regulate RAS/MAPK pathway in human and murine HCC. Data provided by Darjus Tschaharganeh. **(A)** Human HCC microarray IHC and p-ERK staining quantification. **(B)** Survival curves for mice in the Myc;sgTrp53 HTVI experiment. **(C)** Representative tumor IHC comparing RPS6KA3 and p-ERK levels between Myc;sgRps6ka3.2 and Myc;sgTrp53 HTVI cohorts. Scale bar = 100 µm.

I further investigated in an *in vitro* experimental setting in order to investigate whether RPS6KA3 expression status could modulate RAS/MAPK signaling in human and murine HCC cell lines. First, a panel of human HCC cell lines was stratified according to *RPS6KA3* mRNA expression (**Figure 4.13A**). Further, this stratification for high- and low-RPS6KA3-expressing cell lines was also validated at the protein level (**Figure 4.13B**). I selected HuH7 and PLC, which strongly express RPS6KA3 in order to knock it out and Hep3B, which do not express RPS6KA3, to overexpress it. This allowed me to functionally study RAS/MAPK pathway dynamics upon dysregulation of RPS6KA3 expression levels. HuH7 and PLC were chosen as high expressors in order to knockout *RPS6KA3*. Firstly, the cell lines were transduced with a lentiviral plasmid (lentiCas9-Blast) to generate stable cell lines expressing Cas9 nuclease. After blasticidin selection, the cell lines were then transduced with a retroviral plasmid allowing for sgRps6ka3 expression (pLKO-sgRsp6ka3.1 and pLKO-sgRsp6ka3.2) and finally selected with puromycin. To model RPS6KA3 re-expression, Hep3B cells were chosen as low RPS6KA3 expressors and

were then transduced with a retroviral plasmid enabling RPS6KA3 overexpression (MSCV-RPS6KA3). Two Myc;sgTrp53 primary cell lines (#1 and #2) were also engineered in an analogous way. In this case, the cells were both transduced with retroviral vectors allowing for RPS6KA3 knockdown (MLPe-shRps6ka3.1 and MLPe-shRps6ka3.2) and were afterwards selected with puromycin.

These cell lines were used to investigate RAS/MAPK pathway dynamics under different RPS6KA3 expression levels. Briefly, the pathway was deactivated by withdrawing serum from the cell culture medium for 15 minutes and then reactivated by addition of epidermal growth factor (EGF), which is able to stimulate the RAS/MAPK upstream of RPS6KA3 negative feedback inhibition. p-ERK levels were then analyzed and compared among the isogenic cell lines after 15 and 30 minutes since EGF stimulation (**Figure 4.13C**). Both HuH7 and PLC cell lines show that, upon EGF stimulation, p-ERK levels are boosted when compared to the control cell line. The same phenotype was also observed when employing RNAi-mediated gene knockdown (data not shown). The opposite pattern was detected when re-expressing RPS6KA3 in Hep3B cells, in which re-expression of the protein decreases the levels of p-ERK upon EGF stimulation (**Figure 4.13C**). Moreover, to confirm these results in murine cell lines, the same starvation-stimulation experiment was performed with the isogenic murine primary cell lines obtained from Myc;sgTrp53 HTVI experiments, in which RPS6KA3 was knocked down with the use of shRNAs. Also in this setting, the knockdown of the protein led to an increased RAS/MAPK pathway activation after EGF stimulation (**Figure 4.13D**). In an orthogonal approach the same results were observed when inducing CRISPR/Cas9 mediated *Rps6ka3* knockout in the murine cell lines (data not shown). Together, these data show that RPS6KA3 is the most mutated gene in HCC having a role in MAPK pathway and having an impact on its modulation.

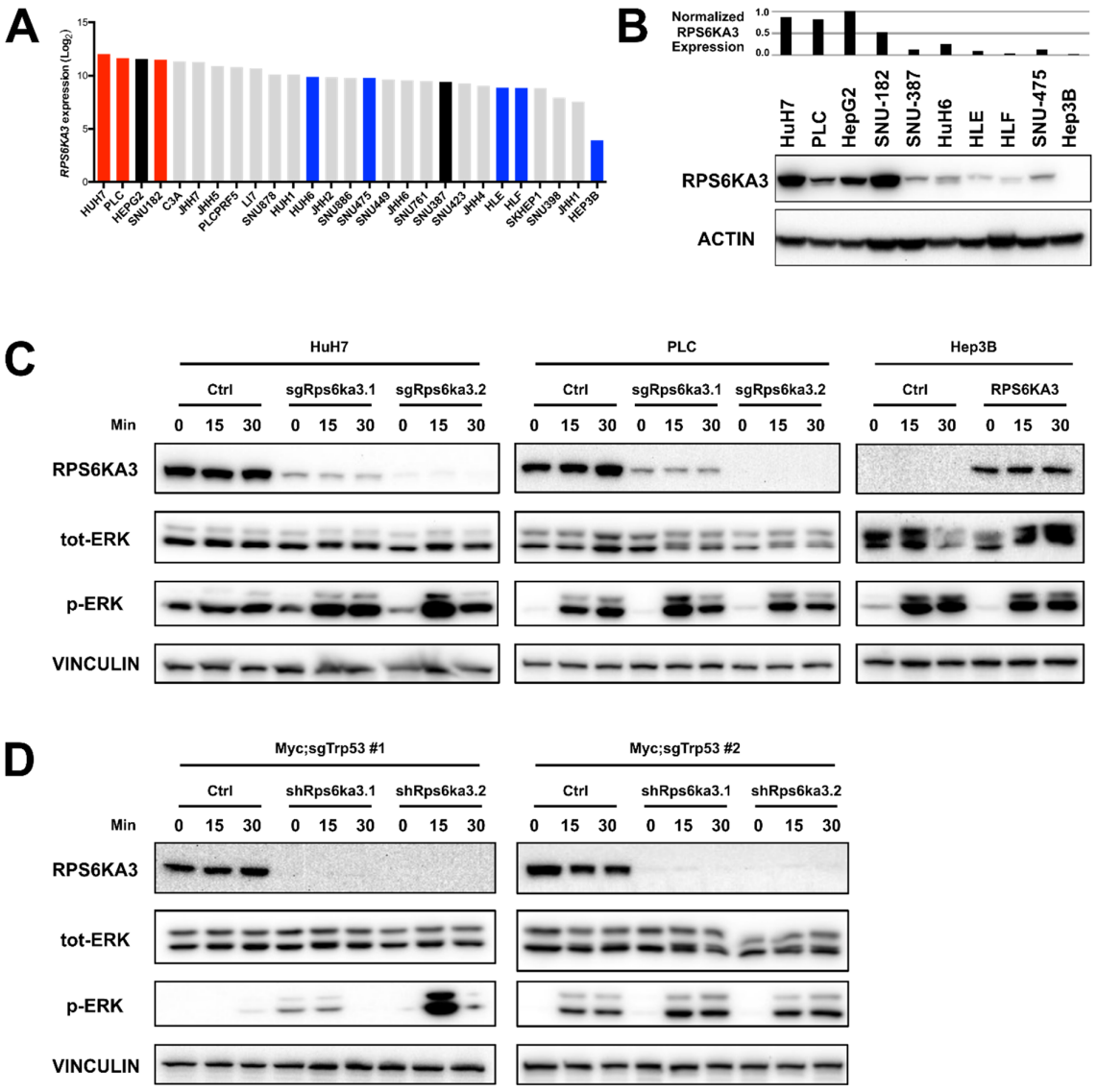

Figure 4.13 | RPS6KA3 expression levels regulate RAS/MAPK pathway in human and murine HCC cell lines. (A) *RPS6KA3* expression in a panel of human HCC cell lines. Red bars = high RPS6KA3 expression. Blue bars = low RPS6KA3 expression. Black bars = cell lines possessing RAS/RAF activating mutations. Data provided by Darjus Tschaharganeh. **(B)** RPS6KA3 expression in a panel of human HCC cell lines. **(C-D)** Serum starvation and EGF stimulation experiments in human and murine cell lines. Min = minutes, 0 = starved cells, 15 = 15 minutes under EGF stimulation, 30 = 30 minutes under EGF stimulation. N = 3.

4.2.2 RPS6KA3 expression levels have a functional impact on HCC progression

Next, I investigated whether RPS6KA3 loss or gain could have a functional impact on HCC progression. To test this hypothesis, I performed subcutaneous injection of the human and murine HCC isogenic cell lines described in **Figure 4.13** in immunodeficient NSG mice and

monitored the growth of the resulting xenografts over time. Upon RPS6KA3 loss, HuH7 grafts showed no significant difference in tumor growth. On the other hand, PLC grafts showed a significant increase in tumor growth upon RPS6KA3 loss (sgRps6ka3.1). PLC cells engineered with shRNAs for RPS6KA3 knockdown were also used in a separate xenograft cohort but showed no significant difference in tumor growth (data not shown). Remarkably, the complete opposite phenotype was achieved with RPS6KA3 overexpression in Hep3B grafts in which re-expressing RPS6KA3 significantly slowed down tumor growth when compared to the control. Also with the murine HCC cell lines grafts, knockdown of RPS6KA3 led to a significant increase in tumor growth over time (**Figure 4.14A**). After tumor lysis and protein extraction, the samples were tested for ERK phosphorylation. Despite no significant difference in tumor growth, HuH7 graft showed a significant increase in p-ERK levels upon RPS6KA3 loss. Conversely, such a difference was not observed in lysates from PLC and Hep3B grafts (**Figure 4.14B**). Furthermore, RPS6KA3 overexpression was not observed in protein lysates from the Hep3B RPS6KA3 samples, suggesting a selective pressure towards RPS6KA3-null cells, possibly explaining delayed tumor initiation and prolonged tumor growth in this experimental setting.

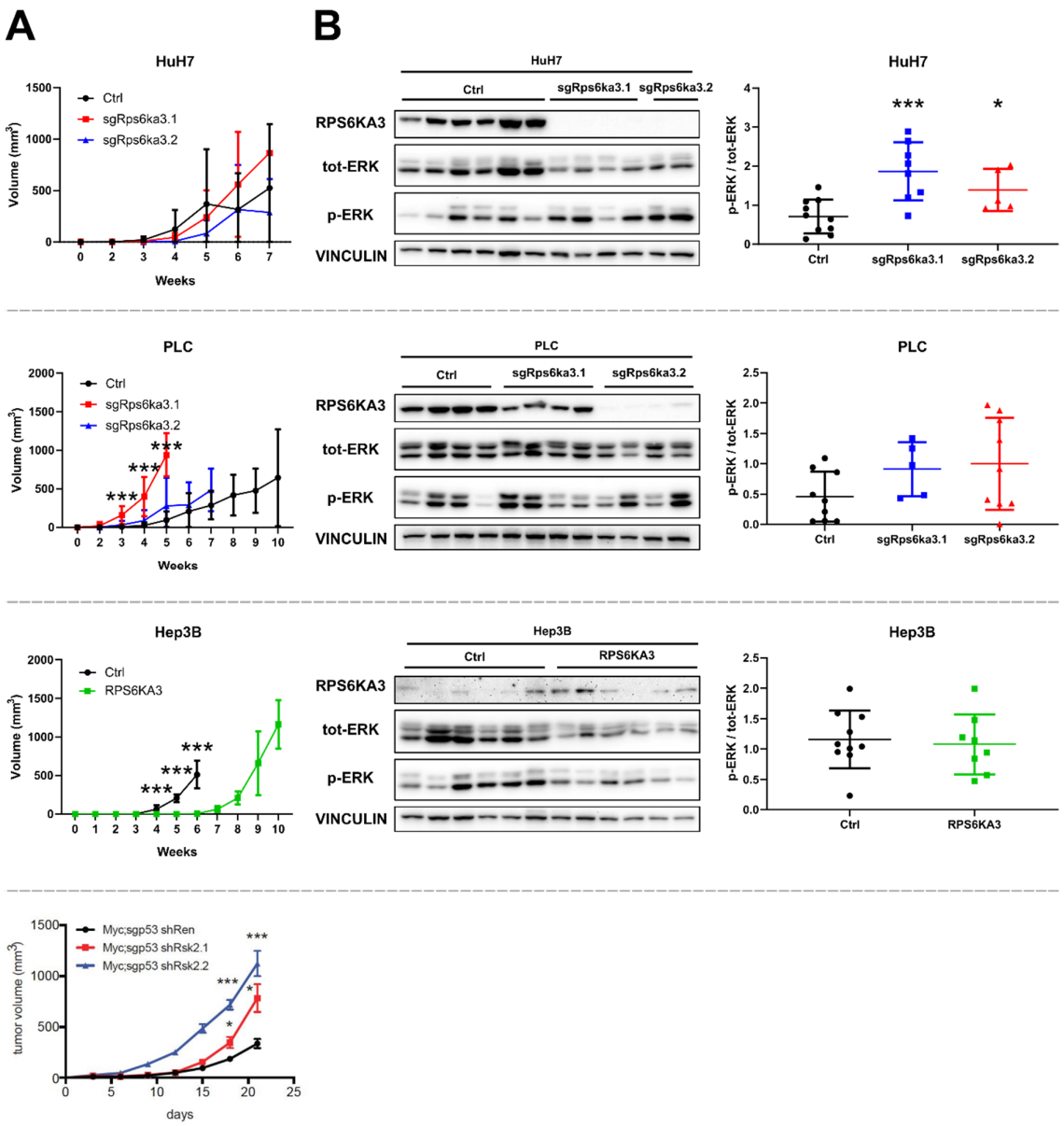

Figure 4.14 | RPS6KA3 has a functional impact in tumor growth *in vivo*. (A) Xenograft growth over time. Bars = SD. N = 10. Experiments and analysis of murine cell line xenograft growth provided by Darjus Tschaharganeh. **(B)** On the left, Representative Western blots of xenograft lysates. On the right, densitometric quantification of p-ERK / tot-ERK levels. Bars = SD. N ≥ 5.

In order to complement the phenotype observed in the *in vivo* xenograft experiment, the isogenic cell lines were used to perform proliferation assays and colony forming assays. These experiments were performed to check whether modulation of RPS6KA3 expression levels could have functional repercussions in cellular growth *in vitro*. Proliferation assays in

HuH7 and PLC isogenic cell lines showed no significant differences in cellular proliferation upon loss of RPS6KA3. On the other hand, re-expressing RPS6KA3 in Hep3B cells significantly reduced cell growth when compared to the control (**Figure 4.15A**). Colony formation assays were also employed as a parallel method to investigate cellular growth. Also with this assay, no significant changes were observed in response to RPS6KA3 loss or gain (**Figure 4.15B**). Together with the previous *in vivo* results, this data showed that modulation of RPS6KA3 expression levels has functional repercussions in tumor growth *in vivo*. On the other hand, this phenotype could not be recapitulated *in vitro*.

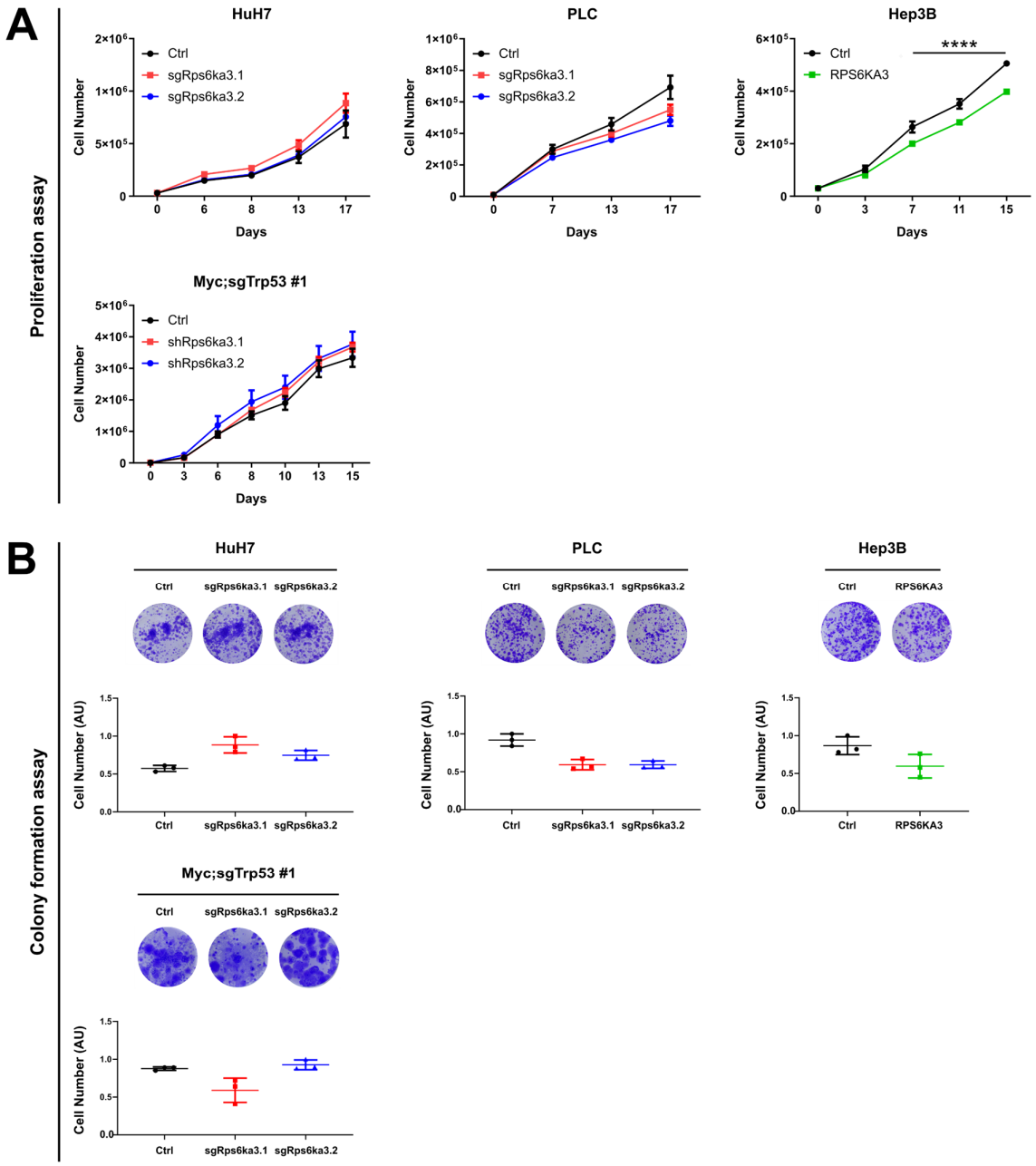

Figure 4.15 | RPS6KA3 expression status does not have a functional impact *in vitro*. (A) Proliferation assay of human and murine isogenic cell lines. Bars = SD. N = 3. **(B)** Representative colony formation assay of human and murine isogenic cell lines. Bars = SD. N = 3.

4.2.3 Investigating the role RPS6KA3 loss as a biomarker

RPS6KA3 loss was demonstrated to be functionally implicated in driving an increased activation of the RAS/MAPK pathway and speeding up tumor growth *in vivo*. Such an increased activation of this pathway was a relevant finding in the context of liver cancer, especially for its potential of being leveraged therapeutically by the employment of RAS/MAPK pathway drug inhibitors.

4.2.3.1 RPS6KA3 is a biomarker *in vivo*

Preliminary experiments investigated whether Trametinib, a MEK inhibitor, could be used to treat RPS6KA3-null tumors. To model this *in vivo*, human HCC cell lines were injected orthotopically in nude mice. SNU-475 were chosen as low RPS6KA3 expressors while PLC were chosen as high RPS6KA3 expressors. After surgery and cell injection, trametinib was administered to the mice. Bioluminescent signal was employed as a redout of tumor growth and, interestingly, trametinib treatment significantly slowed down tumor growth only in SNU-475 grafts, where the RAS/MAPK pathway is driven by the absence of RPS6KA3 (**Figure 4.16A**). In parallel, the isogenic Myc;sgTrp53 #1 cell lines were also injected subcutaneously in nude mice. Remarkably, trametinib treatment significantly reduced tumor growth only when RPS6KA3 was knocked down and not in the control (**Figure 4.16B**).

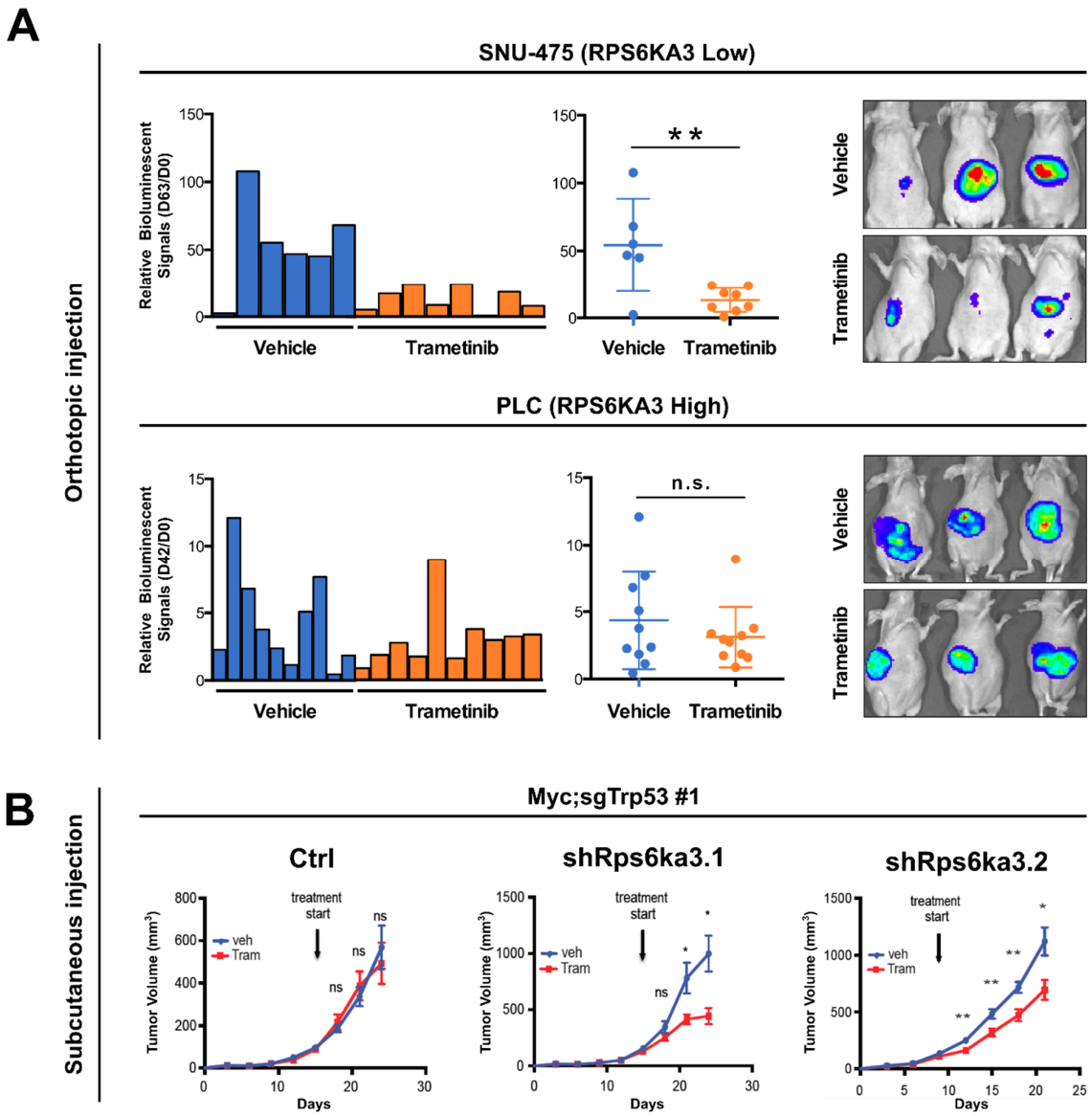

Figure 4.16 | RPS6KA3 is a biomarker *in vivo.* Data provided by Darjus Tschaharganeh. **(A)** Orthotopic injection of human HCC cell lines. On the left, bioluminescent signal relative to injection at day 0. On the right, representative pictures of nude mice in the experiment. **(B)** Subcutaneous injection of isogenic mouse HCC cell lines.

4.2.3.2 RPS6KA3 is not a biomarker *in vitro*

In order to better investigate the role of RPS6KA3 as a biomarker *in vitro*, I selected a panel of drugs to be tested on human HCC cell lines. Trametinib and pimasertib were chosen as MEK inhibitors, ravoxertinib and ulixertinib as ERK inhibitors and finally sorafenib and regorafenib as multi-kinase inhibitors. Human HCC cell lines were chosen based on the

RPS6KA3 panel previously shown (**Figure 4.13B**). I hypothesized that different RPS6KA3 expression levels could influence the response to these drugs; therefore, I selected Hep3B, HLE and SNU-475 as low RPS6KA3 expressors while HuH7, PLC and SNU-182 were chosen as high RPS6KA3 expressors. Furthermore, HepG2 was selected as a control cell line possessing an activating RAS mutation and therefore was expected to strongly respond to MEK and ERK inhibitors. Dose-response curves were generated for each cell line upon three days of treatment with the inhibitors. When observing the curves for MEK and ERK inhibitors, the cell lines responded to the treatment heterogeneously but such response did not cluster according to RPS6KA3 levels (**Figure 4.17A**). Conversely, sorafenib and regorafenib treatments show more homogenous dose-response curves, clustering together with roughly the same IC50 values at higher drug concentrations (~2.5 µM – 5 µM) (**Figure 4.17B**). Together, these results demonstrate that RPS6KA3 is not a biomarker *in vitro.*

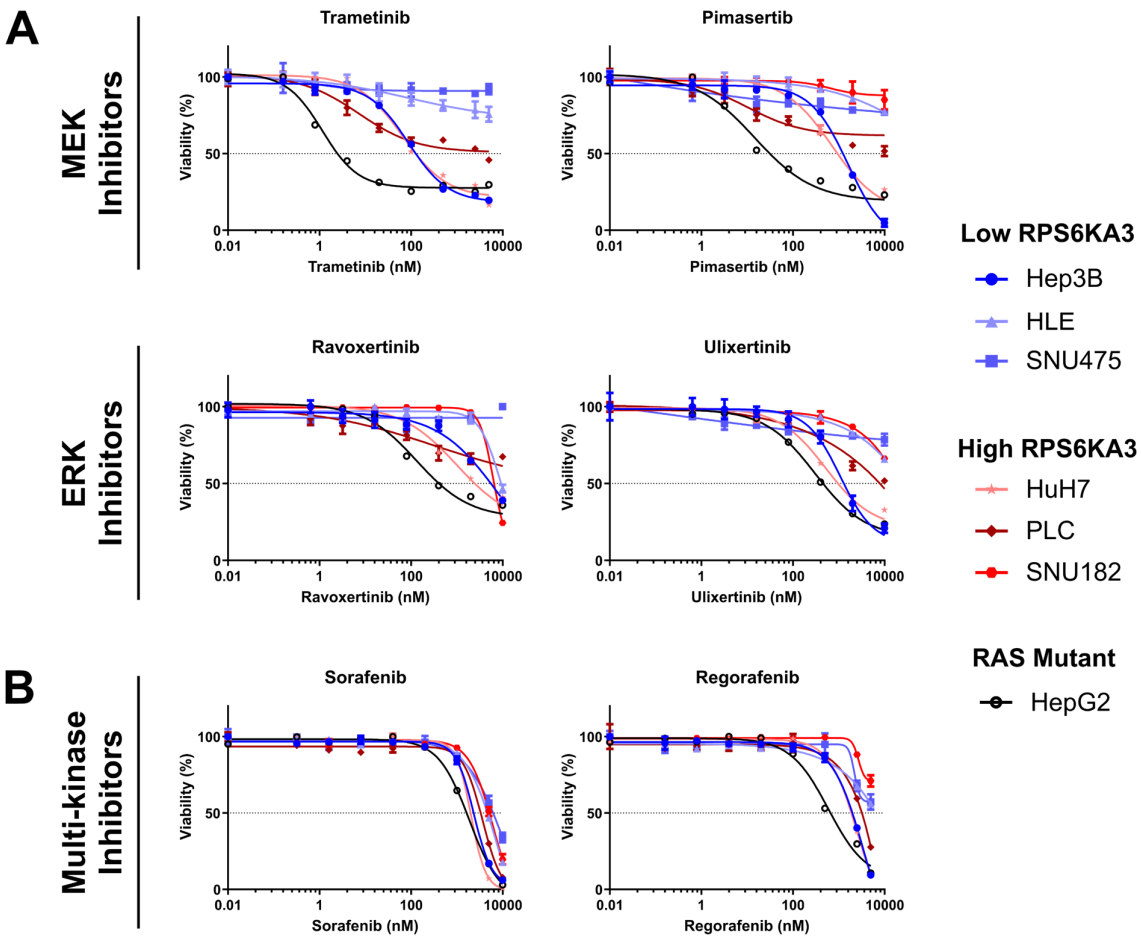

Figure 4.17 | RPS6KA3 is not a biomarker upon MEK, ERK and multi-kinase drug inhibitor treatments. Blu shade = Low RPS6KA3 expressors. Red shade = High RPS6KA3 expressors. Black = RAS mutant. **(A)** Drug response curves upon trametinib, pimasertib, ravoxertinib and ulixertinib treatments. N = 2. **(B)** Drug response curves upon sorafenib and regorafenib treatments. N = 2.

I next investigated whether the previous hypothesis could also be tested by using the isogenic cell lines formerly generated (**Figure 4.13**). Trametinib was employed as the drug of choice for this screening and dose-response curves were generated. Also in this case, both human and mouse HCC cell lines did not respond differently to trametinib treatment upon loss or overexpression of RPS6KA3 (**Figure 4.18**). The same experiments were performed with human PLC and HuH7 cell lines in which RPS6KA3 was knocked down and mouse Myc;sgTrp53 (#1 and #2) cell lines in which *Rps6ka3* was knocked out. Also in this setting, the result was equal (data not shown). Together, these results confirm the previous observation that RPS6KA3 is not a biomarker *in vitro*.

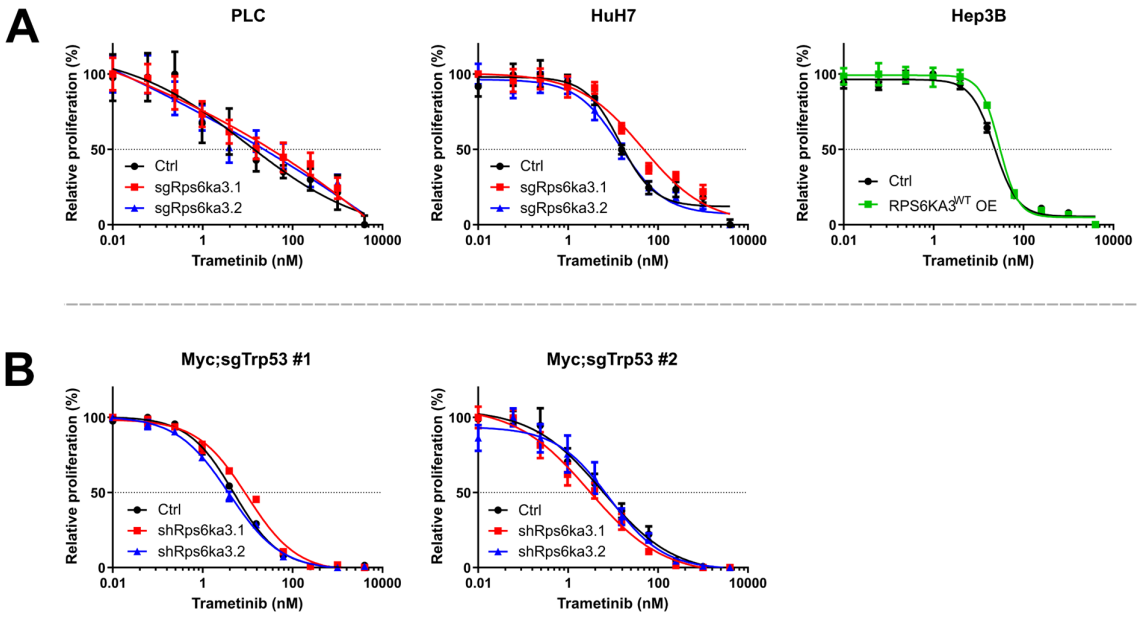

Figure 4.18 | RPS6KA3 is not a biomarker in human and murine isogenic cell lines. (A) Dose-response curves in human HCC isogenic cell lines upon trametinib treatment. N = 3. **(B)** Dose-response curves in murine HCC isogenic cell lines upon trametinib treatment. N = 3.

5 Discussion

Primary liver cancer is a major health concern, being the fifth most occurring cancer and the second most lethal worldwide, with a 5-year survival rate of only 18%.[20] Despite these facts, treatment for primary liver cancer is still lagging behind, with unspecific multi-kinase inhibitors being the only option available for the treatment of advanced disease. However, due to the recent advances in genomic sequencing technologies, we now have precise information about the genetic make-up of liver cancers, which could be utilized to identify specific treatments for individual patients according to their tumor genotype. To push this path forward, it is necessary to understand if a particular genetic alteration is driving tumorigenesis and to identify treatment options, which are specific for a particular genetic alteration, in order to ultimately reach precision medicine in liver cancer. In this work, I aimed to contribute to this concept by interrogating two quite prevalent genetic alterations PBRM1 and RPS6KA3, which are altered in intrahepatic cholangiocarcinoma and hepatocellular carcinoma, respectively.

5.1 PBRM1 depletion does not accelerate tumorigenesis in the liver

PBRM1 loss is considered to be a *bona fide* tumor suppressor gene in many different cancer types.[128] Most notably, PBRM1 loss-of-function mutations are reported to be occurring in ~50% of ccRCCs[129] and have also been described in lung adenocarcinoma, bladder urothelial carcinoma and skin cutaneous melanoma.[130] Based on publicly available human sequencing data, PBRM1 is also found to be preferentially mutated in iCCA rather than HCC.[109,131] Despite this, the mutational status of PBRM1 in iCCA has never been dissected functionally. Therefore, in this dissertation I coupled several established models of liver tumorigenesis with PBRM1 loss in order to test whether PBRM1 depletion could lead to tumorigenesis.

First, in an effort to demonstrate PBRM1 role as a tumor suppressor gene in liver cancer, loss of PBRM1 was investigated in the context of oncogenic signals such as MYC or $KRAS^{G12D}$ overexpression or in a pro-oncogenic background driven by loss of TP53 or loss of PTEN (**Figure 4.5**). None of these combinations resulted in tumor formation, meaning that – at least when coupled with these candidates – PBRM1 inactivating mutations observed in iCCA are

not drivers but rather passenger mutations, not required in tumor initiation but possibly in tumor progression.[132] In support of this view, a study from 2017 described the loss of PBRM1 as a late event during the development of iCCA and as lacking prognostic significance.[133]

Next, PBRM1 involvement in tumorigenesis acceleration was also investigated using the RNAi-transgenic mouse strain, which served as an elegant method of regulating the expression of PBRM1 in liver cells upon doxycycline administration. Initial validation of the mouse model clearly showed that, at least with one of the transgenic mouse strains, precise regulation of PBRM1 expression could be attained (**Figure 4.2**). I coupled PBRM1 loss with dietary models of NASH-induced HCC, by the administration of CD-HFD and WD to the transgenic mouse strains. The results obtained from these cohorts clearly demonstrated that PBRM1 loss in a NASH background does not lead to an acceleration of tumorigenicity in the liver (**Figure 4.6** and **Figure 4.10**). Additionally, I noticed that tumor incidence was lower than previously reported. More specifically, CD-HFD administered to C57BL/6J mice was shown to lead to HCC within 12 months in ~25% of the cases,[35] while WD given to DIAMOND mice was demonstrated to lead to HCC in 89% of the cases within 8-13 months.[36] The transgenic mouse strains were also fed with these diets, but, in my hands, tumor incidence was significantly lower. Specifically, control mice tumor incidence upon CD-HFD was 5.3% to 12.5 % while for WD-fed mice was only 0% to 15.8%.

A drawback of the transgenic mouse model was therefore its resilience in initiating tumorigenesis like described in earlier studies.[35,36] However, this was the first occurrence in which this mouse model was used experimentally to interrogate gene function in liver cancer, therefore, the phenotypic differences observed may have been related to inter-strain differences. Such genetic variances among inbred mouse strains are widely reported to be biologically relevant. For instance, C57BL/6J mice are resistant to hepatic fibrosis, while BALB/c mice are susceptible to it.[134] As another example, when using C57BL/6, 129S and BL6/129S in vascular biology research, it was reported that despite similarities in arterial pressure, the strains differ in underlying vascular properties.[135] In the context of PLC, Inbred mouse strains exhibit susceptibility to liver tumor induction, whereas C57BL/6 and 129 strains have been classified as being “relatively resistant”.[136] This is relevant in the context of my results, as the transgenic mouse strain possessed a C57BL/6 and 129 background, and this

may explain why, in my experimental setting, the strains were so resilient in developing liver cancer. It is beyond the scope of this study to characterize genetic differences and propensions for tumor initiation among different inbred mouse strains, although, future studies with this transgenic mouse model should take this phenotype into consideration. In order to study the impact of PBRM1 loss in these models, a possible solution could be to employ the same strains used in the previously mentioned reports and to model PBRM1 inactivating mutations by HTVI. On the other hand, a drawback of this approach would be settling for an irreversible loss of PBRM1 and thus sacrificing the option of re-expressing PBRM1 by Dox withdrawal, an advantage exclusive of an RNAi-based system.

More interestingly, genomic sequencing of the tumors in the CD-HFD cohort identified a promising drug-actionable mutation in *Hras* as seemingly collaborating with PBRM1 loss in tumorigenesis (**Figure 4.9**). However, modeling of PBRM1 loss in the context of oncogenic HRAS signaling by HTVI in wild-type C57BL/6N mice did not result in tumor formation. This sequencing approach greatly helped in the context of this study in understanding the role of the mutations occurring in a heterogeneous background, like the one observed in NASH, but ultimately was constrained by the limited amount of tumors available for testing.

An unexpected finding was the silencing of the transgene system observed in CD-HFD-fed mice, specifically in the shPbrm1 on Dox cohort (**Figure 4.8**). This phenomenon was implied by the absence of GFP, whose expression was coupled with shPbrm1. Unfortunately, specific loss of PBRM1 could not be directly confirmed in these samples, since a reliable antibody against PBRM1 is not commercially available for IHC. Despite this, subsequent experiments with primary cell lines derived from these tumors clearly demonstrated that the transgene system was still functional when being investigated *in vitro* conditions. A possible explanation for this phenotype may therefore be related to the limited uptake of doxycycline by hepatocytes *in vivo*, which could be hindered by a NASH microenvironment characterized by high steatosis and inflammation. In support of this view, it has been described that during the pathological progression of NASH, expression of uptake transporter genes is significantly downregulated in hepatocytes.[137] Forthcoming studies with this model should take this into account, and a higher dose of doxycycline may be needed in order to achieve hepatocytic uptake *in vivo*. Despite these limitations, a significant portion of hepatocytes in the

parenchyma of CD-HFD- and WD-fed on Dox mice still maintained an active transgene system, in which both shPbrm1.1 and shRen were still expressed. After all, this mosaic expression might reflect better actual tumor formation observed in human patients

5.2 PBRM1 deletion does not influence cell fate during tumorigenesis

When investigating epigenetic modifiers from the perspective of cancer, it is well-known that mutations in these proteins are widely observed in several instances of neoplastic transformation.[138] As an example, in PLC, it was previously reported that gain-of-function mutations in *IDH1* result in an increased conversion of α-ketoglutarate into D-2-hydroxyglutarte.[139] This compound acts as an oncometabolite able to change the epigenetic landscape by blocking hepatocyte differentiation and promoting the formation of biliary cancer,[140] doing so by inducing the inhibition of HNF4A, a master regulator of hepatocytic differentiation.[141] The results of this study are crucial in demonstrating that mutations in IDH not only have a tumorigenic role but are also involved in PLC lineage specification, paving the way for the preferential development of iCCA rather than HCC. In the beginning of the project I hypothesized that PBRM1, being an epigenetic modifier and preferentially mutated in iCCA, could possess a role similar to IDH in influencing cell fate during tumorigenesis.

First, I found that injection of plasmids allowing for PBRM1 loss and myr-AKT overexpression showed no influence on tumor initiation or on cell fate. Notably, my results showed that no liver tumors could be detected upon oncogenic myr-AKT signaling. This result contradicts the claims of Calvisi and colleagues, which, in the same oncogenic background, demonstrated HCC induction in FVB/N mice (**Figure 4.5**).[125]

Furthermore, experiments done to test the possible influence of PBRM1 as a molecular switch in tumorigenesis showed no involvement of PBRM1 in cell fate determination in the context of YAP overexpression and TRP53 loss (**Figure 4.4**). This background was previously shown to lead to the formation of undifferentiated tumors in FVB/N mice.[48] In my hands, HCC was observed when PBRM1 loss was combined with YAP overexpression and TRP53 loss, while in the other conditions no progenitor tumor was observed at all. Thus, the transgenic strain could not reliably reproduce the progenitor tumor phenotype as previously described,

probably also in this case due to inter-strain differences. In accordance to the *in vivo* results, I found no functional repercussions upon modulation of PBRM1 expression levels in *in vitro* experiments with human HCC and iCCA cell lines (**Figure 4.11**).

5.3 Changes in the microenvironment upon PBRM1 deletion

I found that knockdown of PBRM1 in CD-HFD-fed mice conferred significant protection from liver damage, as exhibited by decreased levels of serum transaminases after four months of CD-HFD or WD dietary regimen (**Figure 4.6**), meaning that the loss of this protein could play a different role than previously hypothesized. Moreover, immunological characterization of CD-HFD-fed mice showed an increased infiltration of B cells in the parenchyma of the livers after 12 months since the beginning of the diet (**Figure 4.7**). Whether this B cell involvement is beneficial or deleterious is still a matter of debate in the scientific community.[142] B cells have shown to possess anti-tumorigenic properties through the orchestration of immunological response by the production of tumor-reactive antibodies.[143] Conversely, they also have been shown to possess pro-tumorigenic properties by the release of autoantibodies and tumor growth factors.[142,144] Since NASH is considered to be an inflammatory disease, PBRM1 could play a protective role in an inflammatory landscape and in regulating the immunologic microenvironment, rather than in initiating tumorigenesis.

In support of this view, during the course of this study, several articles were published describing a possible role of PBRM1 loss as a predictive biomarker for immunotherapy. In 2018, it was shown how murine melanomas normally resistant to immunotherapy would then become responsive to the treatments upon PBRM1 loss, which led to a more efficient recruitment of cytotoxic T cells.[145] PBRM1 loss was also associated with an increased likeliness in responding to immune checkpoint inhibitors in metastatic renal cell carcinoma.[146] Conversely, in 2020, a negative correlation between PBRM1 inactivating mutations and response to immune checkpoint blockade was reported in renal cell carcinoma.[147] In the same year, PBRM1 inactivating mutations were also described to be a negative predictive biomarker for immunotherapy in non-small cell lung cancer.[148] Together, these reports are pointing in an exciting new direction in which the role of PBRM1 loss as a predictive biomarker in the context of immunotherapy is still undefined.

Further characterization of the interplay between PBRM1 loss and inflammation in the liver could be a new field to be investigated in more depth. A model currently employed to study short burst of inflammation is achieved by infection with lymphocytic choriomeningitis virus (LCMV), which initially infects resident Kupffer cells and then spreads to hepatocytes. Mice infected with this virus develop a well-characterized transient hepatitis lasting around 7 days. As a consequence, hepatocytes respond by regulating their gene expression and directly influencing B and T cell stimulation.[149] This experimental setting would be ideally suited to better investigate the interplay between PBRM1-null hepatocytes and the immunological microenvironment during hepatitis.

5.4 RPS6KA3 is a tumor suppressor in liver cancer

RPS6KA3 (RSK2) is an effector of the MAPK pathway by acting downstream of ERK. It was recently shown that this kinase is involved in Coffin-Lowry syndrome, a disorder associated with severe mental retardation due to the causative link between its loss and the development of the disease. In 2015, exome sequencing studies identified RPS6KA3 as a putative driver gene in the context of HCC.[150]

In this dissertation, I found that loss of this protein in human and murine cell lines leads to an increased tumor growth upon injection into immunodeficient mice. Analogously, my work demonstrated that re-expression of RPS6KA3 in Hep3B, which exhibit low expression of RPS6KA3, displays the opposite phenotype by slowing down tumor development (**Figure 4.14**). Together, these results showed that RPS6KA3 can be considered a *bona fide* tumor suppressor gene in liver cancer. As of today, there has been no reports investigating the functional repercussions on RPS6KA3 loss in HCC with the exception of a study from Chan and colleagues in 2020. In accordance to my results, the investigators also demonstrated that re-expression of RPS6KA3 in Hep3B led to slower tumor development once injected subcutaneously in immunodeficient mice.[151]

It is a matter of debate whether RPS6KA3 loss-of-function mutations are able to lead to tumor initiation. Preliminary results in this dissertation showed tumorigenicity in the liver upon RPS6KA3 loss in the context of MYC oncogenic signals (**Figure 4.12**), however, since only

one tumor was obtained from this cohort, I performed the same HTVI experiment and could not recapitulate the same phenotype (data not shown). In 2015, Schulze and colleagues proposed a possible cooperation network between the loss of RPS6KA3, the deletion of AXIN1 (involved in Wnt/β-catenin signaling), and ARID1A (involved in epigenetic remodeling).[150] However, the simultaneous loss of these RPS6KA3, AXIN1 and ARID1A did not lead to tumor development (data not shown). Thus, identifying genetic alterations collaborating with RPS6KA3 loss to reliably generate liver cancer would be fundamental for future investigations as this model would allow for the study of RPS6KA3-null tumors directly in the liver microenvironment and in the presence of a physiologically active immune system.

5.5 The influence of RPS6KA3 on RAS/MAPK signaling

Aberrant activation of the RAS/MAPK pathway is a feature commonly observed in many different cancer types. It generally involves gain-of-function mutations in genes involved in this pathway, namely RAS and RAF genes, or an excessive activation of receptor tyrosine kinases.[152] Interestingly, when compared to the majority of solid cancers, a peculiar and poorly understood feature of HCC is the lack of mutations in key players of the RAS/MAPK signaling pathway (**Figure 1.10A**). In this context, investigating the role of RPS6KA3 is pivotal, as not only it acts as a downstream effector of the RAS/MAPK pathway, but also as a negative feedback regulator of the pathway itself by phosphorylation and inhibition of SOS.[122] Loss-of-function mutations in RPS6KA3 could relieve inhibition of SOS upstream of RAS/MAPK and lead to an aberrant overexpression of the signaling pathway (**Figure 1.10B**).

In the present study I addressed this issue by showing the novel finding that RAS/MAPK signaling is modulated by RPS6KA3 expression status in both human and murine HCC (**Figure 4.12**). In accordance to the *in vivo* data, I also showed that RPS6KA3 serves as a negative feedback regulator of the RAS/MAPK pathway by *in vitro* experiments, both with human and murine isogenic cell lines (**Figure 4.13**). This role of RPS6KA3 is particularly relevant in the context of tumorigenesis, considering the central role of RAS/MAPK signaling in controlling key cellular processes such as differentiation, apoptosis, stress responses and proliferation.[153] More specifically in the case of HCC, overactivation of RAS/MAPK pathway upon loss of RPS6KA3 was recently suggested to increase cholesterol biosynthesis.[151] This might be of

interest for future investigations on this topic, considering other recent findings linking high amount of dietary cholesterol to the development of NASH and HCC.[154]

5.6 Therapeutic implications of RPS6KA3 deletion in liver cancer

Preliminary results from my laboratory clearly demonstrated with *in vivo* experiments that xenografts of human and murine cells are more sensitive to trametinib treatment when RPS6KA3 expression is low or absent, thereby demonstrating that RPS6KA3 is a therapeutic biomarker in HCC (**Figure 4.16**). From the perspective of precision medicine, these novel findings are very exciting because FDA-approved RAS/MAPK pathway inhibitors already being used in the clinics to treat many kind of solid cancers – among which we find melanoma,[155] colorectal cancer,[156] breast cancer[157] and pituitary adenoma[158] – and could potentially be used to treat a subset of HCC patients possessing RPS6KA3 mutations.

Next, I found that the results observed *in vivo* could not be translated in an *in vitro* setting. Trametinib treatment in human and murine isogenic cell lines showed no sensitivity to trametinib treatment upon modulation of RPS6KA3 expression levels (**Figure 4.18**). Analogously, treatment of a panel of HCC cell lines with MEK inhibitors (trametinib and pimasertib), ERK inhibitors (ravoxertinib and ulixertinib) and wide-spectrum multi-kinase inhibitors (sorafenib and regorafenib) showed no pattern in drug response dependent on RPS6KA3 expression levels (**Figure 4.17**). In defense of this, *in vivo* studies are more reliable than *in vitro* studies, as they take into account the systemic interactions happening in an organism as a whole.[159,160] Thus, the phenotype observed by *in vivo* experiments may be due to interactions between the cells and the microenvironment in which they are injected, which should be taken into account for future investigations. Finally, the results shown in this dissertation contradict the claims of Chan and colleagues,[151] which demonstrated decreased sensitivity to sorafenib of Hep3B cells upon RPS6KA3 re-expression.

In this context, forthcoming studies employing these inhibitors should take into account increasing concerns regarding crosstalk and redundancy with other pathways.[161] As an example, RAS/MAPK and Pi3K-mTOR pathways have both central roles in physiological control of key cellular processes and have demonstrated to heavily interact with each other,

both through cross-inhibition and cross-activation, but also through pathway convergence.[162] Another point of concern are well-known mechanisms related to drug resistance due to the activation of compensatory feedback loops.[163] An example of this is the recent finding by Jin and colleagues, demonstrating EGFR overexpression upon lenvatinib (a multi-kinase inhibitor) treatment in HCC, leading to activation of RAS/MAPK pathway downstream of lenvatinib inhibition.

A possible solution to these challenges would be targeting aberrant RAS/MAPK signaling downstream at the level of ERK. ERK is placed in a peculiar position within the pathway and could be considered to act at the bottleneck of RAS/MAPK signaling. RAF has few substrates other than MEK, and the same applies to MEK. On the other hand, ERK could be considered the *de facto* effector protein of RAS/MAPK signaling, since it is the only player within the pathway able to modulate the activity of many downstream targets.[164] For this reasons, a great amount of research is currently being carried in the search for potent ERK inhibitors, with ulixertinib leading in phase I and II clinical trials.[164]

5.7 Conclusions

Collectively, this research aimed to functionally dissect the role of two uncharacterized and frequently mutated tumor suppressor genes in the context of primary liver cancer. PBRM1 loss was shown not to be connected to tumorigenesis or determination of cell fate while, on the other hand, suggesting a possible role in reshaping the microenvironment upon inflammatory conditions. Conversely, RPS6KA3 was demonstrated to act as a tumor suppressor gene and as a potential biomarker for MAPK signaling inhibitors. Together, these findings helped on better understanding the role PBRM1 and RPS6KA3 play in such a complex and heterogeneous cancer and paved the way for the development of new targeted therapies for the treatment of PLC.

6 Supplementary Data

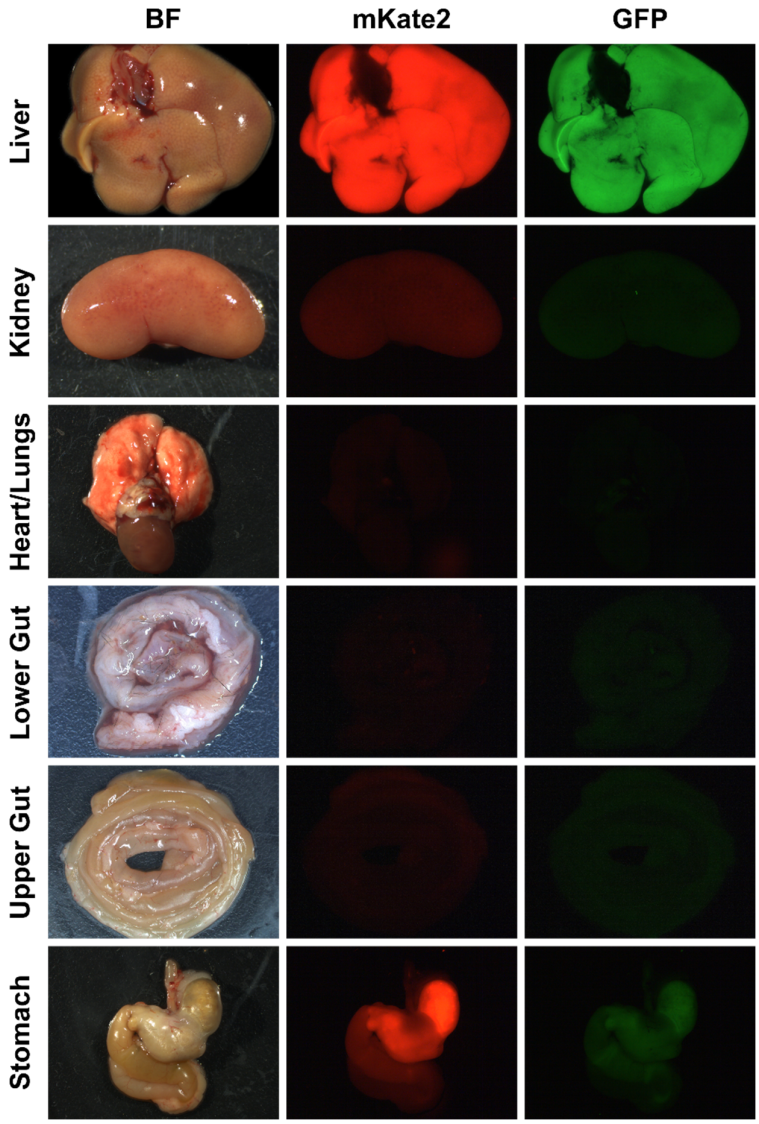

Supplementary Figure 1 | The Alb-Cre x CAGs-LSL-rtTA3 x TGM shPbrm1 strains. Representative dissectoscope picture of different organs after Dox administration. BF = Brightfield picture.

7 Bibliography

1. Bhatia, S. N., Underhill, G. H., Zaret, K. S. & Fox, I. J. Cell and tissue engineering for liver disease. *Sci. Transl. Med.* **6**, 245sr2 (2014).

2. Rappaport, A. M. The microcirculatory hepatic unit. *Microvasc. Res.* **6**, 212–228 (1973).

3. Lautt, W. W. Hepatic Circulation: Physiology and Pathophysiology. in *Hepatic Circulation: Physiology and Pathophysiology* (eds. Granger, D. N. & Granger, J.) 83–108 (Morgan & Claypool Life Sciences, 2009).

4. Jungermann, K. & Kietzmann, T. Zonation of parenchymal and nonparenchymal metabolism in liver. *Annual Review of Nutrition* vol. 16 179–203 (1996).

5. Gordillo, M., Evans, T. & Gouon-Evans, V. Orchestrating liver development. *Development (Cambridge)* vol. 142 2094–2108 (2015).

6. Kalra, A. & Tuma, F. *Physiology, Liver*. *StatPearls* (StatPearls Publishing, 2018).

7. Marquardt, J. U., Andersen, J. B. & Thorgeirsson, S. S. Functional and genetic deconstruction of the cellular origin in liver cancer. *Nat. Rev. Cancer* **15**, 653–667 (2015).

8. Birchmeier, W. Orchestrating Wnt signalling for metabolic liver zonation. *Nature Cell Biology* vol. 18 463–465 (2016).

9. Manco, R. & Itzkovitz, S. Liver zonation. *Journal of Hepatology* vol. 74 466–468 (2021).

10. Almazroo, O. A., Miah, M. K. & Venkataramanan, R. Drug Metabolism in the Liver. *Clinics in Liver Disease* vol. 21 1–20 (2017).

11. Adeva-Andany, M. M., González-Lucán, M., Donapetry-García, C., Fernández-Fernández, C. & Ameneiros-Rodríguez, E. Glycogen metabolism in humans. *BBA Clinical* vol. 5 85–100 (2016).

12. Alves-Bezerra, M. & Cohen, D. E. Triglyceride metabolism in the liver. *Compr. Physiol.* **8**, 1–22 (2018).

13. Doguer, C., Ha, J. H. & Collins, J. F. Intersection of Iron and Copper Metabolism in the Mammalian Intestine and Liver. *Comprehensive Physiology* vol. 8 1433–1461 (2018).

14. Maroni, L. *et al.* Functional and Structural Features of Cholangiocytes in Health and Disease. *CMGH* vol. 1 368–380 (2015).

15. Tabibian, J. H., Masyuk, A. I., Masyuk, T. V, O'Hara, S. P. & LaRusso, N. F. Physiology of cholangiocytes. *Compr. Physiol.* **3**, 541–565 (2013).

16. Naito, M., Hasegawa, G., Ebe, Y. & Yamamoto, T. Differentiation and function of Kupffer cells. *Medical Electron Microscopy* vol. 37 16–28 (2004).

17. Puche, J. E., Saiman, Y. & Friedman, S. L. Hepatic stellate cells and liver fibrosis. *Compr. Physiol.* **3**, 1473–1492 (2013).

18. Hoffmann, C. *et al.* Hepatic stellate cell hypertrophy is associated with metabolic liver fibrosis. *Sci. Rep.* **10**, 1–13 (2020).

19. Robinson, M. W., Harmon, C. & O'Farrelly, C. Liver immunology and its role in inflammation and homeostasis. *Cellular and Molecular Immunology* vol. 13 267–276 (2016).

20. International Agency for Research on Cancer, World Health Organization. https://gco.iarc.fr/today/data/factsheets/cancers/11-Liver-fact-sheet.pdf.

21. Murray, C. J. L. *et al.* Disability-adjusted life years (DALYs) for 291 diseases and injuries in 21 regions, 1990-2010: A systematic analysis for the Global Burden of Disease Study 2010. *Lancet* **380**, 2197–2223 (2012).

22. World Health Organization. Projections of mortality and causes of death, 2016 to 2060 (http://www .who .int/ healthinfo/ global_burden_disease/ projections/ en/).

23. Llovet, J. M. *et al.* Hepatocellular carcinoma. *Nat. Rev. Dis. Prim.* **2**, (2016).

24. Sia, D., Villanueva, A., Friedman, S. L. & Llovet, J. M. Liver Cancer Cell of Origin, Molecular Class, and Effects on Patient Prognosis. *Gastroenterology* vol. 152 745–761 (2017).

25. Marquardt, J. U. & Andersen, J. B. Liver cancer oncogenomics: opportunities and dilemmas for clinical applications. *Hepatic Oncol.* **2**, 79–93 (2015).

26. Raggi, C., Invernizzi, P. & Andersen, J. B. Impact of microenvironment and stem-like plasticity in cholangiocarcinoma: Molecular networks and biological concepts. *Journal of Hepatology* vol. 62 198–207 (2015).

27. Bartolozzi, C., Battaglia, V. & Bozzi, E. Hepatocellular carcinoma. in *Clinical MRI of the Abdomen: Why,How,When* vol. 365 95–116 (Massachusetts Medical Society, 2011).

28. Levrero, M. & Zucman-Rossi, J. Mechanisms of HBV-induced hepatocellular carcinoma. *Journal of Hepatology* vol. 64 S84–S101 (2016).

29. Andrade, L. de O. *et al.* Association between hepatitis C and hepatocellular carcinoma. *J. Glob. Infect. Dis.* **1**, 33 (2009).

30. Rizvi, S. & Gores, G. J. Pathogenesis, diagnosis, and management of cholangiocarcinoma. *Gastroenterology* vol. 145 1215–1229 (2013).

31. Kao, J. H. Hepatitis B vaccination and prevention of hepatocellular carcinoma. *Best Practice and Research: Clinical Gastroenterology* vol. 29 907–917 (2015).

32. Anstee, Q. M., Reeves, H. L., Kotsiliti, E., Govaere, O. & Heikenwalder, M. From NASH to HCC: current concepts and future challenges. *Nature Reviews Gastroenterology and Hepatology* vol. 16 411–428 (2019).

33. Gupta, A. *et al.* Obesity is Independently Associated with Increased Risk of Hepatocellular Cancer-related Mortality. *Am. J. Clin. Oncol. Cancer Clin. Trials* **41**, 874–881 (2018).

34. Burt, A. D., Lackner, C. & Tiniakos, D. G. Diagnosis and Assessment of NAFLD: Definitions and Histopathological Classification. *Semin. Liver Dis.* **35**, 207–220 (2015).

35. Wolf, M. J. *et al.* Metabolic activation of intrahepatic CD8+T cells and NKT cells causes nonalcoholic steatohepatitis and liver cancer via cross-talk with hepatocytes. *Cancer Cell* **26**, 549–564 (2014).

36. Asgharpour, A. *et al.* A diet-induced animal model of non-alcoholic fatty liver disease and hepatocellular cancer. *J. Hepatol.* **65**, 579–588 (2016).

37. Guest, R. V., Boulter, L., Dwyer, B. J. & Forbes, S. J. Understanding liver regeneration to bring new insights to the mechanisms driving cholangiocarcinoma. *npj Regen. Med.* **2**, 13 (2017).

38. Cox, A. G. *et al.* Yap reprograms glutamine metabolism to increase nucleotide biosynthesis and enable liver growth. *Nat. Cell Biol.* **18**, 886–896 (2016).

39. Planas-Paz, L. *et al.* The RSPO-LGR4/5-ZNRF3/RNF43 module controls liver zonation and size. *Nat. Cell Biol.* **18**, 467–479 (2016).

40. Yanger, K. *et al.* Robust cellular reprogramming occurs spontaneously during liver regeneration. *Genes Dev.* **27**, 719–724 (2013).

41. Michalopoulos, G. K., Barua, L. & Bowen, W. C. Transdifferentiation of rat hepatocytes into biliary cells after bile duct ligation and toxic biliary injury. *Hepatology* **41**, 535–544 (2005).

42. Sekiya, S. & Suzuki, A. Hepatocytes, rather than cholangiocytes, can be the major source of primitive ductules in the chronically injured mouse liver. *Am. J. Pathol.* **184**, 1468–1478 (2014).

43. Zong, Y. *et al.* Notch signaling controls liver development by regulating biliary differentiation. *Development* **136**, 1727–1739 (2009).

44. Ishak, K. G., Anthony, P. P. & Sobin, L. H. Histological Classification of Tumours of the Liver. in *Histological Typing of Tumours of the Liver* 5–7 (Springer Berlin Heidelberg, 1994). doi:10.1007/978-3-642-85156-8_2.

45. Guest, R. V. *et al.* Cell lineage tracing reveals a biliary origin of intrahepatic cholangiocarcinoma. *Cancer Res.* **74**, 1005–1010 (2014).

46. Sekiya, S. & Suzuki, A. Intrahepatic cholangiocarcinoma can arise from Notch-mediated conversion of hepatocytes. *J. Clin. Invest.* **122**, 3914–3918 (2012).

47. Fan, B. *et al.* Cholangiocarcinomas can originate from hepatocytes in mice. *J. Clin. Invest.* **122**, 2911–2915 (2012).

48. Tschaharganeh, D. F. *et al.* P53-dependent nestin regulation links tumor suppression to cellular plasticity in liver cancer. *Cell* **158**, 579–592 (2014).

49. Llovet, J. M., Brú, C. & Bruix, J. Prognosis of hepatocellular carcinoma: The BCLC staging classification. *Semin. Liver Dis.* **19**, 329–337 (1999).

50. Villanueva, A. Hepatocellular carcinoma. *N. Engl. J. Med.* **380**, 1450–1462 (2019).

51. Llovet, J. M. *et al.* Sorafenib in Advanced Hepatocellular Carcinoma. *N. Engl. J. Med.* **359**, 378–390 (2008).

52. Bialecki, E. S. & Di Bisceglie, A. M. Diagnosis of hepatocellular carcinoma. *HPB* vol. 7 26–34 (2005).

53. Llovet, J. M. & Hernandez-Gea, V. Hepatocellular carcinoma: Reasons for phase III failure and novel perspectives on trial design. *Clin. Cancer Res.* **20**, 2072–2079 (2014).

54. Ronnekleiv-Kelly, S. M. & Pawlik, T. M. Staging of intrahepatic cholangiocarcinoma. *HepatoBiliary Surg. Nutr.* **6**, 35–43 (2017).

55. Bartolini, I. *et al.* Current management of intrahepatic cholangiocarcinoma: From resection to palliative treatments. *Radiology and Oncology* vol. 54 263–271 (2020).

56. Goodman, A. M. *et al.* Tumor mutational burden as an independent predictor of response to immunotherapy in diverse cancers. *Mol. Cancer Ther.* **16**, 2598–2608 (2017).

57. Rosenberg, S. A. *et al.* Durable complete responses in heavily pretreated patients with metastatic melanoma using T-cell transfer immunotherapy. *Clin. Cancer Res.* **17**, 4550–4557 (2011).

58. Maude, S. L. *et al.* Chimeric Antigen Receptor T Cells for Sustained Remissions in Leukemia. *N. Engl. J. Med.* **371**, 77–87 (2014).

59. Govers, C., Sebestyén, Z., Coccoris, M., Willemsen, R. A. & Debets, R. T cell receptor gene therapy: strategies for optimizing transgenic TCR pairing. *Trends in Molecular Medicine* vol. 16 77–87 (2010).

60. Cooley, S. *et al.* First-in-human trial of rhIL-15 and haploidentical natural killer cell therapy for advanced acute myeloid leukemia. *Blood Adv.* **3**, 1970–1980 (2019).

61. Sahin, U. & Türeci, Ö. Personalized vaccines for cancer immunotherapy. *Science* vol. 359 1355–1360 (2018).

62. Sullivan, K. M., Kenerson, H. L., Pillarisetty, V. G., Riehle, K. J. & Yeung, R. S. Precision oncology in liver cancer. *Ann. Transl. Med.* **6**, 285–285 (2018).

63. Sgambato, A. *et al.* Anti PD-1 and PDL-1 Immunotherapy in the Treatment of Advanced Non-Small Cell Lung Cancer (NSCLC): A Review on Toxicity Profile and its Management. *Curr. Drug Saf.* **11**, 62–68 (2015).

64. Pfister, D. *et al.* NASH limits anti-tumour surveillance in immunotherapy-treated HCC. *Nature* **592**, 450–456 (2021).

65. Finn, R. S. *et al.* Atezolizumab plus Bevacizumab in Unresectable Hepatocellular Carcinoma. *N. Engl. J. Med.* **382**, 1894–1905 (2020).

66. National Cancer Institution at the National Institutes of Health. The Genetics of Cancer - National Cancer Institute. https://www.cancer.gov/about-cancer/causes-prevention/genetics (2015).

67. Malone, E. R., Oliva, M., Sabatini, P. J. B., Stockley, T. L. & Siu, L. L. Molecular profiling for precision cancer therapies. *Genome Medicine* vol. 12 1–19 (2020).

68. Yi, K. & Ju, Y. S. Patterns and mechanisms of structural variations in human cancer. *Experimental and Molecular Medicine* vol. 50 1–11 (2018).

69. Meyerson, M., Gabriel, S. & Getz, G. Advances in understanding cancer genomes through second-generation sequencing. *Nature Reviews Genetics* vol. 11 685–696 (2010).

70. Hanahan, D. & Weinberg, R. A. The hallmarks of cancer. *Cell* vol. 100 57–70 (2000).

71. Hanahan, D. & Weinberg, R. A. Hallmarks of cancer: The next generation. *Cell* **144**, 646–674 (2011).

72. Lodish, H. *et al.* Proto-Oncogenes and Tumor-Suppressor Genes. (2000).

73. Prior, I. A., Lewis, P. D. & Mattos, C. A comprehensive survey of ras mutations in cancer. *Cancer Research* vol. 72 2457–2467 (2012).

74. Simanshu, D. K., Nissley, D. V. & McCormick, F. RAS Proteins and Their Regulators in Human Disease. *Cell* vol. 170 17–33 (2017).

75. Boerner, T. *et al.* Genetic Determinants of Outcome in Intrahepatic Cholangiocarcinoma. *Hepatology* (2021) doi:10.1002/hep.31829.

76. Zou, S. *et al.* Mutational landscape of intrahepatic cholangiocarcinoma. *Nat. Commun.* **5**, 1–11 (2014).

77. Pelengaris, S., Khan, M. & Evan, G. c-MYC: More than just a matter of life and death. *Nature Reviews Cancer* vol. 2 764–776 (2002).

78. Felsher, D. W. & Bishop, J. M. Transient excess of MYC activity can elicit genomic instability and tumorigenesis. *Proc. Natl. Acad. Sci. U. S. A.* **96**, 3940–3944 (1999).

79. Nevzorova, Y. A. *et al.* Overexpression of c-myc in hepatocytes promotes activation of hepatic stellate cells and facilitates the onset of liver fibrosis. *Biochim. Biophys. Acta - Mol. Basis Dis.* **1832**, 1765–1775 (2013).

80. Eilers, M. Control of Cell Proliferation by Myc Family Genes. *Mol. Cells* **9**, 1–6.

81. Ryan, K. M. & Birnie, G. D. Cell-cycle progression is not essential for c-Myc to block differentiation. *Oncogene* **14**, 2835–2843 (1997).

82. Thompson, E. B. The many roles of c-myc in apoptosis. *Annual Review of Physiology* vol. 60 575–600 (1998).

83. Sherr, C. J. Principles of Tumor Suppression. *Cell* vol. 116 235–246 (2004).

84. Wang, L. H., Wu, C. F., Rajasekaran, N. & Shin, Y. K. Loss of tumor suppressor gene function in human cancer: An overview. *Cellular Physiology and Biochemistry* vol. 51 2647–2693 (2019).

85. Aubrey, B. J., Strasser, A. & Kelly, G. L. Tumor-suppressor functions of the TP53 pathway. *Cold Spring Harbor Perspectives in Medicine* vol. 6 (2016).

86. Stracquadanio, G. *et al.* The importance of p53 pathway genetics in inherited and somatic

cancer genomes. *Nat. Rev. Cancer* **16**, 251–265 (2016).

87. cBioPortal for Cancer Genomics. 2014–2016 https://www.cbioportal.org/ (2013).

88. National Cancer Institute. The Cancer Genome Atlas Program - National Cancer Institute. https://www.cancer.gov/about-nci/organization/ccg/research/structural-genomics/tcga (2006).

89. Totoki, Y. *et al.* Trans-ancestry mutational landscape of hepatocellular carcinoma genomes. *Nat. Genet.* **46**, 1267–1273 (2014).

90. Ally, A. *et al.* Comprehensive and Integrative Genomic Characterization of Hepatocellular Carcinoma. *Cell* **169**, 1327-1341.e23 (2017).

91. Tsimberidou, A. M. Targeted therapy in cancer. *Cancer Chemotherapy and Pharmacology* vol. 76 1113–1132 (2015).

92. Tsimberidou, A. M., Fountzilas, E., Nikanjam, M. & Kurzrock, R. Review of precision cancer medicine: Evolution of the treatment paradigm. *Cancer Treatment Reviews* vol. 86 102019 (2020).

93. Sicklick, J. K. *et al.* Molecular profiling of cancer patients enables personalized combination therapy: the I-PREDICT study. *Nat. Med.* **25**, 744–750 (2019).

94. Jennings, L. J. *et al.* Guidelines for Validation of Next-Generation Sequencing–Based Oncology Panels: A Joint Consensus Recommendation of the Association for Molecular Pathology and College of American Pathologists. *Journal of Molecular Diagnostics* vol. 19 341–365 (2017).

95. Sparano, J. A. *et al.* Adjuvant Chemotherapy Guided by a 21-Gene Expression Assay in Breast Cancer. *N. Engl. J. Med.* **379**, 111–121 (2018).

96. Von Hoff, D. D. *et al.* Pilot study using molecular profiling of patients' tumors to find potential targets and select treatments for their refractory cancers. *J. Clin. Oncol.* **28**, 4877–4883 (2010).

97. Salami, S. S. *et al.* Circulating Tumor Cells as a Predictor of Treatment Response in Clinically Localized Prostate Cancer. *JCO Precis. Oncol.* 1–9 (2019) doi:10.1200/po.18.00352.

98. Hiltermann, T. J. N. *et al.* Circulating tumor cells in small-cell lung cancer: A predictive and prognostic factor. *Ann. Oncol.* **23**, 2937–2942 (2012).

99. Nussinov, R., Jang, H., Tsai, C. J. & Cheng, F. Review: Precision medicine and driver mutations: Computational methods, functional assays and conformational principles for interpreting cancer drivers. *PLoS Comput. Biol.* **15**, (2019).

100. Patel, H. *et al.* Current advances in the treatment of braf-mutant melanoma. *Cancers* vol. 12 (2020).

101. Yap, T. A. & Workman, P. Exploiting the cancer genome: Strategies for the discovery and clinical development of targeted molecular therapeutics. *Annu. Rev. Pharmacol. Toxicol.* **52**, 549–573 (2012).

102. Jin, H. *et al.* EGFR activation limits the response of liver cancer to lenvatinib. *Nature* (2021)

doi:10.1038/s41586-021-03741-7.

103. Moosavi, A. & Ardekani, A. M. Role of epigenetics in biology and human diseases. *Iranian Biomedical Journal* vol. 20 246–258 (2016).

104. Weinhold, B. Epigenetics: the science of change. *Environ. Health Perspect.* **114**, A160 (2006).

105. Mazzio, E. A. & Soliman, K. F. Basic concepts of epigenetics impact of environmental signals on gene expression. *Epigenetics* vol. 7 119–130 (2012).

106. Varela, I. *et al.* Exome sequencing identifies frequent mutation of the SWI/SNF complex gene PBRM1 in renal carcinoma. *Nature* **469**, 539–542 (2011).

107. Ong, C. K. *et al.* Exome sequencing of liver flukeg-associated cholangiocarcinoma. *Nat. Genet.* **44**, 690–693 (2012).

108. Chan-On, W. *et al.* Exome sequencing identifies distinct mutational patterns in liver fluke-related and non-infection-related bile duct cancers. *Nat. Genet.* **45**, 1474–1478 (2013).

109. Fujimoto, A. *et al.* Whole-genome mutational landscape of liver cancers displaying biliary phenotype reveals hepatitis impact and molecular diversity. *Nat. Commun.* **6**, 1–8 (2015).

110. Misumi, K. *et al.* Intrahepatic cholangiocarcinoma frequently shows loss of BAP1 and PBRM1 expression, and demonstrates specific clinicopathological and genetic characteristics with BAP1 loss. *Histopathology* **70**, 766–774 (2017).

111. Wilson, B. G. & Roberts, C. W. M. SWI/SNF nucleosome remodellers and cancer. *Nat. Rev. Cancer* **11**, 481–492 (2011).

112. Savas, S. & Skardasi, G. The SWI/SNF complex subunit genes: Their functions, variations, and links to risk and survival outcomes in human cancers. *Crit. Rev. Oncol. Hematol.* **123**, 114–131 (2018).

113. De La Serna, I. L., Ohkawa, Y. & Imbalzano, A. N. Chromatin remodelling in mammalian differentiation: Lessons from ATP-dependent remodellers. *Nature Reviews Genetics* vol. 7 461–473 (2006).

114. Flowers, S., Nagl, N. G., Beck, G. R. & Moran, E. Antagonistic roles for BRM and BRG1 SWI/SNF complexes in differentiation. *J. Biol. Chem.* **284**, 10067–10075 (2009).

115. Isakoff, M. S. *et al.* Inactivation of the Snf5 tumor suppressor stimulates cell cycle progression and cooperates with p53 loss in oncogenic transformation. *Proc. Natl. Acad. Sci. U. S. A.* **102**, 17745–17750 (2005).

116. Nagl, N. G., Zweitzig, D. R., Thimmapaya, B., Beck, G. R. & Moran, E. The c-myc gene is a direct target of mammalian SWI/SNF-related complexes during differentiation-associated cell cycle arrest. *Cancer Res.* **66**, 1289–1293 (2006).

117. Cheng, S. W. G. *et al.* c-MYC interacts with INI1/hSNF5 and requires the SWI/SNF complex for transactivation function. *Nat. Genet.* **22**, 102–105 (1999).

118. Caramel, J., Quignon, F. & Delattre, O. RhoA-dependent regulation of cell migration by the

tumor suppressor hSNF5/INI1. *Cancer Res.* **68**, 6154–6161 (2008).

119. Lemon, B., Inouye, C., King, D. S. & Tjian, R. Selectivity of chromatin-remodelling cofactors for ligand-activated transcription. *Nature* **414**, 924–928 (2001).

120. Thompson, M. Polybromo-1: The chromatin targeting subunit of the PBAF complex. *Biochimie* **91**, 309–319 (2009).

121. Finn, L., Markovic, S. N. & Joseph, R. W. Therapy for metastatic melanoma: The past, present, and future. *BMC Medicine* vol. 10 1–10 (2012).

122. Douville, E. & Downward, J. EGF induced SOS phosphorylation in PC12 cells involves P90 RSK-2. *Oncogene* **15**, 373–383 (1997).

123. Guzmán, C., Bagga, M., Kaur, A., Westermarck, J. & Abankwa, D. ColonyArea: An ImageJ plugin to automatically quantify colony formation in clonogenic assays. *PLoS One* **9**, e92444 (2014).

124. Dow, L. E. *et al.* Conditional reverse tet-transactivator mouse strains for the efficient induction of tre-regulated transgenes in mice. *PLoS One* **9**, e95236 (2014).

125. Calvisi, D. F. *et al.* Increased lipogenesis, induced by AKT-mTORC1-RPS6 signaling, promotes development of human hepatocellular carcinoma. *Gastroenterology* **140**, 1071-1083.e5 (2011).

126. Wang, J. *et al.* Notch2 controls hepatocyte-derived cholangiocarcinoma formation in mice. *Oncogene* **37**, 3229–3242 (2018).

127. Horie, Y. *et al.* Hepatocyte-specific Pten deficiency results in steatohepatitis and hepatocellular carcinomas. *J. Clin. Invest.* **113**, 1774–1783 (2004).

128. Shain, A. H. & Pollack, J. R. The Spectrum of SWI/SNF Mutations, Ubiquitous in Human Cancers. *PLoS One* **8**, e55119 (2013).

129. Brugarolas, J. PBRM1 and BAP1 as novel targets for renal cell carcinoma. *Cancer Journal (United States)* vol. 19 324–332 (2013).

130. Yang, Q. *et al.* Comprehensive analyses of PBRM1 in multiple cancer types and its association with clinical response to immunotherapy and immune infiltrates. *Ann. Transl. Med.* **9**, 465–465 (2021).

131. Jiao, Y. *et al.* Exome sequencing identifies frequent inactivating mutations in BAP1, ARID1A and PBRM1 in intrahepatic cholangiocarcinomas. *Nat. Genet.* **45**, 1470–1473 (2013).

132. McFarland, C. D. *et al.* The damaging effect of passenger mutations on cancer progression. *Cancer Res.* **77**, 4763–4772 (2017).

133. Luchini, C. *et al.* PBRM1 loss is a late event during the development of cholangiocarcinoma. *Histopathology* **71**, 375–382 (2017).

134. Walkin, L. *et al.* The role of mouse strain differences in the susceptibility to fibrosis: A systematic review. *Fibrogenes. Tissue Repair* **6**, (2013).

135. Kishi, T. Appropriate selection of a mouse strain in accordance with the vascular properties. *Hypertension Research* vol. 43 1311–1312 (2020).

136. Maronpot, R. R. Biological basis of differential susceptibility to hepatocarcinogenesis among mouse strains. *Journal of Toxicologic Pathology* vol. 22 11–33 (2009).

137. Lake, A. D. *et al.* Analysis of global and absorption, distribution, metabolism, and elimination gene expression in the progressive stages of human nonalcoholic fatty liver disease. *Drug Metab. Dispos.* **39**, 1954–1960 (2011).

138. Kanwal, R., Gupta, K. & Gupta, S. Cancer epigenetics: an introduction. *Methods in molecular biology (Clifton, N.J.)* vol. 1238 3–25 (2015).

139. Salati, M. *et al.* IDH signalling pathway in cholangiocarcinoma: From biological rationale to therapeutic targeting. *Cancers* vol. 12 1–11 (2020).

140. Saha, S. K. *et al.* Mutant IDH inhibits HNF-4α to block hepatocyte differentiation and promote biliary cancer. *Nature* **513**, 110–152 (2014).

141. Si-Tayeb, K., Lemaigre, F. P. & Duncan, S. A. Organogenesis and Development of the Liver. *Developmental Cell* vol. 18 175–189 (2010).

142. Yuen, G. J., Demissie, E. & Pillai, S. B Lymphocytes and Cancer: A Love–Hate Relationship. *Trends in Cancer* vol. 2 747–757 (2016).

143. Kinker, G. S. *et al.* B Cell Orchestration of Anti-tumor Immune Responses: A Matter of Cell Localization and Communication. *Frontiers in Cell and Developmental Biology* vol. 9 1282 (2021).

144. Ammirante, M., Luo, J. L., Grivennikov, S., Nedospasov, S. & Karin, M. B-cell-derived lymphotoxin promotes castration-resistant prostate cancer. *Nature* **464**, 302–305 (2010).

145. Pan, D. *et al.* A major chromatin regulator determines resistance of tumor cells to T cell-mediated killing. *Science (80-.).* **359**, 770–775 (2018).

146. Miao, D. *et al.* Genomic correlates of response to immune checkpoint therapies in clear cell renal cell carcinoma. *Science (80-.).* **359**, 801–806 (2018).

147. Liu, X. De *et al.* PBRM1 loss defines a nonimmunogenic tumor phenotype associated with checkpoint inhibitor resistance in renal carcinoma. *Nat. Commun.* **11**, 1–14 (2020).

148. Zhou, H. *et al.* PBRM1 mutation and preliminary response to immune checkpoint blockade treatment in non-small cell lung cancer. *npj Precis. Oncol.* **4**, 1–4 (2020).

149. Lang, P. A., Recher, M., Häussinger, D. & Lang, K. S. Genes determining the course of virus persistence in the liver: Lessons from murine infection with lymphocytic choriomeningitis virus. *Cell. Physiol. Biochem.* **26**, 263–272 (2010).

150. Schulze, K. *et al.* Exome sequencing of hepatocellular carcinomas identifies new mutational signatures and potential therapeutic targets. *Nat. Genet.* **47**, 505–511 (2015).

151. Chan, L. K. *et al.* RSK2-inactivating mutations potentiate MAPK signaling and support

cholesterol metabolism in hepatocellular carcinoma. *J. Hepatol.* **74**, 360–371 (2021).

152. Santarpia, L., Lippman, S. M. & El-Naggar, A. K. Targeting the MAPKRASRAF signaling pathway in cancer therapy. *Expert Opinion on Therapeutic Targets* vol. 16 103–119 (2012).

153. Guo, Y. *et al.* ERK/MAPK signalling pathway and tumorigenesis (Review). *Exp. Ther. Med.* **19**, 1997–2007 (2020).

154. JQ, L. *et al.* Dietary cholesterol promotes steatohepatitis related hepatocellular carcinoma through dysregulated metabolism and calcium signaling. *Nat. Commun.* **9**, (2018).

155. Cohen, J. V. & Sullivan, R. J. Developments in the space of new MAPK pathway inhibitors for BRAF-mutant melanoma. *Clinical Cancer Research* vol. 25 5735–5742 (2019).

156. Xie, Y. H., Chen, Y. X. & Fang, J. Y. Comprehensive review of targeted therapy for colorectal cancer. *Signal Transduction and Targeted Therapy* vol. 5 1–30 (2020).

157. Khojasteh Poor, F. *et al.* Mini review: The FDA-approved prescription drugs that target the MAPK signaling pathway in women with breast cancer. *Breast disease* vol. 40 51–62 (2021).

158. Lu, M., Wang, Y. & Zhan, X. The MAPK pathway-based drug therapeutic targets in pituitary adenomas. *Frontiers in Endocrinology* vol. 10 330 (2019).

159. Barré-Sinoussi, F. & Montagutelli, X. Animal models are essential to biological research: Issues and perspectives. *Future Science OA* vol. 1 (2015).

160. S, S., A, M. & M, A. From in vitro Experiments to in vivo and Clinical Studies; Pros and Cons. *Curr. Drug Discov. Technol.* **12**, 218–224 (2015).

161. Braicu, C. *et al.* A comprehensive review on MAPK: A promising therapeutic target in cancer. *Cancers* vol. 11 1618 (2019).

162. Mendoza, M. C., Er, E. E. & Blenis, J. The Ras-ERK and PI3K-mTOR pathways: Cross-talk and compensation. *Trends in Biochemical Sciences* vol. 36 320–328 (2011).

163. Lee, S., Rauch, J. & Kolch, W. Targeting MAPK signaling in cancer: Mechanisms of drug resistance and sensitivity. *International Journal of Molecular Sciences* vol. 21 (2020).

164. Liu, F., Yang, X., Geng, M. & Huang, M. Targeting ERK, an Achilles' Heel of the MAPK pathway, in cancer therapy. *Acta Pharmaceutica Sinica B* vol. 8 552–562 (2018).

Acknowledgements

Writing this dissertation has helped me to summarize and put into perspective four years of my life. I came to appreciate that this thesis became a reality thanks to the constant support of amazing people that I have met since I first set foot in Heidelberg, and I am incredibly thankful for that.

First and foremost, I am extremely grateful to my supervisor, **Prof. Dr. Darjus Felix Tschaharganeh**, for the opportunity to join your lab as a PhD student and giving me the chance to work on this exciting project. Looking back to when I started I can appreciate how much I have grown professionally and I am thankful for that. I would also like to extend my sincere thanks to the members of my TAC committee, **Prof. Dr. Ralf Bartenschlager** and **Prof. Dr. Kai Breuhahn** for the precious feedback over the course of the PhD. Special thanks go to **Prof. Dr. Peter Angel** and **Dr. Richard Harbottle** for enthusiastically joining my doctoral defense examination commission and evaluating my thesis. I would like to acknowledge the support of **Prof. Dr. Mathias Heikenwälder** for his feedback during my second TAC meeting and for offering help with the immunological stainings. Thanks also to **Prof. Dr. Thomas Longerich** for helping with pathological evaluations.

I would not have lasted long for four years without the daily support of great colleagues. **Gege**, thanks for having been a calming presence in the lab, for discussing our projects and for inspiring me to pursue an MBA. **Aga**, thanks for the endless support. You brought an amazing sense of community and positivity in the lab just when I needed it the most. Words cannot describe how grateful I am for that. **Sonia** and **Luise**, we shared the best bike rides and great lunches together, thanks for that! **Kai** and **Lio**, thanks for being the nicest people and for the technical support, I felt part of a team with you in Patho. **Marco**, thanks for brainstorming science with me daily, I learnt a great deal from you. Thanks also to the rest of the present and past members of **AG Tschaharganeh**, there is a lesson to be learnt from everyone.

Working in such a dynamic environments has led me to meet awesome people in the institute. **Yalda**, thanks for the talks and always having the perfect words when I am feeling

down. **Federico** and **Rossella**, what can I say? Thanks for having welcomed me since day one, you are like older siblings to me. Federico, thanks for being a mentor for science and beyond, I cherish every conversation and run we shared together. Let's see if we can run that NY marathon one day! Rossella, thanks for making me believe in my worth and for the emotional support, especially during the last year of my PhD.

To the "**Beiruttini**", you have been a pillar of my life as a PhD student in Heidelberg. **Alice**, you became one of the friends I hold dear the most. Thanks for being the most genuine person and always indulging me when I am goofing around. **Sandro**, thanks for always saying "YES!" whenever I proposed to go and watch some random band playing live. I always enjoyed our trips to the flea markets, our hunts for LPs and our lockdown videogaming sessions. **Silvia** "Coluccia", thanks for the all the time you cooked for us and always made me feel like having Sunday lunch with my family in Italy. **Ilaria**, thanks for being the sweetest friend and having been an irreplaceable colleague, I wished you could have stayed longer in Germany. **Valentina** and **Alessandro**, thanks for the trips, dinners and parties we shared. **Luca**, thanks for the silly times together and teaching me how to ride a unicycle. **Elli**, thanks for being there when I was in need and for always lending me your ear. You have been very supportive, especially during the writing session, and I am very grateful for it! **Ina**, you have been my go-to bouldering buddy, thanks for all the climbing session we shared together. **Lena**, thanks for being a great friend and for offering all those coffees at the "Hotspot". **Karim**, thanks for your kindness and all the help with German bureaucracy.

To my **family**. Thanks for the unconditional love. You always supported my choices, taught me the values that really matter in life and helped me in looking at the big picture when I was stubbornly focused on silly details. You are my strength and I would not have made it without you.

Lastly, thanks to everyone that ever helped me during this journey and supported me in reaching my goals. I hope I did not forget anybody, and if I did, please forgive me!